

UNDERSTANDING EFFICIENCY IMPROVEMENT
IN ORGANIC PHOTOVOLTAICS WITH
MOLECULAR MODIFIERS

by
Jennifer L. Braid

A thesis submitted to the Faculty and the Board of Trustees of the Colorado School of Mines in partial fulfillment of the requirements for the degree of Doctor of Philosophy (Applied Physics).

Golden, Colorado

Date _____

Signed: _____

Jennifer L. Braid

Signed: _____

Dr. Reuben T. Collins
Thesis Advisor

Signed: _____

Dr. Nikos Kopidakis
Thesis Advisor

Golden, Colorado

Date _____

Signed: _____

Dr. Jeff Squier
Professor and Head
Department of Physics

ABSTRACT

Molecular dipole modification of metal oxides has become popular to improve the performance of organic photovoltaic devices through charge transport level matching to the bulk heterojunction species. Properly tuning the work function of a device interlayer can increase charge collection from the active layer, ultimately raising the efficiency of the device.

Here a novel type of molecule is introduced for modulating the work function of charge transport layers in organic photovoltaics: the conjugated phosphonic acid. Due to its longer and double-bonded linkage, as well as its multi-dentate attachment, this type of molecule is shown to shift the work functions of ZnO and ITO through ranges of 2 eV. The vast dipolar aromatic groups possible in conjugated phosphonic acids allow for either increasing or decreasing the work function of the substrate incrementally. This facilitates the energy matching with the Fermi level of a photovoltaic material necessary to achieve maximum efficiency of that solar cell.

The effectiveness of conjugated phosphonic acids is also demonstrated in an operational organic bulk heterojunction solar cell. A self-assembled monolayer of conjugated phosphonic acid on the electron transport layer of an inverted device is shown to significantly increase the power conversion efficiency of that cell, even compared to its non-conjugated counterpart. The improvement to device performance was largely due to an increase in the short circuit current, with minor boosts to the open circuit voltage and fill factor.

Direct measurements of potential distributions inside phosphonic acid modified and unmodified cells are also given. Beneficial modification of the electron transport layer interface is shown to extend the electric field within the active layer. The electric field is thought to aid in carrier separation and extraction from the bulk heterojunction, which correlates with improved short circuit current.

Additionally, the technique for measuring potential distributions within operational solar cells, cross-sectional scanning Kelvin probe microscopy (X-SKPM), is tested in ambient and inert conditions. X-SKPM of organic photovoltaics in air reveals oxygen p-doping of the bulk heterojunction, as well as sensitivity to surface contamination of oxide interlayers, while inert conditions facilitate a reliable measurement of the potential distribution in organic photovoltaics.

TABLE OF CONTENTS

ABSTRACT	iii
LIST OF FIGURES	vii
LIST OF TABLES	ix
LIST OF ABBREVIATIONS	x
ACKNOWLEDGMENTS	xii
CHAPTER 1 GENERAL INTRODUCTION	1
1.1 Thesis Organization	1
1.2 Organic Solar Cell Operation	3
1.3 Contact Interfaces and Interlayers	5
1.4 Work Function Modification of Transparent Conducting Oxides	9
1.5 Potential Distribution in Organic Photovoltaics	15
1.6 Experimental Techniques	17
1.6.1 Solar Cell Processing and Characterization	17
1.6.2 Kelvin Probe	19
1.6.3 Fourier-Transform Infrared Spectroscopy (FTIR)	20
1.6.4 Atomic Force Microscopy (AFM)	21
1.6.5 Cross-Sectional Scanning Kelvin Probe Microscopy (X-SKPM)	21
CHAPTER 2 CONJUGATED PHOSPHONIC ACID MODIFIED ZINC OXIDE ELECTRON TRANSPORT LAYERS FOR IMPROVED PERFORMANCE IN ORGANIC SOLAR CELLS	24
2.1 Introduction	25

2.2	Results and Discussion	28
2.3	Conclusions	32
2.4	Experimental Methods	34
2.5	Acknowledgments	37
CHAPTER 3 MOLECULAR DESIGN FOR TUNING WORK FUNCTIONS OF TRANSPARENT CONDUCTING ELECTRODES		38
3.1	Introduction	39
3.2	Results and Discussion	41
3.3	Summary and Future Outlook	49
3.4	Acknowledgments	50
CHAPTER 4 CROSS-SECTIONAL SCANNING KELVIN PROBE MICROSCOPY OF ORGANIC BULK HETEROJUNCTION SOLAR CELLS		51
4.1	Introduction	51
4.2	Experimental Methods	55
4.3	Results and Discussion	56
4.4	Conclusions	69
4.5	Acknowledgments	70
CHAPTER 5 GENERAL CONCLUSIONS		72
5.1	Discussion and Impact	72
5.2	Recommendations for Future Research	74
REFERENCES CITED		76
APPENDIX A - SUPPLEMENTAL INFORMATION FOR CHAPTER 4		91
APPENDIX B - PERMISSIONS		93

LIST OF FIGURES

Figure 1.1	P3HT and ICBA band structures	3
Figure 1.2	Bulk heterojunction device and P3HT and ICBA chemical structures	4
Figure 1.3	Current-voltage curve for a solar cell depicting device characteristics.	5
Figure 1.4	Band diagram for an inverted architecture device.	6
Figure 1.5	Band diagrams for non-Ohmic and Ohmic contacts	7
Figure 1.6	Fermi-level pinning of contacts to the BHJ	9
Figure 1.7	Electron extraction barrier in OPV device	10
Figure 1.8	Vacuum level shifting by interfacial dipole	12
Figure 1.9	Phosphonic acid attachment to ZnO	14
Figure 1.10	X-SKPM operation	22
Figure 2.1	Novel oF ₂ PAs	27
Figure 2.2	Synthetic preparation of oF ₂ PVPA and oF ₂ PEPA	28
Figure 2.3	FTIR spectra for oF ₂ PEPA and oF ₂ PVPA bonded to ZnO	30
Figure 2.4	J-V characteristics for oF ₂ PA modified devices	32
Figure 3.1	Chemical structures of the seven novel phosphonic acids.	42
Figure 3.2	Linear fit of dipole moment versus work function change for conjugated PAs	43
Figure 3.3	Quantum mechanically calculated geometries of oF ₂ BPA, nc2FPA, and 2FPA.	44
Figure 3.4	Gas-phase dipole vectors for conjugated PAs	45
Figure 3.5	General Synthetic Pathway for Preparing the Conjugated Phosphonic Acids	45

Figure 4.1	Standard architecture device J-V characteristics	57
Figure 4.2	X-SKPM of a standard architecture device	60
Figure 4.3	Inverted architecture device J-V characteristics	62
Figure 4.4	X-SKPM of an inverted architecture device	63
Figure 4.5	Modified inverted device J-V characteristics	66
Figure 4.6	X-SKPM of PA modified inverted devices	68
Figure 4.7	Charge density in modified inverted devices	69

LIST OF TABLES

Table 2.1	Work function of PA modified ZnO and corresponding average device results	33
Table 3.1	Work function changes for ITO and ZnO modified with PAs	43
Table 4.1	Standard architecture device characteristics	57
Table 4.2	Inverted architecture device characteristics	61
Table 4.3	Modified device characteristics	66
Table A.1	Whole standard architecture device characteristics	91
Table A.2	Whole inverted architecture device characteristics	91
Table A.3	Whole modified inverted device characteristics	92

LIST OF ABBREVIATIONS

Cross-Sectional Scanning Kelvin Probe Microscopy	X-SKPM
Highest Occupied Molecular Orbital	HOMO
Lowest Unoccupied Molecular Orbital	LUMO
Poly(3-hexylthiophene-2,5-diyl)	P3HT
Indene-C ₆₀ Bisadduct	ICBA
Bulk Heterojunction	BHJ
Integer Charge Transfer	ICT
Positive Integer Charge Transfer State	E _{ICT+}
Negative Integer Charge Transfer State	E _{ICT-}
Current Density-Voltage	J-V
Open Circuit Voltage	V _{OC}
Short Circuit Current Density	J _{SC}
Fill Factor	FF
Power Conversion Efficiency	PCE
Organic Photovoltaic	OPV
Electron Transport Layer	ETL
Hole Transport Layer	HTL
Work Function	ϕ
Transparent Conducting Oxide	TCO
Indium Tin Oxide	ITO

Fermi Level	E_F
Zinc Oxide	ZnO
Self-Assembled Monolayer	SAM
Poly(3,4-Ethylenedioxythiophene) Polystyrene Sulfonate	PEDOT:PSS
Polytetrafluoroethylene	PFTE
Atomic Force Microscopy	AFM
X-Ray Photoelectron Spectroscopy	XPS
Gallium Arsenide	GaAs
Phosphonic Acid	PA
Contact Potential Difference	CPD
Fourier-Transform Infrared Spectroscopy	FTIR
Alternating Current	AC
Direct Current	DC
Orthodifluorobenzylphosphonic acid	oF ₂ BPA
Orthodifluorophenylvinylphosphonic acid	oF ₂ PVPA, nc2FPA
Orthodifluorophenylethylphosphonic acid	oF ₂ PEPA, 2FPA
Shunt Resistance	R_{SH}
Series Resistance	R_{SE}
Metamethylstyrylphosphonic acid	3TPA
Styrylphosphonic acid	PPA
Paramethoxystyrylphosphonic acid	AnPA
Paratrifluoromethylstyrylphosphonic acid	pCF ₃ PVPA,CF3PA
Paradicyanovinylstyrylphosphonic acid	2CVPA

ACKNOWLEDGMENTS

First, I thank my advisors, Reuben Collins, Nikos Kopidakis, and Dana Olson, who generously provided guidance and encouragement throughout my time at Mines and NREL. Thank you to the other members of my committee: Alan Sellinger, Tom Furtak, and David Wood, for giving crucial feedback and support to this project. I would also like to thank my collaborators for their advice and input, especially Sanjini Nanayakkara and Unsal Koldemir. Your efforts and perspectives were invaluable to the success of this work. Thanks to Tim Ohno for bringing me to Mines and for advising me through my first year, and to Dana for giving me the opportunity to work at NREL.

To my family and friends, thank you for your love and care through my many years of school. To my fellow students and friends at Mines and NREL, thank you for your commiserating and comradery over the past several years.

And finally, to my husband, Ryan, thank you for your undying patience, understanding, and love, and your constant belief in me.

CHAPTER 1

GENERAL INTRODUCTION

Organic photovoltaics have shown promise for producing modules of low cost and reasonable efficiency. However, improving power conversion efficiency of these devices is necessary for them to remain relevant in the solar cell market. One method for improving charge extraction from the device is interfacial transport energy level matching through contact modification. This thesis explores the use of small dipolar molecules to modulate the work function of transparent conducting oxides to improve device performance.

While the effect of work function modification on device characteristics is a very active area of study, the internal mechanisms for device improvement are not well understood. Therefore, direct examination of internal device operation would not only explain the root of device improvement with contact modification, but also inform other methods for increasing solar cell performance.

Cross-sectional scanning Kelvin probe microscopy (X-SKPM) provides a direct look at the potential distribution within a device under operating conditions. This is a relatively new technique that until now has not been well validated; published results give conflicting pictures of the electric potential within organic bulk heterojunction devices. Comparisons of devices measured with this technique in ambient and inert environments will prove reliability of the technique. Then, X-SKPM inspection of molecular dipole modified devices will reveal the origins of improvements to device characteristics through the potential distribution across the solar cell structure.

1.1 Thesis Organization

This thesis examines the use of conjugated phosphonic acids for modifying the work function of transparent conducting oxides and improving performance of organic bulk heterojunction solar cells. In addition to device fabrication and materials characterization, the

impact on solar cell operation is correlated with X-SKPM, which provides direct measurement of the potential distribution of operating devices.

The current chapter provides background information on the basic operation of organic bulk heterojunction devices, as well as the theory of improvement to these devices by molecular dipole modification of transport layer materials. Also provided in the introduction is current theory on organic photovoltaic device behavior in the context of electric potential distribution, and detailed descriptions of the experimental methods used in this work.

Chapter 2 gives Kelvin probe and corresponding device data for phosphonic acid modified zinc oxide. Decreasing the work function of zinc oxide correlates with improved device characteristics, and novel conjugated phosphonic acids are shown to outperform their non-conjugated counterparts. The binding characteristics of these molecules are also examined by Fourier-transform infrared spectroscopy.

Chapter 3 proves the wide range of effective work functions achievable for both zinc oxide and indium tin oxide through modification with a variety of conjugated phosphonic acids. Modeling reveals that changing the head group yields a different net dipole moment of the molecule, allowing for corresponding modulation of the work function of these oxides over a range of 2 eV as measured by Kelvin probe.

Chapter 4 examines the potential distributions within organic photovoltaic devices using X-SKPM. Comprehensive measurements in both ambient and inert conditions and comparison with corresponding current-voltage characteristics reveal the effects of air and applied bias on operating organic solar cells. Then, X-SKPM is used to examine the potential distribution in inverted devices incorporating phosphonic acid modified ZnO electron transport layers. Device performance is shown to correlate with extension of the electric field across the active layer, indicating that the work function of the electron transport layer influences the space charge density within the active layer.

Finally, Chapter 5 discusses the impacts of this work on organic photovoltaics research, as well as larger conclusions for interfacial engineering in other types of solar cells and

electronics. Future topics of research prompted by this work are also suggested in this chapter.

1.2 Organic Solar Cell Operation

Light is absorbed by an organic semiconductor material as determined by its band gap, the range of energies between the highest occupied molecular orbital (HOMO) and lowest unoccupied molecular orbital (LUMO) (similar to the valence and conduction bands in a classical semiconductor). An organic polymer can absorb the portion of the solar spectrum with energy greater than its band gap, though the absorption coefficient is reduced with increasing band gap. When a photon is absorbed, it can excite an electron, forming an electron-hole pair called an exciton, which is bound by the Coulomb force.

In order for energy to be harvested from this solar cell, the exciton must be separated into free charges. This separation occurs at the interface of the polymer electron donor and a second semiconductor material, an electron acceptor. Organic fullerenes, spheres of sixty or seventy-one carbon atoms, fulfill the role of electron acceptor in this work. As seen in Figure 1.1, the polymer:fullerene band structure allows for charges to separate by electrons transferring to the LUMO level of the ICBA fullerene while the holes reside in the HOMO level of the P3HT polymer.

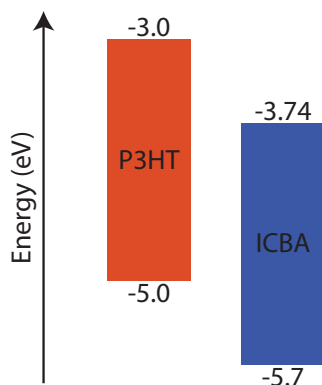


Figure 1.1: P3HT and ICBA band structures

Because exciton separation can only occur where polymer and fullerene meet, and because excitons diffuse only a few nanometers before recombining, it is advantageous to have a large interface between the electron donor and acceptor materials. The bulk heterojunction (BHJ) was introduced to increase the polymer/fullerene interface over traditional bilayer devices. Slow-drying of P3HT:ICBA dichlorobenzene solutions produces optimal domain sizes for balancing the surface area between species for exciton separation with the domain size needed for charges to reach the electrodes. Figure 1.2 shows the mixed domains in a BHJ active layer, as well as the P3HT and ICBA chemical structures.

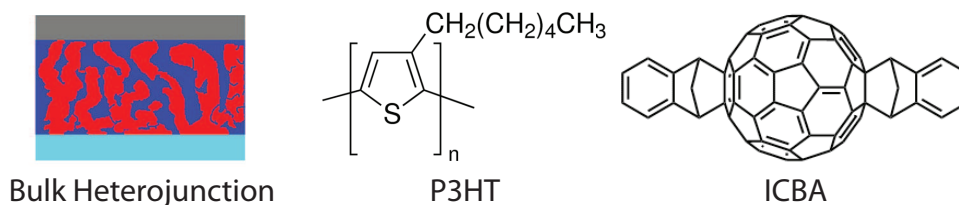


Figure 1.2: Bulk heterojunction device and P3HT and ICBA chemical structures

The picture of band structure in organic materials has been expanded by the integer charge transfer (ICT) model, which describes interfaces with very little hybridization of π -electrons. The lack of hybridization implies that electron transfer occurs via tunneling, a characteristically discrete charge transfer process. In the ICT model, π -conjugated systems experience both geometric and electronic relaxation in the form of polarons, due to the addition or reduction of charge. This leads to states within the formerly forbidden region between the HOMO and LUMO levels of the system, called ICT states, analagous to quasi-Fermi levels. The positive ICT state (E_{ICT+}) is the energy to remove an electron from the material, while the negative ICT state (E_{ICT-}) is the energy gained when an electron is added, both processes creating fully relaxed states.[1]

The BHJ band structure also determines the theoretical maximum device characteristics, depicted in the current density-voltage (J-V) graph for a solar cell in Figure 1.3. The theoretical open circuit voltage (V_{OC}) of an active layer is proportional to the difference in

the ICT states of the BHJ. Some have theorized that this difference builds an internal field that drives charge carrier drift in the active layer. The short circuit current density (J_{SC}) originates from charge generation and extraction, hence the band gap of this material plays a key role. The fill factor (FF) is the ratio of the maximum power density output of the device to the product of its V_{OC} and J_{SC} , and is largely related to exciton recombination. The power conversion efficiency (PCE) is calculated as the maximum power density output of the device divided by the incident light intensity.

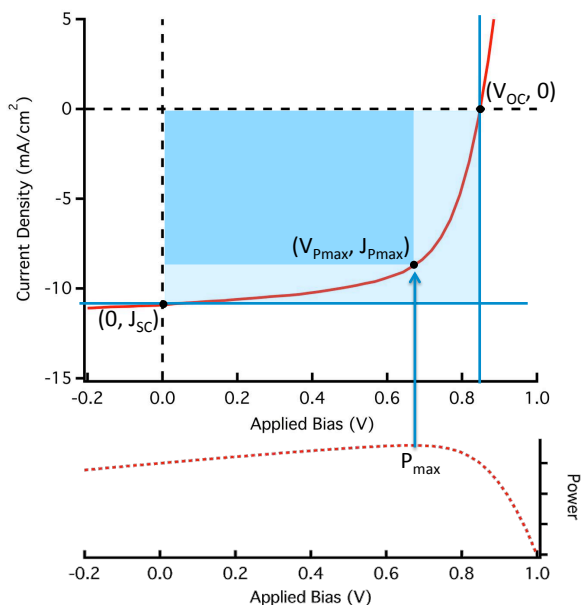


Figure 1.3: Current-voltage curve for a solar cell depicting device characteristics. The fill factor is the maximum power density (darker rectangle) divided by the product of the V_{OC} and J_{SC} (lighter rectangle).

1.3 Contact Interfaces and Interlayers

New organic BHJ constituents, usually polymers[2–4] and fullerenes[5] but also small molecules,[6] are constantly being formulated and synthesized to improve organic photovoltaic (OPV) device characteristics such as V_{OC} and PCE. As these novel active layer materials are introduced, the need for interface engineering of charge transport layers becomes ever greater to realize the best possible devices incorporating these materials. The

energy band diagram of the basic inverted architecture device used in this work is given in Figure 1.4. The use of an electron transport layer (ETL) and hole transport layer (HTL) between the BHJ and electrodes significantly improves device performance by increasing charge extraction efficiency from the active layer over metal/organic interfaces.

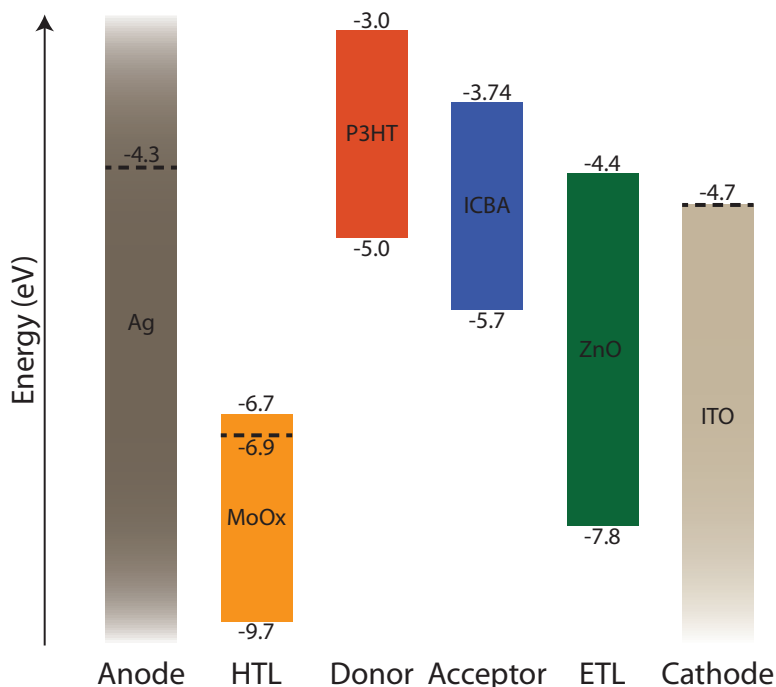


Figure 1.4: Energy band diagram for an inverted architecture device. HOMO and LUMO levels of the BHJ and interlayer materials are shown, and Fermi levels are given as dotted lines.

The interface between a semiconductor and a metal results in a Schottky barrier, defined by the Schottky-Mott rule as the difference in work function of the metal to the electron affinity or ionization energy of the semiconductor. However, metal-induced gap states in the semiconductor can pin to the Fermi-level of the metal, so the Schottky barrier height may vary from this estimate. If the Fermi level of the metal lies within the band gap of the semiconductor, the barrier is large, and the metal/semiconductor interface is a rectifying Schottky junction, which exhibits diode behavior due to the injection barrier. In a solar cell following the Schottky-Mott model, Schottky junctions result in V_{OC} determined by the difference in work functions ($\Delta\phi$) of the electrodes, significantly lower than the maximum

possible V_{OC} . Similarly, the metal-insulator-metal (MIM) model often used for OPV and shown in Figure 1.5 describes a barrier for charges crossing a non-Ohmic contact resulting from a contact Fermi level within the band gap, which also reduces the V_{OC} of the device. Charge transport interlayers can drastically improve the V_{OC} of a device by making Ohmic contacts, or non-rectifying (linear) junctions that eliminate the injection barrier at the interface by pinning of the Fermi levels of electrodes to ICT states.[1, 7, 8] However, the doping level in the semiconductor also plays a major role in determining whether the metal/semiconductor interface behaves as an Ohmic or Schottky junction.

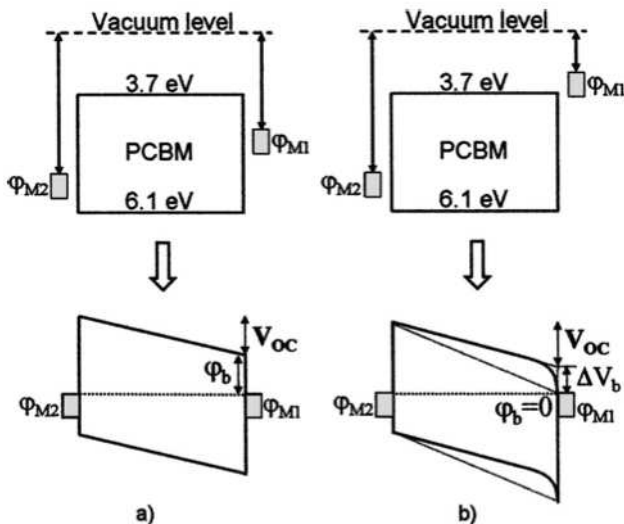


Figure 1.5: Band diagram of a metal-insulator-metal device with vacuum levels (top) and Fermi levels (bottom) aligned for a) non-Ohmic and (b) Ohmic M1 contact. ϕ_b is the injection barrier height for electrons at the non-Ohmic contact, and ΔV_b is the voltage loss at the Ohmic contact. Reprinted from [9] with the permission of AIP Publishing.

In addition to Ohmicity of the interface, several other factors contribute to a charge transport material's effect on device performance, including charge transfer efficiency and selectivity, surface energy, conductivity, and chemical stability. Specifically for solar applications, it is also advantageous for these materials to have high transparency in the absorbing wavelengths of the cell, be mechanically robust, and show ease of thin film formation. In showing good metrics in all of these areas, transparent conducting metal oxides (TCOs) are

a common type of charge transport material in the current state of the art.

In both standard and inverted architecture OPVs, indium tin oxide (ITO) is the most frequently used transparent electrode, due to its very good stability, durability, conductivity, and transparency in the relevant wavelengths. However, ITO's work function, usually reported around 4.2 to 4.7 eV, falls between the ICT states of common BHJs, meaning that its Fermi level cannot be pinned to these states, and consequently Ohmic behavior cannot occur for a BHJ/ITO interface.[10, 11] This effect is depicted in Figure 1.6. When the work function of the substrate is greater than the positive ICT state of the organic semiconductor (a), electrons spontaneously flow from the ICT state into the substrate, creating a dipole across the substrate/organic and consequently a charge transfer-induced shift in the vacuum level at the interface such that the substrate Fermi level is pinned to the positive ICT state of the organic. Conversely, if the work function of the substrate is less than the negative ICT state of the organic (c), a similar process occurs with electrons flowing from substrate to organic and pinning the substrate Fermi level to the negative ICT state. If the Fermi level of the substrate lies between the positive and negative ICT states of the organic (b), no pinning occurs. In addition to its unfavorable Fermi level position, ITO also suffers from inconsistent conductivity. Therefore, ITO can be used as either a cathode or anode, but requires a buffer layer for reasonable performance with current active layer materials.

Zinc oxide (ZnO) is an n-type, electron selective material with high conductivity and optical transmittance, making it a frequent choice as an electron transport layer between ITO and the BHJ in inverted organic solar cells. Solution-processing of ZnO using a zinc acetate sol-gel was introduced to improve cost and scalability of devices, and successfully resulted in robust and environmentally stable films with good crystallinity.[12–14] The size of crystalline domains, and hence the electronic properties of the material, were further increased by high temperature annealing (300 °C), though this hinders future high-throughput reel-to-reel manufacturing of these devices. More recently, the use of a diethyl zinc precursor allowed for low-temperature annealing (120 °C) and was shown to increase long-term device stability

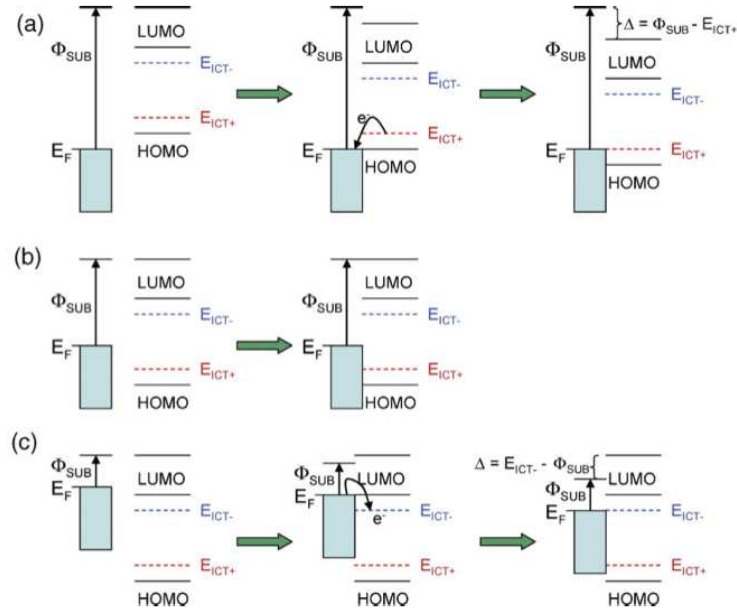


Figure 1.6: Pinning of the Fermi-level of a surface to the BHJ integer charge transfer (ICT) states when a) $\phi_{\text{SUB}} > E_{\text{ICT}+}$: Fermi-level pinning to $E_{\text{ICT}+}$, b) $E_{\text{ICT}-} < \phi_{\text{SUB}} < E_{\text{ICT}+}$: no pinning, c) $\phi_{\text{SUB}} < E_{\text{ICT}-}$: Fermi-level pinning to $E_{\text{ICT}-}$. Reprinted with permission from [1]. Copyright 2009 Wiley-VCH.

versus zinc acetate.[15]

Although ZnO shows promise as an electron transport layer, there is a natural barrier for electron extraction from common fullerene electron acceptors into ZnO. This energetic barrier is the result of the electron affinity of the oxide being significantly smaller than that of the fullerene as shown in Figure 1.7. Changing the work function of the electron transport layer relative to that of the BHJ may decrease the electron extraction barrier, thereby increasing PCE, V_{OC} , FF, and J_{SC} of the device.

1.4 Work Function Modification of Transparent Conducting Oxides

In order to permanently modify the work function of a material, one must modify the material itself. Work function adjustment is viable by a few methods, most notably substitutional doping and surface modification. ITO was developed through tin substitutional doping of indium oxide, though the optimization of optical transmittance and carrier con-

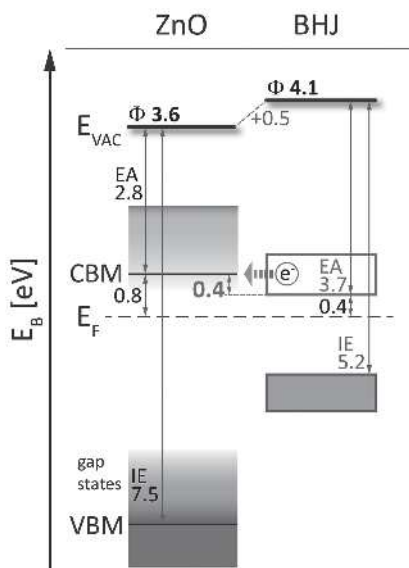


Figure 1.7: Electron extraction barrier of 0.4 eV between the electron affinity of PC₇₁BM and the conduction band minimum (CBM) of ZnO. Reproduced in part with permission from [16]. Copyright 2014 Wiley-VCH.

centration severely limits the allowed percentages of tin,[17] meaning that doping is not a viable strategy for greatly changing the work function of ITO. Doping of other transparent conducting oxides, especially ZnO, has been somewhat successful in shifting the work function of the oxide, as well as improving conductivity and transparency. Aluminum and other group-XIII dopants have been used to move the Fermi level of the oxide toward the conduction band,[18] with gallium earning the most attention as it results in minimal lattice distortion and less oxidation than aluminum.[19] Alternatively, the work function of ZnO can be increased up to 250 meV by substitution of magnesium into the lattice.[20] Doping can therefore be used to tune the work function by varying concentration, though the change is limited as issues of opacity and charge transfer arise at higher dopant concentrations.

Conveniently, surface modification is also an effective method of improving the TCO/BHJ relationship. The goal of surface modification is to form a dipole layer at the surface in order to tune the work function and/or surface energy without affecting the bulk properties of the oxide. This has been demonstrated, for example, through plasma treatments of the surface,

which can change surface stoichiometry and/or defect structure. Another approach, and the one discussed in detail here, introduces a self-assembled monolayer (SAM) of molecules on the TCO surface. On ZnO and ITO, this method has been used with a variety of small molecules, as well as fullerenes and polymers. Fullerene derivatives have been successful in reducing recombination at the electron transport layer/BHJ interface and decreasing contact resistance through improved electronic coupling and alignment.[21–25] Thin films of polymers, while not SAMs, are even more frequently used as anode modifiers, especially PEDOT:PSS on ITO. PEDOT:PSS is a high work function material with sufficient transparency that increases the work function of ITO and thereby improves hole collection. However the high acidity and hygroscopic nature of the material lead to rapid device degradation.[26] With similar function, PFTE (Teflon) has been cited as another possible polymer for modifying the ITO surface.[27]

Meanwhile, SAMs of small molecules can be used to directly shift the work function of a TCO relative to the ICT levels of the bulk heterojunction by forming an interfacial dipole layer on the oxide surface, without affecting the bulk properties of the underlying oxide. The change in work function is actually a change in the vacuum level of the oxide resulting from the perpendicular component of the total interfacial dipole moment. The total dipole moment at the interface is dominated by the intrinsic dipole of the molecule, but the bond dipole resulting from charge redistribution at the attachment site also contributes significantly. In the negative-to-positive pointing dipole convention, if the total interfacial dipole moment points away from the oxide, the work function of the oxide is decreased. Alternatively, if the dipole moment points toward the oxide, the work function increases as a result of modification, as shown in Figure 1.8. The intrinsic dipole moment of the molecule depends on its chemical structure, especially placement of electron donating and withdrawing groups. The bond dipole depends on the attachment group of the molecule: an acidic group protonates the oxide, resulting in a bond dipole pointing toward the surface, while a basic group yields a bond dipole pointing away from the oxide. The surface coverage

and orientation of these molecules also play very influential roles in determining the strength of the total dipole moment, and hence the change in work function.

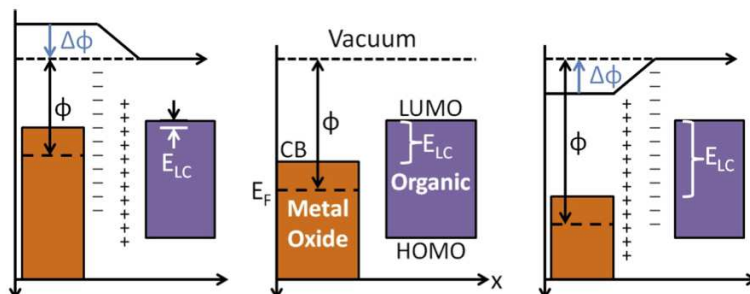


Figure 1.8: Energy level diagram of a metal oxide/BHJ interface with dipolar surface modifiers. The magnitude and direction of the dipole determine the change in vacuum level for the oxide. E_{LC} is the electrostatic potential shift to charges crossing the interface. Reproduced in part from [28] with permission of The Royal Society of Chemistry.

Extensive work has been done to investigate small molecule modification of ZnO for the purpose of improving organic device performance. A wide range of molecules has been employed for various purposes, with largely successful results. One of the simplest molecules studied on ZnO is pyridine, which reduced the work function of ZnO by 2.9 eV through cooperation of the intrinsic and bond dipoles.[29] AFM and XPS studies of functionalized alkenes on ZnO show good packing and coverage, while inducing a small field in the underlying oxide.[30] Succinic acids deposited on ZnO have been shown to tune the height of the Schottky barrier at the ZnO/metal interface, with ZnO showing a greater response to dipole modification than GaAs.[31] ZnO/metal interface modification was further studied with carboxylic acids in standard architecture OPVs, where the dipolar molecules were successful in raising/lowering the work function of ZnO to create Ohmic contact between ZnO and high work function metals.[32, 33] At the interface in ZnO/P3HT bilayer devices, silane and thiol molecules with the same alkyl chains were shown to increase and decrease the work function of ZnO, respectively, and resulted in modulation of the V_{OC} of the device.[34] Mixed monolayers of triethoxysilanes with opposing dipoles were shown to tune the work function of modified ZnO, which produced a corresponding trend in the V_{OC} of inverted BHJ solar

cells.[35] In the same device structure, various dipolar benzoic acids on ZnO raise and lower both the V_{OC} and J_{SC} of the solar cell.[36]

In addition to improving charge transport and energy level alignment in organic devices, small molecule modification affects the surface energy of the modified oxide, which can determine the morphology of the subsequently deposited BHJ. In standard architecture devices, the distribution of BHJ species has been shown to be slightly fullerene rich near the PEDOT:PSS HTL.[37–39] In inverted devices, surface energy of ZnO was shown to change linearly with the surface coverage of alkylsilanes, while work function was stable through the range. By tuning the surface energy for optimal BHJ morphology, the J_{SC} and PCE of the device were increased.[40] Similarly, benzoic acid modified ZnO with higher surface energy caused smaller fullerene aggregates in the adjacent BHJ, which led to increased J_{SC} and FF in devices.[36] Alkanethiols and silanes were also shown to improve π -stacking of the P3HT on modified ZnO in bilayer devices, leading to an increase in J_{SC} . [41]

Compared to the modifiers listed above, phosphonic acids (PAs) have become the frontrunners in small molecule modification of ZnO. Phosphonic acids bind to ZnO via multidentate attachment, with tridentate binding being most energetically favorable.[42–44] Multidentate attachment, shown in Figure 1.9, provides PAs with a distinct advantage over molecules with fewer ligaments, as they form more robust SAMs on ZnO. Compared to thiols, PAs form less uniform layers on ZnO, but withstand rinsing and also cause less etching of the oxide surface.[45] Phosphonic acids also have greater thermal stability and preferentially bind to ZnO when directly compared with thiols.[46] In addition to the issue of carboxylic acids actively etching ZnO,[47] dually functionalized carboxyl alkyl phosphonic acids were shown to preferentially bind to ZnO via the phosphonic acid group with increasing alkyl chain length.[48]

Phosphonic acids are also effective in tuning the work function of ZnO through a range of over 1eV by using various aromatic groups to change the molecular dipole moment.[16, 43, 49] The modulation of the work function of ZnO at the BHJ interface was exploited in increasing

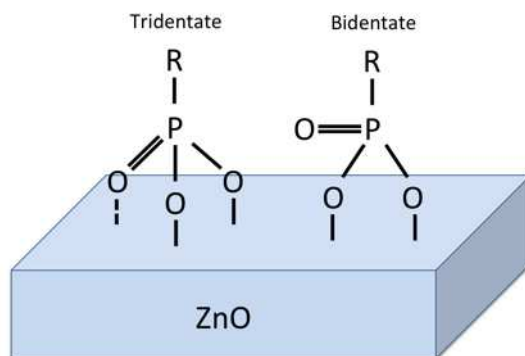


Figure 1.9: Bidentate and tridentate attachment of phosphonic acids to zinc sites on ZnO.

the V_{OC} and PCE of an inverted solar cell.[15, 16] Furthermore, PA modification of ZnO in the inverted BHJ device increases long-term stability by passivating interstitial Zn defects on the oxide surface.[15] Phosphonic acids bind quickly to ZnO, enabling spin-coating or even spray coating to further minimize etching effects.[50] A possible disadvantage for PAs on ZnO is that the acidic nature of the attachment group leads to a bond dipole pointing toward the oxide and increasing the work function. This is undesirable in inverted BHJ devices where the work function of ZnO must be lowered, so it is necessary to have a strong aromatic group with a dipole moment pointing away from the surface that is sufficiently large to overcome the bond dipole moment. However the fast multidentate attachment along with minimal etching, increased device stability, and work function tunability still make PAs one of the best choices for modifying ZnO.

While phosphonic acid modification of TCOs has become a model system for solar cell improvement, the way in which device characteristics are affected has not been made clear. Often when a change in V_{OC} is expected, the J_{SC} is also affected. Since charge extraction efficiency directly impacts the J_{SC} , the electric field in the device is suspected to change with interlayer dipole modification. Therefore measuring the potential distribution within phosphonic acid modified solar cells would better our understanding of the mechanism behind device improvement in these devices.

1.5 Potential Distribution in Organic Photovoltaics

Previous attempts have been made to measure the electric potential distribution in OPV devices, which is not trivially calculated due to the BHJ structure of the active layer. It is important to pursue study of the electric field distribution in organic solar cells as this may influence the charge collection and hence photocurrent of the device. A few models have been suggested to represent the band structure of OPV devices, including MIM, expanded p-n junction, and Schottky models.[51, 52] The use of interlayers increases the complexity of the system, but potential mapping of OPV device cross-sections has still been aimed at determining the proper system for describing the energy levels. The primary difference in these models is the location of the electric field. In the MIM model, the BHJ is considered as a single material with uniform electric field resulting from the work function difference between the electrodes. The expanded p-n junction treats the interface of the two active layer species (the donor and acceptor making up the BHJ) as a depletion layer. In an evenly doped BHJ, this is equivalent to a uniform electric field in the active layer, as for the MIM model. The Schottky junction model treats the BHJ as an evenly doped semiconductor that in contact with a metal electrode forms a Schottky barrier. Therefore the Schottky model is associated with a large field-free region in the active layer, with the contact layer interfaces hosting the electric field. The electric field has been cited as critically important to charge carrier extraction due to the limitations on carrier mobility and lifetime,[52–54] however some suggest that the internal field has very little impact on device operation.[55]

Electric field distribution has been studied in a handful of organic solar cell structures, but common methods extract the field profile indirectly.[56] Calculating the potential distribution in an organic bulk heterojunction device from such measurements is fundamentally difficult due to the mixed electron donating and accepting groups in the active layer (compared to a bilayer device). Studies using time-of-flight measurements,[57] light intensity photocurrent measurements,[58, 59] nonlinear optical microscopy,[56] and impedance spectroscopy[60, 61] have speculated on the electric field distribution in organic bulk heterojunction devices,

with most concluding Schottky diode behavior and diffusion-dominated charge transport in the device. With the exception of the optical microscopy, these measurements are indirect and require interpretation to achieve this result. Nonlinear optical microscopy requires lateral device architecture for transmission, which does not reflect normal device structure or operation.

Alternatively, the potential distribution across the operational device structure can be directly measured via cross-sectional scanning Kelvin probe microscopy (X-SKPM). X-SKPM measurements may be performed on a device that is in short circuit condition, or that is biased at some voltage. Short circuit conditions allow for measurement of the local vacuum level shifts across a device, which grants direct comparison of work functions for each of the layers. Few studies have used SKPM in unbiased conditions to map the topography and work function of polymer:fullerene films in the dark and under illumination.[62–65] Biased conditions on a device cross-section reflect device operation, and by subtracting the short circuit condition from the biased conditions, only direct effects of the applied bias may be seen.[66] This method has been used to identify charge transport barriers from potential drops in the device cross-section.

Saive et al. identify the X-SKPM measured distribution of relative potential in a device as primarily affected by vertical species separation within the BHJ, and by charge injection/extraction barriers at the electrodes.[66] Some X-SKPM studies have seen a large potential drop at the cathode of OPV BHJ devices. A theory is that a p-n junction forms between the p-type BHJ and a small layer of the BHJ at the cathode interface, which is n-doped by electron injection from the ETL. This potential drop near the cathode, along with the near-zero field through the majority of the BHJ, may indicate that BHJ devices primarily exhibit expanded p-n junction behavior.[51, 52, 67] However, potential drops at the interfaces of transport layers and the BHJ have also been attributed to charge transport barriers between these materials.[66]

X-SKPM presents is not without limitations, as the exposure of a device cross-section may cause unintentional doping or defects on the exposed surface. Although a few studies of X-SKPM on OPV devices have already been published and sample preparation has been well documented,[68] no previous reports have validated the technique on these materials in air. Because both sample cleaving and measurement have been commonly performed in air, it is necessary to prove the reliability of this measurement technique on the device surface in ambient conditions. These issues are further discussed below.

1.6 Experimental Techniques

The experimental techniques used in this work focus on identifying the effectiveness of conjugated phosphonic acids for increasing organic solar cell efficiency. Electronic consequences and attachment of conjugated phosphonic acids on TCOs are measured, and the applied potential distribution within device structures is mapped. In addition to fabricating and directly measuring the diode characteristics of devices, these methods aim to reveal the underlying mechanisms for improving device performance.

1.6.1 Solar Cell Processing and Characterization

Device processing is a major part of determining whether surface treatments are successful in improving the efficiency of organic electronics. While we have other methods of measuring the direct effect of molecular dipoles on the work function of modified oxides, these do not always indicate if a device will be successful, as other factors such as surface energy and film quality play major roles in the performance of organic photovoltaics.

Fabrication techniques for organic photovoltaic devices in this thesis include spin-casting, annealing, and thermal evaporation, which will take place in ambient, nitrogen, and high vacuum conditions as required for optimal performance. Spin-casting is employed due to its quick and consistent results in depositing oxides, molecular monolayers, and bulk heterojunction active layers from solutions of various types and viscosities. The spin speed is optimized based on the wetting properties of the solution and the desired thickness of the resulting

layer. This method may be performed in either air or nitrogen environments, furthering the variety of layers that may be applied in this way. Thermal evaporation is also advantageous for organic device processing, as it allows for deposition of oxides and metals in high vacuum conditions on top of other device layers. The use of this procedure prevents damage to the existing device structure, while providing reliable application of several different electrode materials.

Organic photovoltaics are processable in two architectures, namely standard and inverted. In a standard architecture device, light is passed through the hole-collecting contact materials, usually ITO and PEDOT:PSS, to reach the active layer. However, it is the electron-collecting contact materials, ITO and ZnO in this study, on the illuminated side of the inverted device. The work in this thesis includes both architectures to demonstrate how the potential distribution changes as a result of different transport materials, and the inverted device will be modified with phosphonic acids. Each device structure will contain a bulk heterojunction active layer, consisting of a polymer fullerene blend. The bulk heterojunction that will be used is P3HT:ICBA, a well-known system with relatively high device efficiency, depending on the contacts.

As this study will focus on the interaction of the bulk heterojunction with the charge transfer materials, the processing and quality of the oxides used for these layers are of particular importance. Indium tin oxide is commonly used as a hole transport layer in standard architecture devices, as well as a cathode in inverted devices. The ITO used here has been purchased patterned on glass slides. Zinc oxide, an electron transport layer in inverted devices, is deposited from a solution of diethyl zinc in tetrahydrofuran and then annealed in air to grow the oxide. This procedure produces thin, high quality, robust films that are easily modified. Molybdenum oxide is thermally evaporated onto active layers to act as a transport layer, and aluminum and silver are also applied as electrodes via thermal evaporation.

In order to compare the effects of various modifiers in organic photovoltaics, the devices must be measured accurately. A home-built solar simulator in a nitrogen environment is employed for this purpose. In this system, devices are masked to eliminate current bleed from outside the device area. Additionally, devices may be light-soaked and measured both with and without illumination. By sweeping the applied bias, the system allows for examination of the diode characteristics of each device such as open circuit voltage, short circuit current, fill factor, power conversion efficiency, shunt resistance, and series resistance. An additional solar simulator system in air provides the capability to measure partial devices after cleaving and exposure of the cross-section.

1.6.2 Kelvin Probe

A Kelvin probe measures the contact potential difference (CPD) between a probe and sample, operating on the basic principle of capacitance. The CPD is the difference in work function between the probe and sample. Placing the tip and sample in electrical contact forces their Fermi levels into alignment, so the CPD is equal to the change in vacuum level. This difference results in a force between the tip and sample, which can be negated by applying a voltage to the probe equal to the CPD. The CPD provides a relative work function measurement, so a known and stable reference must be used in order to determine the absolute work function of a sample. In this work we are concerned with relative work functions whereby measuring both modified and unmodified substrates, the effect of a molecular dipole may be determined from the difference in their CPDs. The surface-sensitivity of the measurement is convenient for the work presented here, as phosphonic acids don't change the bulk work function of a material, but Kelvin probe can still measure the change in effective work function of the modified oxides.

Kelvin probe measurements have been performed with a KPTechnology SKP/SVP/LE 450 system. The sample surface is grounded, while voltage is applied at the Kelvin probe tip during measurement. It is crucial for the sample to be conductive, or to be deposited on a conductive substrate to avoid charging effects due to poor grounding during measure-

ment. However, the Kelvin probe has been shown to be reliable as compared to ultraviolet photoelectron spectroscopy measurements of work function.

1.6.3 Fourier-Transform Infrared Spectroscopy (FTIR)

Fourier-transform infrared spectroscopy uses infrared radiation transmitted through a sample to determine which bonds are present in a sample. A range of infrared frequencies are collected simultaneously, and the transmitted sample signal is resolved by Fourier transform. The sample spectrum is compared with a background spectrum, usually from a blank or unmodified substrate. Here FTIR is employed to determine how phosphonic acids attach to the zinc oxide surface to determine whether the linkage inside the molecule affects binding characteristics.

The frequencies of peaks returned in a background-corrected absorption spectrum are matched with known vibrational and stretching modes of molecular and surface bonds. Many compounds oscillate at unique frequencies, corresponding to absorption of a very small and consistent fraction of the infrared spectrum. The amplitude, width, and position of the absorption peaks can change as a result of the concentration, orientation, and strength of the bonds. In this work, absorption information is used to determine the attachment and orientation of phosphonic acids on ZnO.

The FTIR spectroscopy in this work was performed on a Thermo Scientific Nicolet 6700 FT-IR Spectrometer with liquid nitrogen cooled Hg-Cd-Te detector and KBr beam splitter. Transmission measurements were taken for samples on polished silicon wafers, with ZnO and modifiers deposited on one side of the wafer. The background transmission measurement was of ZnO on silicon without the modifier. The measurement environment was purged with nitrogen to reduce water and carbon dioxide, which also absorb infrared wavelengths. This technique will allow us to not only confirm the attachment of ZnO modifiers, but also estimate surface coverage and identify binding characteristics of these molecules.

1.6.4 Atomic Force Microscopy (AFM)

AFM uses a macroscopic cantilever with a tiny tip that extends toward the sample. The van der Waals interaction of the tip with the sample causes deflection of the cantilever, which is measured by a laser and position-sensitive photodiode. In contact mode, the movement of the AFM tip contours the surface of the sample. A less destructive method is tapping mode, in which the cantilever is driven with an alternating current (AC) voltage at its resonant frequency to oscillate the tip perpendicular to the sample surface, and a feedback loop is used to maintain constant amplitude of the tip oscillation while contouring the sample. This method is ideal for performing AFM on soft organic materials such as bulk heterojunction solar cells to reduce sample destruction.

1.6.5 Cross-Sectional Scanning Kelvin Probe Microscopy (X-SKPM)

Scanning Kelvin probe microscopy is an advanced AFM technique that measures the local CPD between a conducting AFM tip and a sample surface. In this specific setup, tapping mode AFM is used to image both surface topography and potential simultaneously. In addition to the AC voltage required for tapping mode, the cantilever is driven with a second AC modulation, as well as a direct current (DC) voltage to match the local CPD of the tip and sample. This causes a capacitive force between the tip and sample with constant, ω , and 2ω components, where ω is the modulating frequency. When the DC voltage is equal to the CPD, the force of oscillation at frequency ω is zero (while the force at 2ω is nonzero). Therefore by adjusting the DC voltage to eliminate cantilever oscillation at the driving frequency, the CPD is determined from the DC input. This allows for simultaneous mapping of the CPD and topography of a sample.

SKPM measurements of topography and potential are the convolution of tip and sample features. In order to use this method for mapping the potential distribution in a device, we must break our samples to expose the cross-section and scan across the layers of the solar cell. A diagram of the setup is shown in Figure 1.10. The tip used in X-SKPM may be

large compared to some features in the sample, so the interaction of the two includes large areas of both. Topographically this results in smoothing or sharpening of sample features, while the CPD measurement may be an average of the local area. Also, the interaction of the cantilever with the sample consistently results in a measured CPD lower than the actual value. Due to these factors, the lateral resolution of SKPM is approximately 30-50 nm, while the electronic resolution is around 30 mV. X-SKPM is employed to map the cross-sectional topography, phase, and CPD of organic solar cells.

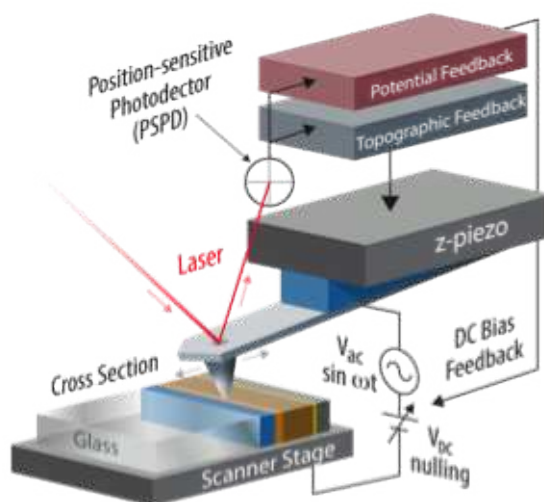


Figure 1.10: Diagram of cross-sectional scanning Kelvin probe microscopy of a photovoltaic device. Adapted with permission from [69]. Copyright 2015 American Chemical Society.

The method used to cleave, mount, and wire the device cross-section allows for an applied bias across the device structure during cross-sectional imaging. Under short circuit conditions, the CPD map of a device shows the change in work function across the device structure. Applying bias across the device changes the CPD across the device. At the point at which bias is applied, the CPD should change by the applied voltage. At the point at which the device is grounded, the CPD should be the same as for the short circuit case. Intermediate points should show CPD changing between these values. The shape of the CPD across the device has several implications about device performance, including charge injection and extraction barriers, doping, and surface effects. The latter is of particular

concern since X-SKPM is performed on an exposed device cross-section, and may not truly reflect bulk device operation. For example, X-SKPM measurements of device cross-sections at applied bias do not show the full applied voltage difference in the CPDs of the electrodes. Therefore surface defects and cantilever convolution are suspected as major players in CPD mapping of device cross-sections.

One way to ensure accuracy of potential mapping is to measure the CPD at various biases, including +0.0 V (short circuit), so that the potential images at nonzero bias may be corrected by subtracting the zero bias potential.[66] This relative potential is useful for determining if a CPD feature is topographic and how the device responds to only applied bias (less work function changes). The electric potential may also be differentiated to obtain the electric field through the device.

Device cleaving, mounting, and wiring were performed in a nitrogen-purged glovebox. This was followed by initial X-SKPM measurements in nitrogen (As Fabricated) and subsequent testing in air. The device was then annealed in nitrogen and re-measured in this system (Annealed), followed by testing in air. Next, X-SKPM was performed in air (Ambient), and the device was tested afterward. The device was measured a final time in the nitrogen X-SKPM system (Post-Ambient), and again tested in air. By this systematic methodology, we investigate the effect of air exposure, interlayer materials, and transparent conductive oxide modifiers on the work function, electric potential, and electric field distribution across an active device. X-SKPM is conducted on a Veeco 5000 AFM housed in nitrogen, as well as a Park Instrument XE-70 AFM in air.

CHAPTER 2
CONJUGATED PHOSPHONIC ACID MODIFIED ZINC OXIDE ELECTRON
TRANSPORT LAYERS FOR IMPROVED PERFORMANCE IN ORGANIC SOLAR
CELLS

Reproduced with permission from *ACS Applied Materials and Interfaces*, 2014, 6 (21), pp
19229–19234. Copyright 2014 American Chemical Society.

Jennifer L. Braid^{1,2}, *Unsal Koldemir*³, *Alan Sellinger*^{2,3}, *Reuben T. Collins*¹, *Thomas E.
Furtak*¹, *Dana C. Olson*²

Attributions: JLB wrote the manuscript, prepared samples and conducted FTIR and Kelvin probe measurements, and fabricated and tested solar cells. UK synthesized the phosphonic acids and performed NMR.

Abstract: Phosphonic acid modification of zinc oxide (ZnO) electron transport layers in inverted P3HT:ICBA solar cells was studied to determine the effect of conjugated linkages between the aromatic and phosphonic acid attachment groups. For example, zinc oxide treated with 2,6-difluorophenylvinylphosphonic acid, having a conjugated vinyl group connecting the aromatic moiety to the phosphonic acid group, showed a 0.78 eV decrease in the effective work function versus un-modified ZnO, while non-conjugated 2,6-difluorophenylethylphosphonic acid resulted in a 0.57 eV decrease, as measured by Kelvin probe. This resulted in an average power conversion efficiency of 5.89% for conjugated 2,6-difluorophenylvinylphosphonic acid modified solar cells, an improvement over un-modified (5.24%) and non-conjugated phosphonic acid modified devices (5.64%), indicating the importance of the conjugated linkage.

¹Department of Physics, Colorado School of Mines, Golden, Colorado, 80401, USA

²National Renewable Energy Laboratory, Golden, Colorado 80401, USA

³Department of Chemistry and Geochemistry, Colorado School of Mines, Golden, Colorado, 80401, USA

2.1 Introduction

Organic photovoltaics are a viable source of scalable, renewable energy due to their potentially low cost, lightweight, low temperature, and high throughput manufacturing. Single junction power conversion efficiencies have recently reached 9.2% for polymer:fullerene cells,[70] with tandem polymer device efficiency having already surpassed 10%.[71] These bulk heterojunction cells can be prepared by two architectures, namely traditional and inverted. The traditional architecture in an organic solar cell generally uses PEDOT:PSS as a hole transport layer with a transparent electrode, indium tin oxide (ITO), that collects the holes. Inverted devices, on the other hand, use an electron transport layer, such as ZnO, thereby employing ITO to collect electrons. As such, the inverted device architecture avoids stability problems associated with both the PEDOT:PSS/ITO interface, as well as diffusion of water and oxygen into the low work function anode, usually Al or Ca/Al for traditional devices.[12] Thus, inverted devices have led to increased device stability and performance and therefore longer lifetimes, especially with the introduction of ZnO as a charge-selective interlayer.[14, 26]

As an electron transport layer, ZnO has been commonly used due to its electron selectivity, ease of thin film formation by a variety of deposition methods, high electron mobility, good transparency, earth abundance, and low cost.[16, 35, 36, 43, 44, 50] It is worth noting that any mismatch between the Fermi level of ZnO and the electron transport level of the active layer may result in energy loss during charge extraction.[16, 72] Due to this energy loss, quasi-Fermi level matching between the active layer and the charge transport layers has become an important attribute in maximizing efficiency in organic hybrid photovoltaics. Adjusting the alignment of the effective work function of charge transport layers to the charge transport levels of the active layer has been shown to influence the efficiency of charge extraction and the open circuit voltage of bulk heterojunction solar cells,[16, 35, 36, 72–75] as well as charge injection in organic light emitting diodes.[1, 76–78]

In this context, a molecular dipolar surface modifier may be used to alter the alignment of the effective work function of ZnO relative to the lowest unoccupied molecular orbital (LUMO) of the electron acceptor material at the BHJ interface, without changing the intrinsic Fermi level or carrier density of the bulk oxide. Better energy alignment at the interface reduces the energy lost during electron extraction/injection, increasing the open circuit voltage, the built-in field, and thereby the fill factor of the device.[16, 35, 36, 72, 79] The relationship between the work function of the contact and open circuit voltage has also been shown on ITO in standard architecture devices.[74, 75]

Changes in the effective work function of a surface modified with a molecular dipole can result from the change in vacuum level and the bond dipole created by the surface bond.[49, 74, 80–82] The change in the vacuum level across the monolayer itself is defined to be proportional to the component of the molecular dipole moment perpendicular to the surface. Therefore, the influence of a molecular dipolar surface modifier on effective work function is divided into two contributions: (i) the dipole of the molecular monolayer along the surface normal, and (ii) the interfacial dipole created by charge redistribution due to the surface bond. As molecular dipolar surface modifiers, benzylphosphonic acids have shown promise; effectively increasing or decreasing the work function of various transparent conductive oxides, including ITO,[50, 74, 75, 77, 79, 81, 83, 84] GZO,[49] and ZnO,[16, 50] by up to 1 eV depending on the orientation and strength of the molecular dipole. Recently, benzylphosphonic acids with various head groups, and therefore different dipole moments, have been used to alter the work function of the modified oxide by shifting the vacuum level of the oxide (i), while the bond dipole (ii) remains relatively constant.[16, 74, 75, 79, 83]

Orthodifluorobenzylphosphonic acid (oF₂BPA), which has been investigated previously,[16, 43, 49, 74, 75, 79, 81, 83, 85] decreases the work function of zinc oxide, and is shown to increase the open circuit voltage in inverted architecture devices.[16] In this study, we introduce two small polar phosphonic acids with the same attachment and head groups as oF₂BPA, but different linkages connecting the two moieties (Figure 2.1). Specifically, we utilize a

conjugated trans double bond as a linker between the aromatic ring and the phosphonic acid group in 2,6-orthodifluorophenylvinylphosphonic acid (oF₂PVPA), and compare it with the non-conjugated orthodifluorophenylethylphosphonic acid (oF₂PEPA), having a saturated ethyl linkage. These molecules, having similar lengths and molecular dipole moments should therefore have similar effects on the vacuum level of ZnO. However, the different linkages may allow for variation in the bond dipole through direct conjugation with the acid binding group.

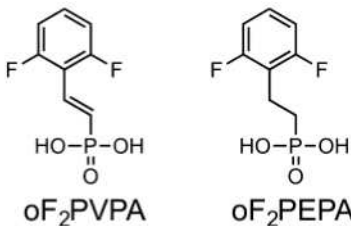


Figure 2.1: Two phosphonic acids used in this study: orthodifluorophenylethylphosphonic acid (oF₂PEPA), and orthodifluorophenylvinylphosphonic acid (oF₂PVPA).

A double bond between two carbon atoms allows for delocalization of the associated π -electrons of the aromatic ring into the phosphonic acid attachment group, potentially facilitating a change in the molecular dipole as well as improved charge transport between the molecule and the oxide. We hypothesized that the introduction of the conjugated double bond would increase the electron charge redistribution at the interface, increase the bond dipole, and accentuate the shift in work function. Our results show the conjugated oF₂PVPA does outperform the non-conjugated analogue, oF₂PEPA, in modification of the effective work function of zinc oxide by 0.21 mV. The conjugated linkage led not only to an improvement in work function, but also to increased open circuit voltage, short circuit current, and power conversion efficiency (PCE) of devices compared to the non-conjugated modifier. Overall the PCE was increased by over 12% versus the un-modified ZnO interface (5.89 vs. 5.24%). Infrared spectroscopic characterization of these phosphonic acids on ZnO indicates that they bind in a bidentate and/or tridentate fashion, with similar surface

coverage.

2.2 Results and Discussion

Synthesis of oF₂PEPA, oF₂PVPA. The conjugated orthodifluorophenylvinylphosphonic acid (oF₂PVPA) and non-conjugated orthodifluorophenylethylphosphonic acid (oF₂PEPA) were synthesized as shown in Figure 2.2, with all synthetic details outlined in the Experimental Methods section. Preparation of oF₂PVPA was achieved via Heck coupling between 2,6-difluoroiodobenzene (**1**) and diethyl vinylphosphonate using Herrmann's palladacycle in 66% yield. As Heck coupling is more prevalent for styrenyl and acrylate based systems, performing this on vinylphosphonates is not very common and required careful experimental optimization. The intermediate vinyl bridged compound (**2**) was used to prepare both the oF₂PVPA and oF₂PEPA. The oF₂PVPA was prepared via deprotection of the vinyl bridged phosphonic ester using a combination of trimethylsilyl bromide/potassium iodide (TMSBr/KI) in acetonitrile (ACN). In the case of oF₂PEPA, the vinyl group was hydrogenated using triethyl silane (TES) as a hydrogen source over Pd/C catalyst under mild conditions to afford the ester precursor (**3**) in 67% yield. The desired oF₂PVPA and oF₂PEPA phosphonic acid products were obtained in 48 and 42% yield, respectively.

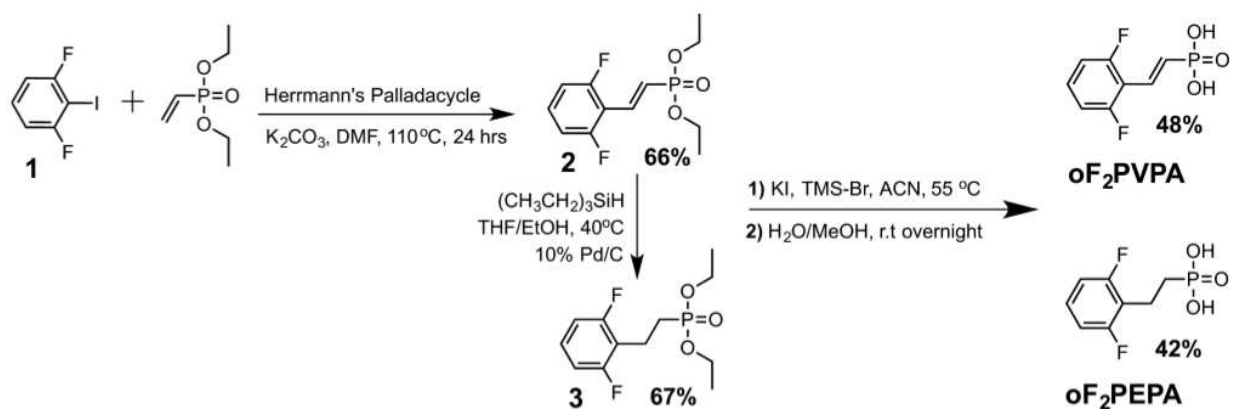


Figure 2.2: Synthetic Preparation of the Conjugated Orthodifluorophenylvinylphosphonic Acid (oF₂PVPA) and Nonconjugated Orthodifluorophenylethylphosphonic acid (oF₂PEPA)

Binding Characteristics on Zinc Oxide. The oF₂PVPA and oF₂PEPA are spin-cast via ethanol solutions onto zinc oxide that had been deposited from a dilute solution of diethyl zinc in a toluene/tetrahydrofuran solvent mixture. After spin-casting, the films are annealed at 120 °C and rinsed with ethanol to ensure monolayer or sub-monolayer coverage of the respective phosphonic acids. Next, we performed Fourier-transform infrared spectroscopy (FTIR) to identify the vibrational fingerprints of these molecules bonded to zinc oxide, which allows us to verify attachment as well as compare the surface coverage and binding configurations of these modifiers.

As may be seen in Figure 2.3, the region of 900-1300 cm⁻¹ contains several characteristic vibrations of the P=O and P-O-(H) terminations. Due to similar feature sizes across the FTIR spectra, we infer that the surface coverage is roughly equal for both molecules. The peaks at ~1000 and 1070 cm⁻¹ for both oF₂PEPA and oF₂PVPA, shown in region A, are associated with symmetric and asymmetric P-O stretching in PO₃²⁻, respectively.[86, 87] This indicates fully deprotonated phosphonic acids, bonded to Zn sites with both P-O-(H) ligaments. The lack of features at 925 and 940 cm⁻¹, normally attributed to P-O-H stretching,[88] points to few or no unattached P-O-H ligaments. Also absent is a large band centered at 1230 cm⁻¹, which would signify unbound P=O terminations.[44] Instead, we find smaller features in 1130-1300 cm⁻¹, labeled region B. Peaks in this region could represent $\nu(\text{PO}_2^-)$ stretching vibrations associated with one bound and one free P-O-H ligament,[87] though we should also see free P-O-H signatures at 925 and 940 cm⁻¹ with this mode. Therefore we suspect that the peaks between 1130 and 1300 cm⁻¹ are P-O-Zn and P=O-Zn vibrations, expected between 1160 and 1230 cm⁻¹. [87] Since these modes are known to shift with electron affinity, we credit the variation in peak position to the change in linkage between these molecules, because of delocalization of the π -electrons of the aromatic ring. Specifically, we suspect the pair of peaks in the oF₂PEPA spectrum at 1140 and 1160 cm⁻¹ is shifted to higher energies (1200 and 1225 cm⁻¹) for oF₂PVPA due to the conjugation. However some of the features in region B could belong to unbound P=O ligaments,[48] shifted

by P-O-(H) terminations binding to Zn sites and different linkages within the phosphonic acids, suggesting the possibility of some unbound P=O terminations. We conclude that both oF₂PVPA and oF₂PEPA bind to ZnO via multidentate attachment, most likely a mixture of bidentate and tridentate configurations.

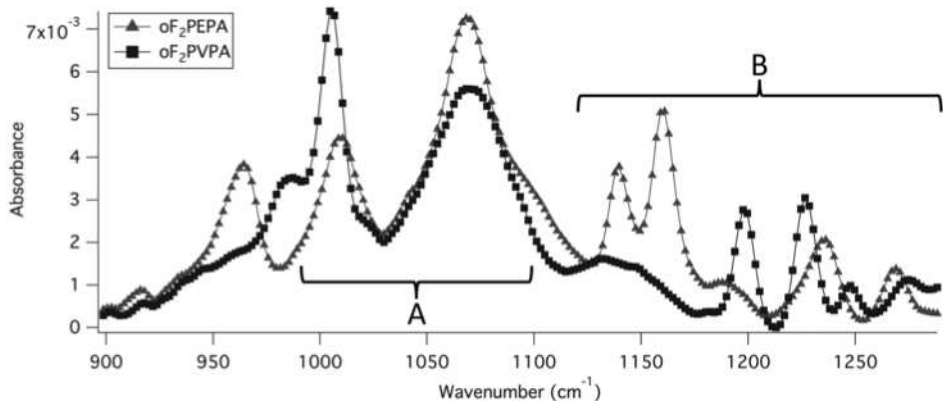


Figure 2.3: FTIR spectra for oF₂PEPA and oF₂PVPA bonded to ZnO. Region A, 990-1100 cm⁻¹, contains stretching modes of PO₃²⁻. Region B, 1125-1300 cm⁻¹, shows P-O-Zn and P=O-Zn vibrations, and may exhibit free P=O signatures for both molecules.

Work Function Modification and Device Results. After confirming the attachment of these phosphonic acids on zinc oxide, work function measurements of treated and untreated zinc oxide were performed with a Kelvin probe setup at ambient conditions to determine the extent of change in work function as shown in Table 2.1. We observed a large shift in the effective work function of zinc oxide when modified with each phosphonic acid, with conjugated oF₂PVPA decreasing the work function by 0.78 eV, a 0.21 eV greater change versus the similarly sized oF₂PEPA. We attribute the enhanced shift in work function for zinc oxide modified with oF₂PVPA over oF₂PEPA to better charge delocalization between oF₂PVPA and ZnO via the π -electrons of the conjugated linkage.

Changing the linkage within our phosphonic acid would have some effect on the intrinsic dipole moment of the molecule, but it may also alter the bond dipole created at the phosphonic acid/oxide interface. We see a larger change in the work function of ZnO modified with oF₂PVPA versus oF₂PEPA, which lacks conjugation in its linkage. The conjugation likely

improves the change in work function in two ways: (i) a larger molecular dipole moment, and (ii) a larger bond dipole contribution, both resulting from the delocalized π -electrons in the aromatic ring having better communication with the bonding phosphonic acid through the vinyl linkage.

Finally, inverted architecture devices were fabricated on ITO-patterned glass substrates. The ZnO electron transport layer was deposited from the diethyl zinc solution, onto which phosphonic acid modifiers were spin-cast. These films were then annealed at 120 °C to promote binding, and rinsed with ethanol to remove unbound species and promote mono-layer coverage of phosphonic acids. P3HT:ICBA bulk heterojunction active layers were subsequently spin-cast and slow-dried, followed by thermal evaporation of the MoO₃ hole transport layer and the Ag cathode. The solar cell device parameters are summarized in Table 2.1, and J-V curves are presented in Figure 2.4. At first glance, we observe a systematic increase in the open circuit voltage, due to the decrease in effective work function for oF₂PEPA and oF₂PVPA-modified ZnO. The sub-unity relation between change in V_{OC} and work function shift has been previously attributed to Fermi-level pinning as the oxide work function approaches the LUMO level of the BHJ.[1, 9, 35, 89]

The short circuit current was also improved for oF₂PVPA versus the control device and non-conjugated oF₂PEPA. This agrees with the prediction of improved energy level alignment at the BHJ/ETL interface and a resulting increase in the electron transfer rate. The boost in fill factor from 69.1% for the unmodified device to 71.7% for oF₂PEPA and 71.6% for oF₂PVPA is the result of reduced recombination associated with the change in effective work function of the ZnO contact and a corresponding increase in the electric field across the active layer. Additionally, the shunt resistance (R_{SH}) is improved with modification by both oF₂PEPA and oF₂PVPA, signifying that these modifiers may inhibit leakage current in reverse bias. Since low R_{SH} can result in a decrease in V_{OC}, the effect of these modifiers on leakage current may also be contributing to the improved open circuit voltage of the PA-modified devices. However, the modifiers also increase the series resistance (R_{SE}) of the

device, which may explain why fill factor did not further improve for the oF₂PVPA-modified device.±

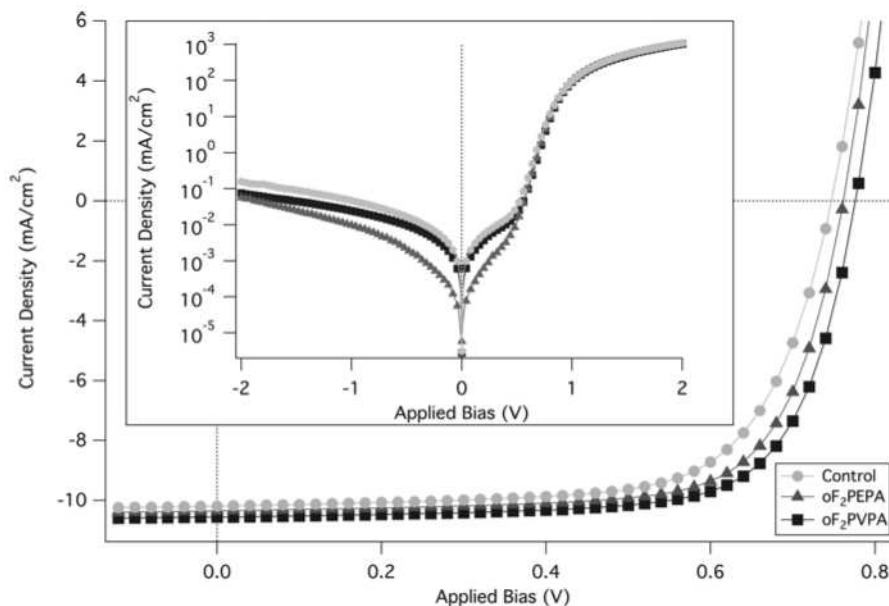


Figure 2.4: Average J-V characteristics for PA modified ZnO devices under illumination. The inset shows average J-V characteristics in the dark on a semi-log scale. (Corresponding parameters in Table 2.1)

2.3 Conclusions

Zinc oxide modified with 2,6-difluorophenylvinylphosphonic acid (oF₂PVPA) measured with Kelvin probe showed a 0.78 eV decrease in the effective work function compared to unmodified ZnO, while non-conjugated 2,6-difluorophenylethylphosphonic acid (oF₂PEPA) decreased the effective work function of ZnO by only 0.57 eV. Inverted P3HT:ICBA solar cells modified with the conjugated oF₂PVPA improved both open circuit voltage and power conversion efficiency over oF₂PEPA, and showed a 40 mV boost in open circuit voltage and increased power conversion efficiency over unmodified solar cells. Through FTIR characterization, the attachment of these molecules was found to be predominantly bidentate/tridentate to ZnO, and the conjugated linkage is shown to affect binding energy. That this conjugated linkage dramatically accentuates the effect of the molecule on the work func-

Table 2.1: Work function of PA modified ZnO and corresponding average device results

	$\Delta\phi$ (eV)	V_{OC} (V)	J_{SC} (mA/cm ²)	FF (%)	PCE (%)	R_{SH} (k Ω)	R_{SE} (Ω)
ZnO	-	0.74 \pm 0.01	10.19 \pm 0.13	69.1 \pm 0.8	5.24 \pm 0.05	158 \pm 2	18.7 \pm 0.1
oF ₂ PEPA	0.57 \pm 0.01	0.76 \pm 0.01	10.35 \pm 0.14	71.7 \pm 0.2	5.64 \pm 0.09	369 \pm 7	17.7 \pm 0.1
oF ₂ PVPA	0.78 \pm 0.01	0.78 \pm 0.01	10.55 \pm 0.12	71.6 \pm 0.3	5.89 \pm 0.04	344 \pm 4	20.3 \pm 0.3

tion of the modified surface shows it to be an interesting approach in improving quasi-Fermi level alignment in organic photovoltaics. An important finding was that the open circuit voltage of modified devices was shifted by a much smaller, but dependent amount to the change in work function, as is common in this type of device. Furthermore, the simple synthesis of conjugated molecules from commercially available precursors makes this type of linkage extremely viable for continued study with other types dipolar molecules on various contact surfaces for use in organic hybrid electronics.

2.4 Experimental Methods

Synthesis of oF2PVPA, oF2PEPA. Diethyl (E)-(2,6-difluorostyryl)phosphonate (oF₂PVPA):[90] A 100 mL Schlenk flask was charged with the aromatic halide (1 equiv.), diethyl vinyl phosphonate (1 equiv.) Herrmann's catalyst (2 mol %) potassium carbonate (1 equiv.) and 20 mL of anhydrous dimethylformamide. The reaction mixture was heated to 110 °C for 24 h under argon. After cooling to room temperature, water (100 mL) was added and the mixture was stirred for 30 min. The organic layers were extracted with dichloromethane (100 mL) three times and dried over magnesium sulfate. Then, the solvent was evaporated under vacuum resulting in the yellow oil crude product. The product was obtained after purification by column chromatography eluting with petroleum ether: ethyl acetate (1:1). Start with 1g (4.16 mmol) of 1,3-difluoro-2-iodobenzene. The product was obtained 0.76 g (66%) of a yellow oil. ¹H NMR (500 MHz, CDCl₃): δ = 7.48-7.57 (dd, 1H, J = 20 Hz), 7.24-7.31 (m, 1H), 6.88-6.92 (m, 2H), 6.59 (t, 1H, J = 20 Hz), 4.12 (t, 4H, J = 10 Hz), 1.31-1.35 (m, 6H). ¹³C NMR (125 MHz, CDCl₃) δ = 162.53, 160.56, 134.81, 131.20, 129.19, 120.70, 111.99, 111.78, 62.02, 16.43.

Diethyl (2,6-Difluorophenethyl)phosphonate (oF₂PEPE):[91] A 100 mL oven-dried Schlenk flask was charged with diethyl (E)-(2,6-difluorostyryl)phosphonate (0.9 g, 3.25 mmol), 10% Pd/C (0.11 mg), anhydrous THF (15 mL) and anhydrous ethanol (2 mL). To this mixture, triethylsilane (3.78 g, 5.22 mL, 32.5 mmol) was added dropwise. After bubbling was quenched, the reaction was heated to 40 °C for 4 h. After cooling to room temperature,

solvents were evaporated under vacuum. The resulting crude was suspended in DCM (50 mL) and filtered through a plug of Celite. After evaporating the volatiles, the product was obtained 0.6 g (67%) of a colorless oil. ^1H NMR (500 MHz, CDCl_3): $\delta = 7.02\text{-}7.13$ (m, 1H), 6.75-6.80 (m, 2H), 4.00-4.07 (m, 4H), 2.85-2.89 (m, 2H), 1.92-1.98 (m, 2H), 1.21-1.27 (m, 3H) ^{13}C NMR (125 MHz, CDCl_3) $\delta = 162.34, 160.38, 128.04, 116.73, 111.27, 111.06, 61.71, 61.65, 25.90, 24.79, 16.41, 16.36$.

General Reaction Protocol for the Synthesis of Vinylphosphonic Acids:[81] A 100 mL two neck flask equipped with a condenser and a stir bar was charged with the phosphonic ester (1 equiv.), potassium iodide (3 equiv.), and 20 mL of anhydrous acetonitrile. The mixture was cooled to 0 °C and then bromotrimethylsilane (3 equiv) was added dropwise. Ice-water bath was removed and the reaction mixture was heated to 55 °C for 6 h under argon forming pink color with white precipitates. Next, the reaction mixture was cooled down to room temperature and the volatiles were removed under vacuo yielding a brown solid. Then, 50 mL of methanol:water (1:1) solution was added and the reaction mixture was stirred at room temperature overnight. After cooling to room temperature, the solvents were evaporated under vacuum yielding crude product as brown solid. The respective products were obtained by recrystallization as white powders.

(E)-(2,6-difluorostyryl)phosphonic acid (oF₂PVPA): Start with 0.74 g (2.83 mmol) diethyl (E)-(2,6-difluorostyryl)phosphonate. The product was obtained 0.30 g (48%) of a white powder after recrystallization from acetonitrile. ^1H NMR (500 MHz, DMSO-d_6): $\delta = 7.43\text{-}7.51$ (m, 1H), 7.15-7.23 (m, 3H), 6.57 (t, 1H, $J = 15$ Hz). ^{13}C NMR (125 MHz, DMSO-d_6) $\delta = 161.58, 159.57, 131.41, 129.00, 128.62, 127.58, 112.41, 112.21$.

(2,6-Difluorophenethyl)phosphonic Acid (oF₂PEPA). Start with 0.6 g (2.16 mmol) diethyl (2,6-difluorophenethyl)phosphonate. The product was obtained 0.20 g (42%) of a white powder after recrystallization from acetonitrile: ^1H NMR (500 MHz, DMSO-d_6): $\delta = 7.27\text{-}7.33$ (m, 1H), 7.02-7.09 (m, 2H), 3.99 (s, br, -POOH), 2.78-2.83 (m, 2H), 1.69-1.76 (m, 2H) ^{13}C NMR (125 MHz, DMSO-d_6) $\delta = 161.86, 159.91, 128.71, 117.24, 111.81, 111.61, 27.41$,

16.32.

Fourier-Transform Infrared Spectroscopy. Polished silicon wafers (525 μm thick) are cut into 1" squares, which are then cleaned and prepared with ZnO and PA films using the same procedure for glass/ITO substrates for devices, including the subsequent rinse and annealing steps. FTIR spectroscopy was completed using a Thermo Scientific Nicolet 6700 FT-IR Spectrometer with a liquid nitrogen cooled Hg-Cd-Te detector and KBr beam splitter. Normal-incidence transmission measurements were completed for thin films of PAs on ZnO on Si.

Kelvin Probe Measurements. Glass/ITO substrates are cleaned and prepared with ZnO and PA films as for devices, including the subsequent rinse and annealing steps. A KPTechnology SKP/SVP/LE 450 system is utilized for Kelvin probe measurements of the work function and calibrated with Al and Au reference samples in air. All work function measurements are then calculated as change from the ZnO control.

Device Fabrication. Devices were fabricated on 1" x 1" glass substrates with patterned ITO (Thin Film Devices), with better than 84% optical transparency and sheet resistance of approximately 10 Ω/sq . The substrates are cleaned by sonicating first in acetone, then isopropanol, for 15 minutes each. Next, they are treated with a Jelight Company, Inc. Model 42 UV-O₃ cleaner for 15 minutes and used immediately afterward. Zinc oxide is deposited from a solution prepared in an inert environment from a 1.1M diethyl zinc precursor (Sigma Aldrich) in toluene mixed (1:2 by volume) with anhydrous tetrahydrofuran (Sigma Aldrich). The zinc oxide film is spin-cast in air at 6000 rpm for 60 s, followed by annealing in air at 120 °C for 10 minutes. 10 mM ethanol solutions of oF₂PEPA and oF₂PVPA are prepared and spin-cast in air at 2000 rpm for 60s. The samples are then annealed in air at 120 °C for 10 minutes, rinsed with ethanol, blown dry with nitrogen, and annealed again at 120 °C for 5 minutes. The active layer solution is prepared with equal weights of P3HT (BASF) and ICBA (Plextronics), for total solids of 34 mg/mL in 1,2-dichlorobenzene. The solution is stirred overnight at 60 °C. The bulk heterojunction is spin-cast in an inert (N₂) environment at 800

rpm for 30 seconds. The samples are allowed to dry for several hours in covered petri dishes, and then annealed at 155 °C for 10 minutes in the nitrogen environment. Molybdenum oxide (Strem Chemicals) is thermally evaporated at a rate of 0.1 Å/s, followed by the Ag cathode at 0.5 Å/s, with base pressure below 1E-7 Torr.

Device Characterization. Devices were tested using a solar simulator with a quartz halogen lamp (1.1 spectral mismatch factor as compared with the solar spectrum for PCDTBT:PC₇₁BM) in an inert (N₂) environment. A 0.06 cm² aperture was used to avoid edge effects. A voltage bias was applied via the ITO and Ag electrodes and the resulting current density was measured. Series resistance was measured at 1.2 V applied bias.

2.5 Acknowledgments

This work was supported by the U.S. Department of Energy under Contract DE-AC36-08-GO28308 with the National Renewable Energy Laboratory through the DOE SETP program. Partial support from the National Science Foundation through Grant DMR-0907409 and the Renewable Energy Materials Research Science and Engineering Center is also acknowledged for RTC and TEF.

CHAPTER 3
MOLECULAR DESIGN FOR TUNING WORK FUNCTIONS OF TRANSPARENT
CONDUCTING ELECTRODES

Reproduced with permission from *The Journal of Physical Chemistry Letters*, 2015, 6 (12),
pp 2269–2276. Copyright 2015 American Chemical Society.

*Unsal Koldemir*¹, *Jennifer L. Braid*^{2,3}, *Amanda Morgenstern*¹, *Mark Eberhart*¹, *Reuben T.
Collins*², *Dana C. Olson*³, and *Alan Sellinger*^{2,3}

Attributions: UK and JLB jointly wrote this manuscript. UK synthesized the phosphonic acids and conducted NMR. AM performed gas-phase dipole calculations. JLB fabricated samples, conducted Kelvin probe measurements, and analyzed the data.

Abstract: In this perspective, we provide a brief background on the use of aromatic phosphonic acid modifiers for tuning work functions of transparent conducting oxides, e.g., zinc oxide (ZnO) and indium tin oxide (ITO). We then introduce our preliminary results in this area using *conjugated* phosphonic acid molecules, having a substantially larger range of dipole moments than their un-conjugated analogues, leading to the tuning of ZnO and ITO electrodes over a 2 eV range as derived from Kelvin probe measurements. We have found that these work function changes are directly correlated to the magnitude and the direction of the computationally derived molecular dipole of the conjugated phosphonic acids, leading to the predictive power of computation to drive the synthesis of new and improved phosphonic acid ligands.

¹Department of Chemistry and Geochemistry, Colorado School of Mines, Golden, Colorado, 80401, USA

²Department of Physics, Colorado School of Mines, Golden, Colorado, 80401, USA

³National Renewable Energy Laboratory, Golden, Colorado 80401, USA

3.1 Introduction

The need for transparent conducting electrodes has increased proportionally to the growing development of consumer electronics such as flat panel displays,[92–96] solar cells,[12, 70, 71, 97, 98] lasers,[99–102] sensors,[103–106] and UV LEDs[107–110] to name a few. Frequently, transparent conducting oxides (TCOs) are chosen to allow not only light transmission but also charge injection to and from the active layer of the device. As such, indium tin oxide (ITO) and zinc oxide (ZnO) have been benchmark materials due to their high optical transmittance and conductivity. However, conductivity and transparency are not the only criteria for contacts in high performance devices, as the alignment of energy levels between the electrodes and active materials is another crucial factor in obtaining high efficiency.[16, 73, 74, 111] By correctly tuning the effective work function of a given oxide, the charge transfer barrier at the oxide interface may be greatly reduced. Additionally, this interface requires comparable surface energies between the electrode and the active material to prevent delamination, improve film quality, promote enhanced contact, and limit other defects that lead to device instability.[112–115]

Few methods have been used to modify energy levels of transparent conducting oxides to improve their performance in devices. Especially for ZnO, doping has been explored to shift work function, with gallium- (GZO) and aluminum- (AZO) doped oxides being the most common. While substitutional dopants are successful in tuning the work function of ZnO and result in increased conductivity, the range of electronic properties is limited by the extremes of the dopant concentration.[19]

In this context, small molecule surface modifiers have been widely employed for tuning the work function, surface energy, and wettability of transparent electrodes over a wide span.[33, 49, 81, 83, 116–122] Of the most common TCO modifiers (silanes, carboxylic acids, thiols, and phosphonic acids), phosphonic acids have demonstrated promise as they bind effectively and densely via multidentate attachment to metal oxides using simple processing conditions and cause minimal etching, whereas other molecular surface modifiers show weaker

binding or may damage the oxide surface.[44, 123] The main advantage of phosphonic acids as surface modifiers is that the molecular dipole normal to the surface can tune the electrode work function in either direction as determined by the aromatic group.[82, 124] For example, depending on the nature of the electron withdrawing or electron donating substituents of the surface modifier, the molecular dipole can move the effective work function of the oxide toward either higher or lower energy with respect to vacuum level. To date, benzylphosphonic acids as surface modifiers have shown effectiveness in terms of work function shifts of 1 eV for ITO and ZnO depending on the nature of the molecular dipole.[16, 50, 74, 77, 124] As these molecules are applied with monolayer coverage, phosphonic acid modification does not alter the optical or bulk electrical characteristics of the modified oxides. Furthermore, phosphonic acids have been shown to passivate interstitial zinc defects on the surface of solution processed ZnO, leading to greater stability.[15]

We have recently reported on the preparation of simple *conjugated* phosphonic acids and the importance of the conjugated vinyl linkage between the phosphonic acid binding site and the aromatic ring. The vinyl linkage allows for enhanced electronic communication between the acid binding group and the “functionalized” aromatic ring by delocalization of the π electrons, leading to increased dipoles that in turn greatly affect the electrode work function. We have shown the significance of this conjugated linkage with respect to a saturated bond in terms of the magnitude of the work function change in ZnO leading to an improvement in solar cell device performance.[125] Our aim in this perspective is to introduce how gas-phase molecular dipole calculations can lead to the design of novel conjugated phosphonic acids that are effective in tuning the work functions of both ZnO and ITO through a range of 2 eV. In this work, we present a series of conjugated phosphonic acids, their quantum mechanically calculated gas phase dipoles, and the relationship between molecular dipole and work function change of the metal oxide electrode as determined by Kelvin probe measurements.

3.2 Results and Discussion

Gas-Phase Dipole Computational Calculations. It has been shown in previous work that the work function of an idealized ITO surface is shifted linearly with the gas-phase dipole moment of the molecular modifier.[81, 126] We have performed theoretical calculations of gas-phase dipoles on seven novel phosphonic acids (the structures are given in Figure 3.1) to be correlated with the work function change of the electrode surfaces. Dipole moments were calculated using the Amsterdam Density Functional Package (ADF) version 2014.01,[127, 128] with all calculations being performed spin-unpolarized in the gas phase. A conformer search was conducted to find the lowest-energy conformation of each molecule using the RDKit package. Initial geometry optimizations were done on all conformers within the lowest 5 kcal/mol for each conjugated phosphonic acid with a nonrelativistic all-electron double- ζ singly polarized (DZP) basis set and the Vosko, Wilk, and Nusair parametrized local density approximation (LDA) functional.[129] Single-point calculations were run on all geometries in the lowest 1 kcal/mol using a triple- ζ singly polarized (TZP) basis set and the Becke-3-Lee-Yang-Parr functional (B3LYP) with 20% Hartree-Fock exchange.[130] The dipole moments for the lowest-energy structures are reported here. The magnitude of the dipole moment was calculated along the phosphorus-carbon bond (henceforth the z-axis) for each molecule as this is the approximate orientation of the ligand perpendicular to the surface. Fourier transform infrared spectroscopy has shown that the conjugated 2FPA binds to ZnO by a combination of bidentate and tridentate configurations, which imply the approximate phosphonic acid orientation that we have selected for our dipole calculations.[125]

The computational normal-component dipole moments are reported in Table 3.1 and plotted in Figure 3.2. Looking first at the very well studied (2,6-difluorobenzyl)phosphonic acid (oF₂BPA) presented the lowest dipole value of the ortho-2,6- difluoro-type phosphonic acids at 0.97 D. The variance in dipole moment in this series of related molecules is due in part to the conjugation and geometry of each molecule. The conjugated molecule, 2FPA, is forced into a perpendicular orientation relative to the surface due to the restriction of the

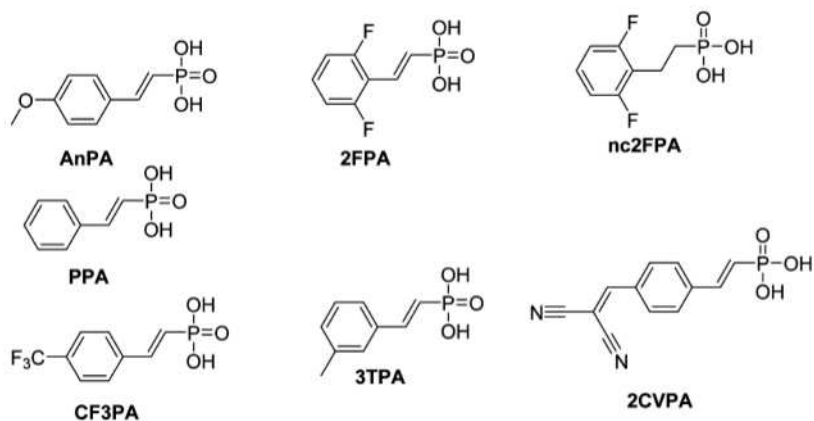


Figure 3.1: Chemical structures of the seven novel phosphonic acids.

double bond, as shown in Figure 3.3. The planar and conjugated configuration of 2FPA orients and electronically connects the active 2,6-difluoro aromatic ring with the carbon-phosphonic acid binding site, thereby increasing the magnitude of the dipole normal to the surface (see Figure 3.4 for the gas-phase dipole vectors). While the same fluorinated aromatic ring on nc2FPA is still normal to the surface, the ring is electronically decoupled from the carbon-phosphonic acid binding group, thus decreasing the magnitude of the dipole in the normal direction. For oF₂BPA, not only is the linkage between the aromatic ring and binding site unconjugated, the aromatic ring is also bent even further away from the linear geometry at an angle of 114° from the surface. Thus, the deviation from planarity and disruption of conjugation decreases the magnitude of the dipole perpendicular to the surface through this series of molecules.

Further, the dipole moment values of (E)-(3-methylstyryl)- phosphonic acid (3TPA) and (E)-styrylphosphonic acid (PPA) are lower compared to those of 2FPA but greater than the dipoles of its phenylethyl and benzyl analogues. (E)-(4- methoxystyryl)phosphonic acid (AnPA) has an even greater dipole moment of 3.18 D, largely due to the para-methoxy group on the aromatic ring. Alternatively, (E)-(4-(trifluoromethyl)- styryl)phosphonic acid (CF3PA) resulted in a molecular dipole of -1.26 D, toward the surface, due to the placement of the electronegative trifluoromethyl group in the para position on the benzene ring. The

Table 3.1: Average Measured Work Function Changes with Respect to Unmodified ITO and ZnO for the Novel Conjugated Phosphonic Acids. The dipole moment is calculated along the z-axis.

phosphonic acid	$\Delta\phi_{\text{ITO}}$ (eV)	$\Delta\phi_{\text{ZnO}}$ (eV)	μ_z (Debye)
AnPA	$+0.63\pm 0.08$	$+0.27\pm 0.14$	3.18
2FPA	$+0.99\pm 0.08$	$+0.82\pm 0.09$	3.06
3TPA	$+0.40\pm 0.07$	$+0.39\pm 0.01$	2.48
PPA	$+0.33\pm 0.03$	$+0.27\pm 0.04$	2.09
nc2FPA	$+0.98\pm 0.09$	$+0.61\pm 0.15$	1.79
oF ₂ BPA	$+0.48\pm 0.07$	$+0.31\pm 0.17$	0.97
CF ₃ PA	-0.80 ± 0.15	-1.12 ± 0.27	-1.26
2CVPA	-0.32 ± 0.02	-0.45 ± 0.12	-1.55

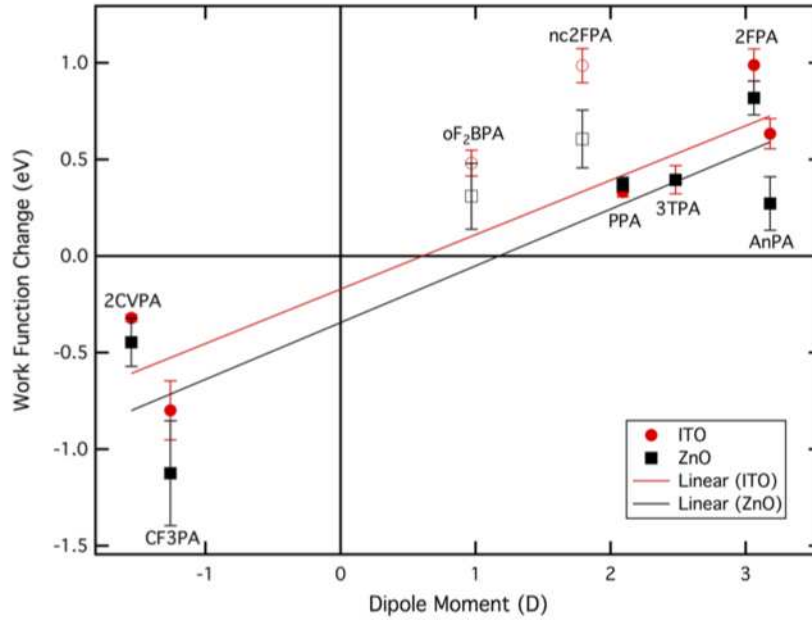


Figure 3.2: Values of the magnitude of the dipole moments along the phosphorus-carbon bond of phosphonic acids versus the work function change of modified ZnO (black squares) and ITO (red circles) with respect to unmodified oxides. Hollow points indicate unconjugated molecules, which have been excluded from the linear fits.

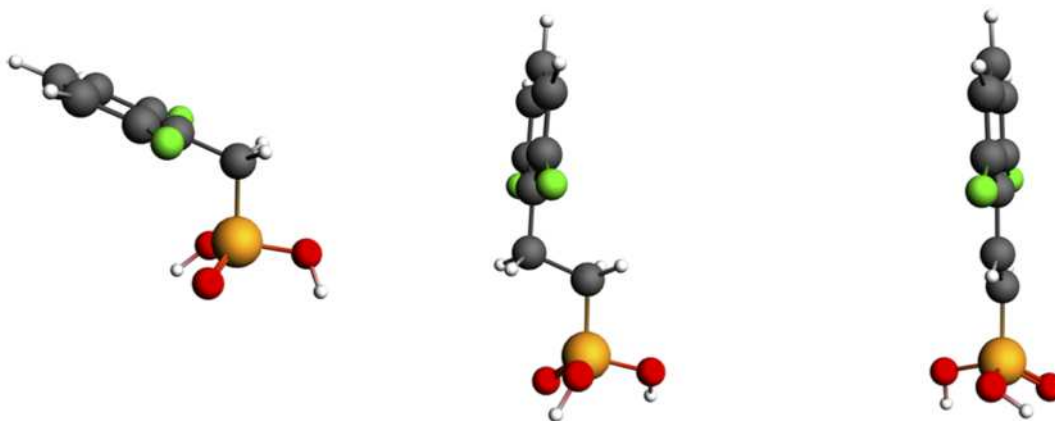


Figure 3.3: Quantum mechanically calculated geometries of oF2BPA, nc2FPA, and 2FPA.

dicyanovinyl ligand of (E)-(4-(2,2-dicyanovinyl)styryl)phosphonic acid (2CVPA) allowed for the most extreme negative dipole moment at -1.55 D.

Synthesis. The molecular modifiers were prepared based on the results of the molecular dipole calculations above. Synthetic details for the chemical synthesis of seven novel conjugated phosphonic acids are given in the Supporting Information, while the chemical structures and a general outline of the synthetic methodology are shown in Figure 3.5. We have applied an uncommon protocol of the Heck coupling of commercially available aromatic halides with vinyl-diethylphosphonate using Herrmann's palladacycle to generate a trans-conjugated bond between the aromatic group and the phosphonic ester. In this process, the Heck coupling provides milder conditions with a higher tolerance to other functional groups, as well as higher yields as compared to the Arbuzov reaction for generating benzylphosphonic acids. Next, conversion of the esters to the target phosphonic acids was achieved by sequential treatment of the phosphonic esters with trimethylsilyl bromide/potassium iodide (TMSBr/KI) and water/methanol (H₂O/MeOH) at room temperature.[131] The compounds were obtained as white solids with yields greater than 40%, and their structures were confirmed with NMR spectroscopy (¹H and ¹³C).

For only the saturated nc2FPA molecule, we applied a subsequent hydrogenation procedure with triethylsilane (TES) over a palladium on carbon (Pd/C) catalyst under ambient

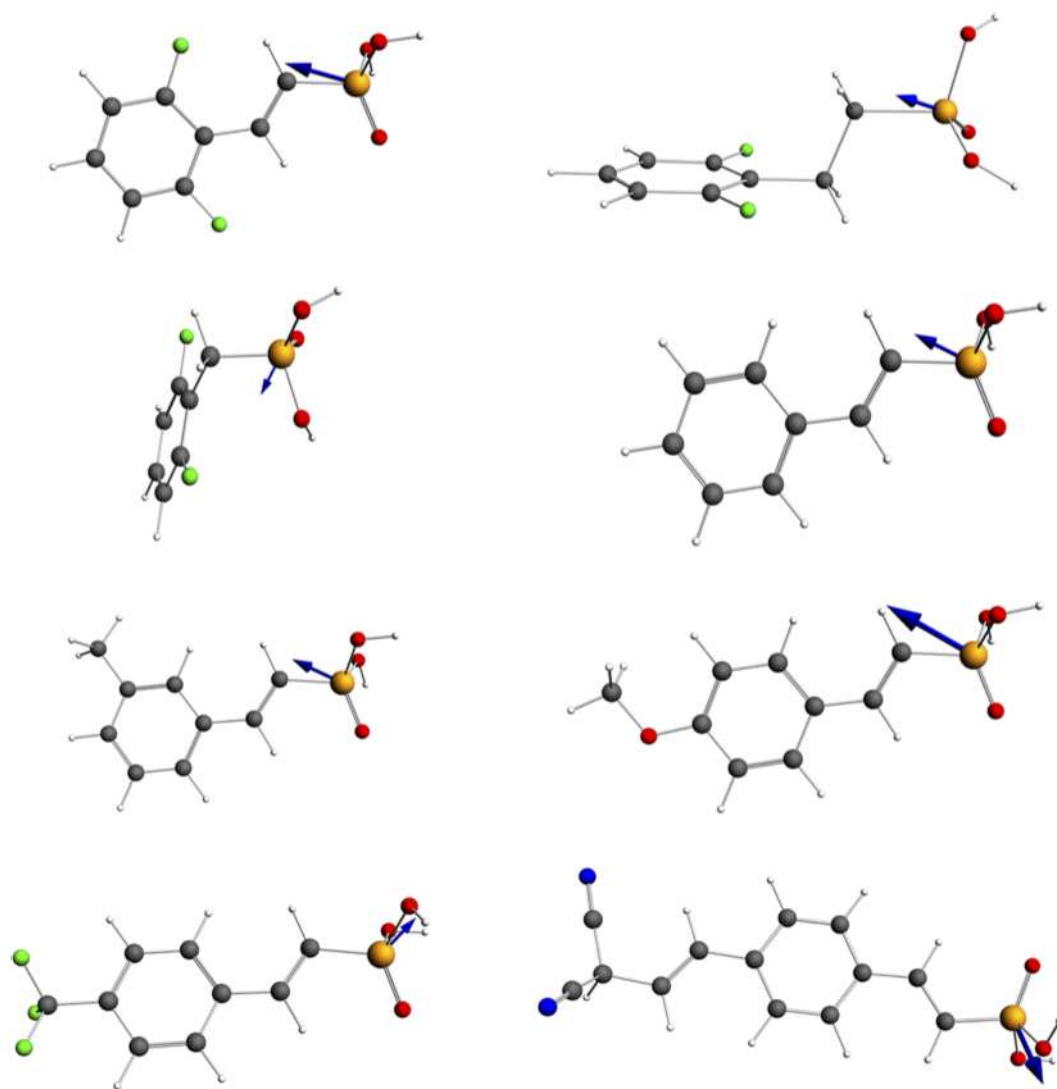


Figure 3.4: Gas-phase dipole vectors using the phosphorus atom as the origin for 2FPA, nc2FPA, oF2BPA, PPA, 3TPA, AnPA, CF3PA, and 2CVPA (left to right, top to bottom).

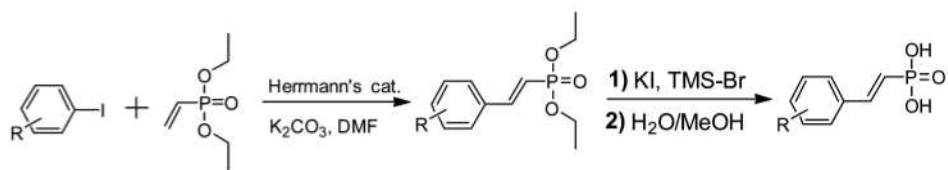


Figure 3.5: General Synthetic Pathway for Preparing the Conjugated Phosphonic Acids

conditions to reduce the vinyl to an ethyl bridge, forming the saturated phosphonic ester intermediate that was then converted to the acid.[125] Additionally, a Knoevenagel condensation reaction between malononitrile and the aldehyde group of (4- formylstyryl)phosphonic acid was performed in water without any base catalyst to afford 2CVPA in a quantitative yield.[132]

Sample Preparation. The 1 in. x 1 in. glass substrates, patterned with ITO (Thin Film Devices) or unpatterned (Colorado Concepts), were cleaned by 15 minutes sonicating in each acetone then isopropanol. This was followed by 15 minutes of UV-O₃ cleaning in a Jelight Company, Inc. model 42. ZnO was deposited on top of ITO from a 1.1M diethyl zinc precursor (Sigma-Aldrich) in (1:2) toluene with anhydrous tetrahydrofuran (Sigma-Aldrich) by spin-casting in air at 6000 rpm for 60 seconds. The ZnO samples were then annealed in air at 120 °C for 10 minutes. 10 mM MeOH solutions of phosphonic acids were spin-cast on the ITO/glass and ZnO/ITO/glass substrates in air at 2000 rpm for 60 seconds, followed by annealing in air at 120 °C for 10 minutes. Finally, the samples were rinsed with methanol and blown dry with nitrogen, and annealed again at 120 °C for 10 minutes.

Kelvin Probe Measurements. Kelvin probe measurements were performed at ambient conditions on ITO and ZnO on ITO, each treated with the novel phosphonic acids in order to investigate the work function change with respect to untreated ITO and ZnO/ITO controls. Both patterned and unpatterned ITO substrates were used, and samples were prepared as described above. Measurements were performed using a KPTechnology SKP/SVP/LE 450 system, calibrated with Al and Au reference samples in air. Work function measurements have been calculated as the average change from ITO and ZnO/ITO control samples for the two types of ITO substrates, calculated from twenty data points for each sample. Relative work function values are given in Table 3.1.

At first glance, we observed two extremes of the ZnO work function change: a decrease of 0.82 eV induced by 2FPA, and an increase of 1.12 eV by CF₃PA, thus leading total relative change in the work function of 1.94 eV for ZnO. Similar effects were observed for

ITO modified with the same phosphonic acids, resulting in a total work function change in a range of 1.79 eV. 2FPA, which resulted in the second largest calculated normal dipole moment (only 0.12 D lower than AnPA), corresponds to the largest work function shift in the positive direction on both ITO and ZnO. Compared to the un-conjugated nc2FPA and oF₂BPA, 2FPA shows a larger decrease of the work function of ZnO as the vinyl conjugated linker is suspected to contribute in the electronic communication between the aromatic ring and the phosphonic acid functional group. On ITO, 2FPA again outperforms its un-conjugated counterparts, though trivially compared to nc2FPA. This indicates that binding morphology may vary not only between acid types and linkages, but also between oxides modified with the same molecule. PPA and 3TPA result in intermediate work functions relative to 2FPA due to their smaller dipole moments.

The gas-phase dipole moments of the conjugated molecules are plotted versus the average measured change in work function for modified ITO and ZnO in Figure 3.2. Immediately apparent is that the changes in work function of both ZnO and ITO largely correlate with the magnitude and direction of the gas-phase dipole moments of the surface modifiers. The linear fit data has a slope of 0.28 eV/D for ITO and 0.29 eV/D for ZnO, with R² values of 0.87 and 0.81, respectively. While the data generally follow this trend, the scatter from these lines is also noteworthy.

Unconjugated oF₂BPA and nc2FPA are shown in Figure 3.2 but have been omitted from the fit as the difference in linkage results in a change in the bond dipole, and therefore, we expect deviation from the conjugated molecular dipole versus work function trend. Still a concern for the conjugated molecules is that the change in work function of phosphonic-acid-modified metal oxides has been shown to vary with binding mode of the modifier.[43] Therefore, the attachment geometry of these molecules plays a role for which we cannot account in this graph. Furthermore, the aromatic groups of the phosphonic acids can influence the work function beyond just the dipole contribution. 2CVPA, having the largest negative molecular dipole, increased the ZnO and ITO work functions by only 0.45 and 0.32 eV, re-

spectively, less than half of the work function shifts produced by the smaller dipole CF3PA. This may be caused by non-normal orientation of the dicyanovinyl ligand in 2CVPA as it is much larger compared to CF3PA. Another possibility that would also explain why AnPA similarly underperformed in altering the work function of ZnO and ITO compared to its calculated dipole moment is the more hydrophilic nature of these ligands. As the oxide surfaces are hydrophilic in nature, water can be easily absorbed on the surface, leading to changes in optoelectronic properties. Having a more hydrophobic ligand containing fluoro groups and no oxygen atoms may minimize water absorption on the surface, while hydrophilic ligands like 2CVPA and AnPA may be less effective barriers.[33] If we remove the outlying 2CVPA and AnPA from our fit, the slope and R^2 values increase to 0.37 eV/D and 0.95 for ITO and 0.43 eV/D and 0.99 for ZnO, respectively. This indicates that the slopes shown in Figure 3.2 may be somewhat shallow.

Despite these other factors for modifying electrical properties, our results demonstrate that the calculation of the normal incidence gas-phase dipole moment is a reasonably good predictor of the effect of a conjugated phosphonic acid on the work function of transparent metal oxides and allows for relevant design of dipolar modifiers through simulation. Our rate of change in work function is not only consistent between the oxides studied here but is also comparable to values derived from theoretical calculations and UPS measurements of phosphonic acids on GZO[49] and ITO.[74, 81] Other studies differ more widely from our results, with our slope being somewhat higher than that shown by Khodabakhsh et al. for ITO modified with various chlorinated dipolar molecules[133] and somewhat lower than the theory of phosphonic acids on ZnO.[43] The dipole moments in these previous studies were calculated for monolayers bonded to the surface rather than for free molecules as in our case. We suspect that any mismatch in slope from these previous findings arises from either discrepancy in calculation of the molecular dipole moment or the difference in measurement technique.

As this study is limited to gas-phase dipole moments of phosphonic acids, linear offset of our fit from the origin may be attributed to the interfacial dipole formed by charge redistribution due to the surface bond. This offset is greater for ZnO than ITO, suggesting a difference in strength of the bond dipole on these substrates. Future work including the calculation of dipoles for ligands attached to surfaces may elucidate this variation in results.

3.3 Summary and Future Outlook

We have developed and studied conjugated phosphonic acids that are effective in tuning the work function of ZnO and ITO over a range of nearly 2 eV. We have also shown that our calculated gas-phase dipole moments correlate well with the experimentally measured work function changes. We expect that the reliability of dipole moment calculations in predicting work function modification, in conjunction with our new synthetic methodology, will lead to additional conjugated phosphonic acid groups with different electron-donating and -withdrawing ligands. In organic photovoltaics, the development and implementation of these materials will increase the versatility of electrode materials via work function modification, allowing any TCO to work as a contact for a variety of active layer species. This fine-tuning of work functions enables maximization of the open-circuit voltage of organic solar cells by optimizing interfacial energy alignment. Additionally, these materials will benefit other organic electronic devices in a similar manner, where quasi-Fermi level matching has improved built-in voltage and injection efficiency.

In the future, it is important to pursue modeling of these molecules on a variety of substrate materials to understand the influence of interfacial dipoles on not only work function but also other properties of the modified oxides as benzyl phosphonic acids have been shown to alter the defect structure and surface states of ZnO. More specifically, the bonding and orientation of these molecules on various surfaces should be studied to determine a more accurate picture of the roles of molecular and bond dipoles in work function tuning. Furthermore, simulations may shed some light on how modified TCOs interact with the active layer and influence device characteristics such as open-circuit voltage, device stability, and

short-circuit current. The latter is particularly interesting due to the poor conductivity of these molecules above monolayer coverage.

Still, this methodology for production has already proven useful in anticipating the change in the work function of TCOs as a function of the dipole of the molecular modifier. The novel conjugated phosphonic acids presented are a marked improvement over traditional benzyl phosphonic acids because of the larger dipole moments for conjugated molecules using the same aromatic group, as well as enhanced electronic interaction with the TCO via the double-bonded linkage. The simple synthesis and predictive dipole correlation make conjugated phosphonic acid modification a straightforward approach to bettering TCOs for use in organic electronics.

3.4 Acknowledgments

The authors acknowledge financial support for this research through the U.S. Department of Energy under Contract No. DE- AC3608-GO28308 with the National Renewable Energy Laboratory through the Department of Energy Solar Energy Technology Program. A.M. acknowledges financial support through ONR Grant No. N00014-10-1-0838.

CHAPTER 4
CROSS-SECTIONAL SCANNING KELVIN PROBE MICROSCOPY OF ORGANIC
BULK HETEROJUNCTION SOLAR CELLS

Jennifer L. Braid^{1,2}, *Nikos Kopidakis*², *Reuben T. Collins*¹, *Sanjini U. Nanayakkara*²

Attributions: This manuscript was written by JLB, who also fabricated OPV devices and measured J-V characteristics. SUN cleaved and mounted devices for X-SKPM measurement. JLB and SUN performed X-SKPM in nitrogen. JLB performed X-SKPM in air, and processed all X-SKPM data. Bobby To provided SEM images of device cross-sections.

Abstract: Cross-sectional scanning Kelvin probe microscopy (X-SKPM) has become a valuable tool for studying the fundamental operation mechanisms of many types of solar cells, including organic bulk heterojunction solar cells. However, more information on the effects of device structure and measurement environment on the electric field distribution is needed to better interpret X-SKPM results and understand device mechanics. Here we show that oxygen p-doping of the bulk heterojunction greatly affects the potential distribution in organic solar cells, and that organic photovoltaics are highly susceptible to surface effects during ambient measurement. We also explore the effect of modulating the cathode work function on the potential distribution of devices. The decrease of cathode work function is shown to extend the electric field in the active layer, correlating with an improvement in device short circuit current and efficiency.

4.1 Introduction

Organic photovoltaic (OPV) devices made a major leap in efficiency with the introduction of the bulk heterojunction (BHJ) active layer, in which electron donor and acceptor materials are mixed to form a network of polymer/fullerene interfaces for efficient charge

¹Department of Physics, Colorado School of Mines, Golden, Colorado, 80401, USA

²National Renewable Energy Laboratory, Golden, Colorado 80401, USA

carrier separation and extraction. Modeling of the electric potential in a BHJ OPV device has indicated a linear variation in potential and a constant electric field across the active layer, generally following metal-insulator-metal (MIM) device behavior.[53, 134, 135] In the MIM model, the linear potential sweeps photogenerated charge carriers out of the device to be collected at the contacts, though the Schottky model and other theories suggest charge extraction by diffusion rather than field induced drift.[55]

Until recently, indirect methods such as time-of-flight measurements[57] and light intensity varying photocurrent measurements[58, 59] have been used to determine the spatial extent of the electric potential in BHJ OPV devices. Many of these studies, including impedance spectroscopy,[60, 61] have been taken as evidence for a large field-free region within the active layer, leading to the conclusion that the electric field is isolated at the contact interfaces which exhibit Schottky barrier behavior. In this view, charge transport in the BHJ is dominated by diffusion, rather than drift. However, all of these methods require model-dependent interpretation of the data to extract a potential distribution, rather than direct observation.

Cross-sectional scanning Kelvin probe microscopy (X-SKPM) offers direct measurement of the potential distribution within the device structure. This tapping mode atomic force microscope (AFM) technique is sensitive to topography and differences in local work function across the sample, allowing both to be mapped in registry and providing a contact potential difference map of the device cross-section. The few prior X-SKPM studies of BHJ OPVs that have been reported are not in complete agreement on the potential distribution across BHJ devices.

Standard architecture devices, illuminated through the device anode, have shown non-linear potential across the BHJ under X-SKPM investigation.[51, 52, 54, 66, 67] Specifically, all of these studies reveal two regions of slope in potential: a near-zero field region through the bulk of the BHJ, and a sharp increase in potential in a small region near the cathode. This is indicative of Schottky junction behavior at the BHJ/cathode interface, rather than

the expected MIM or expanded p-n junction behavior across the BHJ. However, p-n junction behavior may also fit this potential distribution if the BHJ could be n-doped by electron injection from the cathode, creating a p-n junction between the differently doped regions of the active layer.[52] A bilayer standard architecture device shows the same behavior in potential though, and a charge transport barrier at the cathode is said to cause both this potential distribution as well as s-shaped J-V curves.[136]

Inverted architecture devices have been less studied, but an inverted bilayer device showed a sharp drop in potential at the donor/acceptor interface where these materials act as a p-n junction.[67] In an inverted BHJ device, the potential has been shown to behave linearly in the active layer.[66] This difference from the standard device was attributed to a lack of injection barriers between the BHJ and contact materials.

Previous X-SKPM studies of OPV devices have failed to address the rapid degradation of device characteristics catalyzed by biasing of the device in the presence of oxygen, and the effect of this degradation on the potential distribution in the device, despite many performing X-SKPM in air. BHJ OPV devices have been shown to degrade via p-doping of the BHJ by the formation of immobilized superoxide anions and mobile holes (reversible with annealing) and carboxylic and carbonyl groups with P3HT (irreversible).[60] In addition to changing the potential distribution within the device, oxygen doping reduces current and fill factor in devices.[137] Strong p-doping of the active layer results in p-n junction behavior at a semiconductor cathode, or Schottky junction behavior with a metal cathode. The effect on the potential distribution would be a near-zero slope through the majority of the active layer and a sharp change in potential at the BHJ/cathode interface.[60] This is very similar to the two region potential distribution seen in previously published X-SKPM studies of OPV BHJ devices.

In this study, we prove that the Schottky type of potential distribution is indeed affected by oxygen doping of the active layer in standard architecture devices. Furthermore we show that X-SKPM in air causes other complications when performed on an inverted architecture

BHJ OPV device incorporating zinc oxide (ZnO) and molybdenum oxide (MoO_x) interlayers. The effects of surface hydroxides on the work functions of these materials cause variations in ambient X-SKPM profiles, yielding potential distributions that do not reflect bulk device operation. The effect of varying the work function of metal oxide contacts on the potential distribution is also demonstrated by X-SKPM of inverted devices incorporating molecular dipoles to modulate the work function of ZnO.

Molecular dipole modification of the ZnO electron transport layer has been shown in several studies to increase some combination of the short circuit current, fill factor, and open circuit voltage of organic bulk heterojunction devices.[15, 16, 36, 40] Small molecules with correct dipole strength and orientation applied to the ZnO surface create a monolayer to shift the effective work function of the oxide to improve compatibility with the electron transport level of the active layer material. Recently, we have reported on a novel type of molecule for contact modification, conjugated phosphonic acids, which have very large dipole moments and can shift the effective work function of ZnO through a range of 2 eV by way of the double-bonded linkage between the attachment and aromatic groups,[138] shown here in Chapter 3. In Chapter 2, modification of ZnO in an inverted device structure with oF_2PVPA conjugated phosphonic acid increased device efficiency by 12% compared to the unmodified device.[125] ZnO modification was predicted to improve device performance by boosting the open circuit voltage. Better electron transport level matching between ZnO and the active layer decreases energy loss at this interface, increasing the built-in voltage in the device. While this effect only slightly raised the open circuit voltage, improvements to the short circuit current and fill factor also contributed to the increase in efficiency. Here we provide a direct measurement of the potential distribution on cross-sections of unmodified, beneficially modified, and detrimentally modified organic bulk heterojunction devices, revealing the mechanics of device performance and improvement associated with molecular modification of the electron transport layer.

4.2 Experimental Methods

Device processing & characterization. Devices were built on glass substrates patterned with approximately 265 nm of ITO with sheet resistance 10 Ω /sq (Thin Film Devices). Substrates are sonicated in acetone and then isopropanol for 15 min each, followed by 5 min in a 100 °C oven and 15 min in a UV-ozone cleaner (Jelight Company, Inc.).

Substrates for standard architecture devices are spin-coated with PEDOT:PSS (Baytron P VP Al 4083) at 6000 rpm for 60 s and annealing at 140 °C in air for 10 min. Next, 34 mg/mL total solids 1:1 by weight P3HT:ICBA (BASF and Plextronics, respectively) in dichlorobenzene is spin-coated in a nitrogen environment at 500 rpm for 30 s. The active layer is allowed to dry before annealing at 150 °C. Finally, the Al contact is evaporated at a rate of .5 Angstroms/s at a base pressure of 10^{-7} Torr.

For inverted devices, substrates are spin-coated with a 1:2 diethyl zinc solution in tetrahydrofuran (both Sigma-Aldrich) at 2000 rpm for 60 s. The sample is annealed in air at 140 °C for 10 minutes to form zinc oxide. Conjugated phosphonic acids were spin-coated at 2000 rpm for 60 s from 10 mM solutions in methanol, followed by a methanol rinse, blowing dry with nitrogen, and 140 °C anneal for 5 min in air. P3HT:ICBA is applied and treated as for the standard device. 10 nm of MoO_x (Strem Chemicals) is evaporated at .1 Angstroms/s, followed by 50 nm of Ag at .5 Angstroms/s at a base pressure of 10^{-7} Torr.

J-V characteristics of whole devices were measured using a home-built solar simulator in a nitrogen purged glove box, with Oriel Sol3A illumination calibrated to 1 sun with a KG5-filtered mono-Si reference cell. Device area is 0.1 cm², but was masked to 0.06 cm² during measurement. Partial devices were measured in a like solar simulator system in air after X-SKPM investigation of the cross-section in nitrogen or air. Bias was applied between -2 and +2 V, incremented by 0.01 V.

X-SKPM preparation & measurement. Devices were cleaved in nitrogen to expose the cross-section of the solar cell. Samples were scribed outside the device area to direct breakage. Glass pliers were used to break the sample by tension across the device area to expose all

layers of the working device. Devices were then mounted on sample holders to present the device cross-section perpendicular to the AFM tip. Devices were wired so the cathode was grounded and a bias could be applied to the anode, regardless of standard or inverted device architecture.

X-SKPM was performed on a Veeco 5000 AFM, housed in nitrogen, in tapping mode. The Pt/Ir coated Si probe (Nanosensors PPP-EFM) has a cantilever resonant oscillation of 50-70 kHz, used for topographic imaging, while the second resonant oscillation, 300-400 kHz, was used for potential measurement. Images were collected with pixel density 512 pixels/ μm , at a scan rate of .2 Hz. Additional X-SKPM measurements were conducted with a Park Instrument XE-70 AFM in air using BudgetSensors Multi75E-G Cr/Pt coated Si probes with the first resonant frequency, 18 kHz, used for potential and the second resonant frequency, 75 kHz, used for topography. Topography and potential profiles presented here are the averages of 100 nm wide strips (50 pixels) of the device cross-section.

4.3 Results and Discussion

Standard architecture device. J-V characteristics for the standard architecture solar cell of the structure ITO/PEDOT:PSS/P3HT:ICBA/Al are given in Table 4.1 and Figure 4.1. Note that the As Fabricated device is a different device from the same substrate as the following three measurements, which were all performed on the same device, and information is presented for partial, cleaved devices. The two devices used had very similar device characteristics before cleaving, which may be found in Appendix A. The J-V characteristics listed here were obtained after each step of X-SKPM. Annealing the device at 140 °C for 10 minutes (before cleaving) improves the short circuit current, open circuit voltage, and fill factor of the device. X-SKPM characterization of the device in air (which involves externally biasing the device during air exposure) leads to reduction of the short circuit current of the device. Further, these reductions are maintained during X-SKPM investigation of the device in a nitrogen environment immediately following the ambient measurement.

Table 4.1: Standard architecture device characteristics

	V_{OC} (V)	J_{SC} (mA/cm ²)	FF (%)	PCE (%)
As Fabricated	0.37	10.13	42.8	1.63
Annealed	0.48	11.30	49.0	2.65
Ambient	0.49	10.13	49.3	2.48
Post-Ambient	0.50	9.65	49.2	2.38

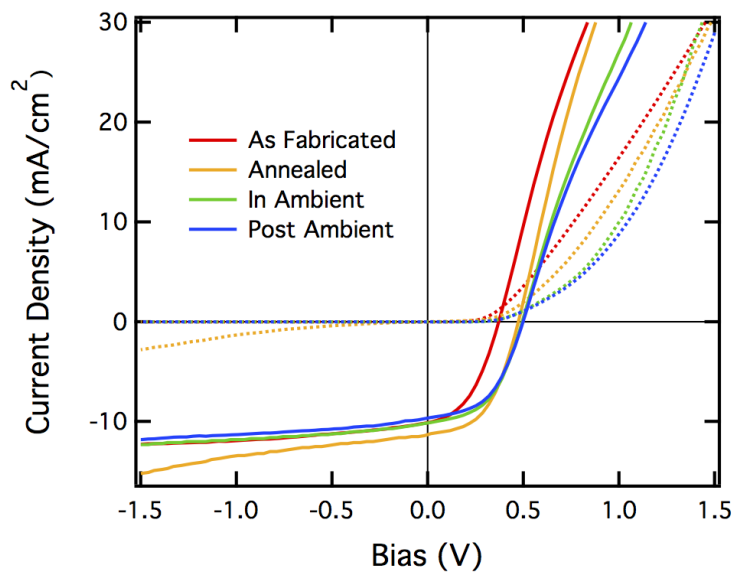


Figure 4.1: Applied voltage vs. current density for the standard architecture device. Solid lines represent illuminated device characteristics, while dotted lines represent dark.

X-SKPM of the standard architecture device shows a significant difference in the electric potential distribution for the device before and after exposure to oxygen and applied bias. Figure 4.2 shows the raw potential and electric field, as well as relative potential and electric field distributions for the standard architecture device as annealed and after external biasing in air. A variety of external biases were applied to each device, color-coded as shown for the As Fabricated Potential measurement. This figure also includes topography for each cross-sectional measurement, and scanning electron microscope (SEM) images of the two device cross-sections. SEM agrees well with our layer thicknesses as determined by X-SKPM, allowing the potential distribution to be plotted in registry with the layers making up the device. It is also important to note that the variation in X-SKPM-measured topography varies by less than 150 nm over each cross-sectional measurement. The devices measured here by X-SKPM and SEM are the same devices whose characteristics are shown above in Table 4.1 and Figure 4.1. Only the Ambient measurement was performed in an open-air AFM, while the rest of the measurements were performed in an AFM housed in a nitrogen glove box.

The As Fabricated device, measured in a nitrogen ambient, shows a relatively uniform electric field throughout its active layer. This uniform field is maintained even after annealing the device. The raw potential is very asymmetric between reverse and forward bias in both of these measurements, with forward bias being the normal device operating condition. The raw electric field has a negative value in the active layer for all of the biases applied. The relative electric field, obtained by first derivative of the relative potential, shows the difference in device behavior under forward and reverse biases more clearly, with a nearly field-free active layer and a peak at the device cathode under forward bias for both the As Fabricated and Annealed measurements.

The raw potential distribution changes greatly upon biasing in air. There is a large negative electric field at the cathode, occurring in both the Ambient and Post-Ambient measurements, as well as a field-free region in the BHJ and through the PEDOT:PSS interface.

The relative potential and electric field show symmetric responses under forward and reverse applied bias, though the field is located only at the cathode in both cases. While the magnitude of the electric field changes between the Ambient and Post-Ambient measurements, the shape and location of the field are essentially the same, verifying that our air- and nitrogen-housed measurement systems are at least qualitatively equivalent. The difference in electric field magnitude likely originates from the attachment of surface hydrogen or hydroxides to the aluminum surface during Ambient measurement. Attachment of hydroxides or hydrogen increases the work function of a material, causing a greater change in potential at the BHJ/Al interface and therefore a larger electric field magnitude, as we see here. The location and shape of the electric field in the BHJ and the rest of the device are unaffected by these species.

The electric potential seen in our As Fabricated and Annealed measurements is very close to the linear distribution expected for BHJ devices. There is a negative electric field across the entire active layer under operating conditions for these measurements, which aids in the extraction of charge carriers. The asymmetry in potential distribution between forward and reverse bias indicates that our electron and hole transport layers have good selectivity for the intended charges.

Biasing the device in air during Ambient measurement results in a very different potential distribution due to oxygen p-doping of the active layer. Oxygen p-dopes P3HT, creating a more Schottky-like junction between the BHJ and Al. The effect on the potential distribution is a field-free region extending approximately halfway through the p-type active layer, and a high field region near the n-type cathode.

Device characteristics agree with our SKPM results. The As Fabricated and Annealed cross-sections showing good field extension have higher efficiencies due to the charge extraction aided by the electric field through the BHJ. The increased carrier extraction leads to a higher short circuit current than in the Ambient and Post-Ambient device measurements where there is a large field-free region in the active layer.

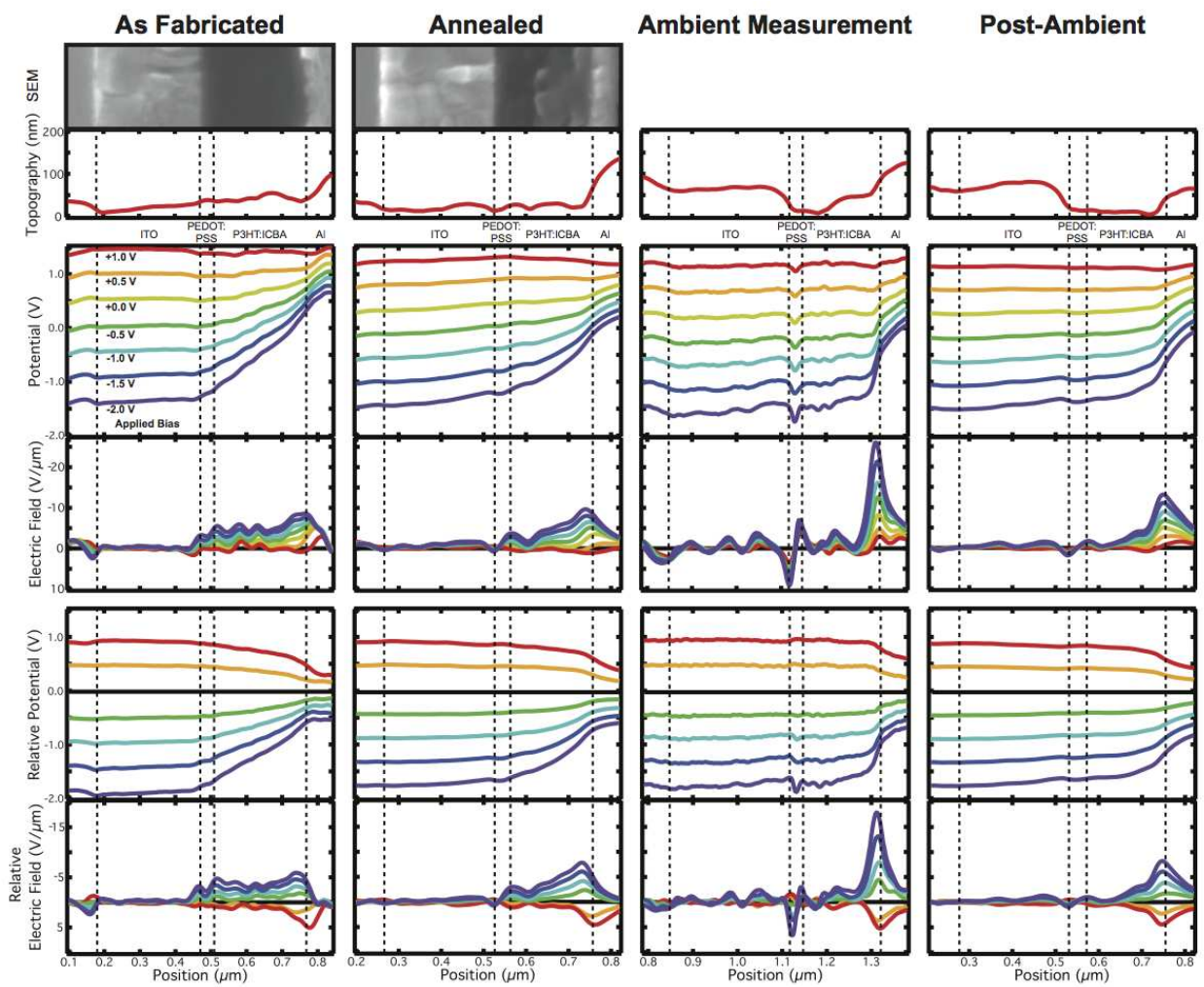


Figure 4.2: X-SKPM results for the standard architecture device. Colors correspond to the bias applied across the device.

Inverted architecture device. Device characteristics are given in Table 4.2 and Figure 4.3 for inverted devices of the structure ITO/ZnO/P3HT:ICBA/MoO_x/Ag. Note that again the As Fabricated device is a different device from the same sample as the device used for the other X-SKPM and efficiency measurements, and these devices began with similar performance. (See Appendix A.) The inverted device underwent the same steps for obtaining J-V characteristics and X-SKPM as the standard architecture device.

In contrast to the Standard Architecture devices, annealing the inverted device structure decreases its efficiency compared to the As Fabricated state, probably due to adverse effects of heating the MoO_x layer. Again we see that short circuit current, open circuit voltage, and efficiency are further reduced with biasing in the presence of oxygen for the Ambient measurement. After Post-Ambient X-SKPM measurement, the device characteristics were unchanged; hence bulk device operation did not change during measurement in the nitrogen environment.

Table 4.2: Inverted architecture device characteristics

	V _{OC} (V)	J _{SC} (mA/cm ²)	FF (%)	PCE (%)
As Fabricated	0.82	8.80	44.1	3.19
Annealed	0.69	6.56	50.8	2.30
Ambient	0.66	5.75	47.6	1.81
Post-Ambient	0.67	5.73	47.6	1.82

The X-SKPM behavior of the inverted device in Figure 4.4 is much more complex than the standard architecture due to the oxide transport layers in this structure. As Fabricated, the device shows a positive electric field throughout the active layer at reverse bias, and a negative field through approximately half of the active layer in forward bias (operating condition). The raw potential and electric field reveal asymmetric behavior between forward and reverse applied biases, showing a slight positive built-in electric field under short circuit conditions. Annealing increases the electric field magnitude and symmetry between forward and reverse bias in the region of the BHJ near the anode, giving a slight negative electric

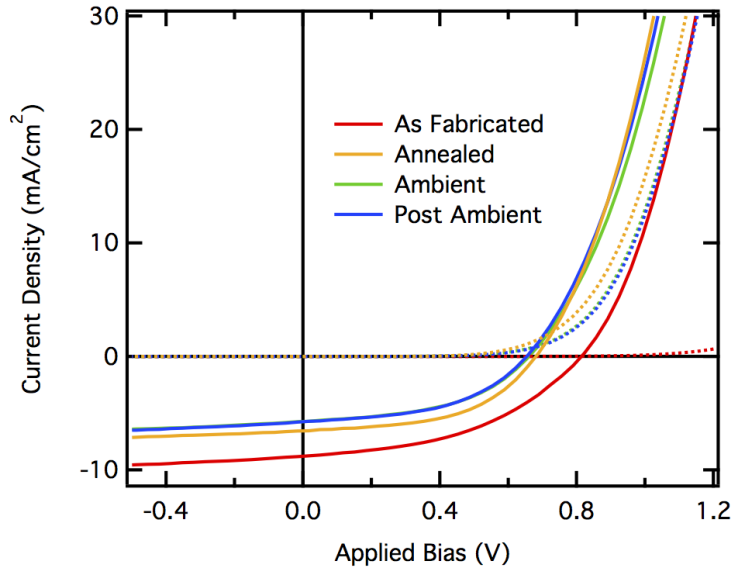


Figure 4.3: Applied voltage vs. current density for the inverted architecture device. Solid lines represent illuminated device characteristics, while dotted lines represent dark.

field across the entirety of the active layer in forward bias.

Biassing the device in air during Ambient measurement gives a similar result as in the standard device: the electric field is localized to the ZnO/BHJ interface, and a field-free region appears in the BHJ near the anode. The electric field magnitude also becomes much more symmetric between forward and reverse bias in this condition. However, the Post-Ambient X-SKPM measurement does not agree with the Ambient measurement as it did for the standard architecture device. Rather, the electric field in the Post-Ambient measurement extends throughout the BHJ, with greater magnitude near the anode and more symmetry between forward and reverse bias than even the As Fabricated or Annealed measurements.

The potential distribution in our As Fabricated measurement of the inverted device is not as close to the expected linear distribution as we found for the standard architecture device. The decrease in electric field in the region of the BHJ near the active layer points to p-doping. However, the active layer has not been exposed to air at this point, so this doping must not originate from oxygen p-doping of P3HT as we explored earlier. Instead, the very high work function of as-deposited MoO_x may cause contact-induced p-doping of the

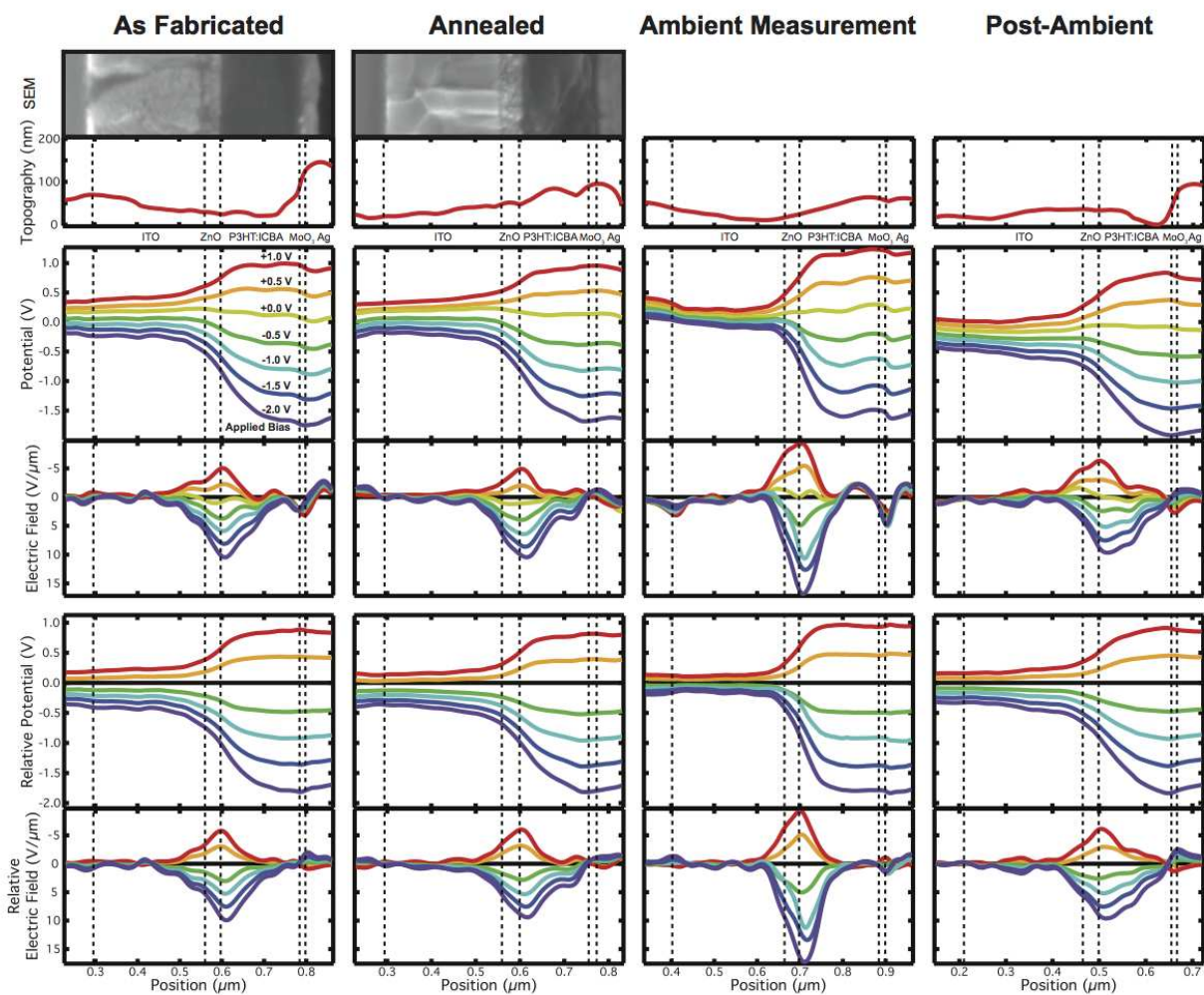


Figure 4.4: X-SKPM results for the inverted architecture device. Colors correspond to the bias applied across the device.

active layer.[139] When the positive integer charge transfer state of the bulk heterojunction is mismatched with the work function of the hole transport layer, electrons flow from the bulk heterojunction to the oxide, effectively p-doping the active layer of the device.[140] Slight p-doping of the active layer would cause the diminished electric field in the BHJ near the anode and the larger field at the ZnO/BHJ interface where a p-n junction would occur between these materials.

Annealing the device at our selected temperature of 140 °C drives excess oxygen out of both the zinc oxide layer and the bulk heterojunction. However, the device has been exposed to air briefly during J-V measurement before the anneal, and this temperature is not high enough to reverse the effect on the work function of MoO_x. Air exposure reduces the work function of MoO_x by up to 0.8 eV,[139] which not only negates the contact-induced doping of the active layer, but also decreases the built-in voltage in the device. A reduction in the built-in voltage decreases the open circuit voltage and short circuit current of the device, consistent with the measured device characteristics for the Annealed solar cell. Reduction of contact-induced doping from MoO_x also agrees with the potential distribution, as the electric field in the BHJ near the HTL has a greater magnitude in the Annealed measurement.

Measuring the device in Ambient conditions introduces oxygen into the BHJ, MoO_x, and ZnO layers. Oxygen exposure causes p-doping of the active layer, as shown in the standard architecture device. Additionally, increasing the oxygen content of ZnO decreases the charge carrier concentration and increases the resistivity of the material.[141] Surface adsorption of hydroxides and hydrogen on ZnO also depletes the surface of electrons and increases the effective work function.[142, 143] In our Ambient X-SKPM measurement, the large electric field at the ZnO/BHJ interface is reflective of the high effective work function ZnO with adsorbed hydroxides. Furthermore, the field-free region in the active layer near MoO_x is characteristic of oxygen p-doping of P3HT.

Returning the device to the nitrogen system highlights the surface effects on zinc oxide. Time-dependent desorption of surface hydrogen and hydroxide from ZnO in a nitrogen envi-

ronment reduces its effective work function over the course of a few hours (within the time scale of our experiment).[144] So in the inverted device, the extension of the electric field across the active layer seems to be almost entirely dependent on the work function of the electron transport layer, ZnO. The effective work function of ZnO is low when the device is in the nitrogen system, and high only while in the ambient AFM. Because this is a surface effect on the exposed cross-section only, the bulk of the device is not affected, and device characteristics remain the same for the Ambient and Post-Ambient measurements. However, this greatly affects the X-SKPM measurements, since the technique directly measures the work function predominantly along the surface of the cross-section. Therefore, we attribute the change in potential distribution between Ambient and Post-Ambient X-SKPM to a shift in the surface work function of ZnO due to hydroxides which absorb on the ZnO surface upon exposure to air. This is further supported by X-SKPM of phosphonic acid modified inverted devices below, where modulating the work function of ZnO by modification with molecular dipoles also changes the shape of the potential distribution. Additionally, the work function of MoO_x has been further reduced by air exposure during Ambient measurement, negating the effects of contact-induced p-doping and increasing the field in the BHJ near the anode.

Modified inverted devices. As has been shown in our previous work, device characteristics are improved by modification of ZnO with oF₂PVPA. Figure 4.5 and Table 4.3 show device characteristics for the unmodified, oF₂PVPA modified, and pCF₃PVPA modified inverted devices after X-SKPM measurement (cleaved). Whole device characteristics are given in Appendix A and do not change significantly with cleaving, but do change during X-SKPM measurement in the glove box. All devices show a mild increase in open circuit voltage after measurement, but the unmodified and pCF₃PVPA modified devices show significant drops in short circuit current and fill factor. Meanwhile the oF₂PVPA modified device shows improved short circuit current and significantly less impact on the fill factor compared to the other devices. Reduced degradation of the phosphonic acid modified devices has been attributed to passivation of interstitial Zn defects on the ZnO surface by the attached molecules.[15]

When compared to the unmodified devices, oF₂PVPA modification significantly improves both short circuit current and fill factor, with minor improvement to the open circuit voltage as well. pCF₃PVPA, on the other hand, has a dipole moment pointing toward the oxide surface that increases the effective work function of the oxide and drastically reduces device performance. The V_{OC}, J_{SC}, FF, and PCE of the pCF₃PVPA modified device are all significantly reduced compared to the unmodified device.

Table 4.3: Modified device characteristics

	$\Delta\phi_{\text{ZnO}}$ (eV) [138]	V _{OC} (V)	J _{SC} (mA/cm ²)	FF (%)	PCE (%)
Unmodified	-	0.82	8.80	44.1	3.19
oF ₂ PVPA	+0.82	0.83	10.79	60.0	5.39
pCF ₃ PVPA	-1.12	0.20	0.49	22.0	0.02

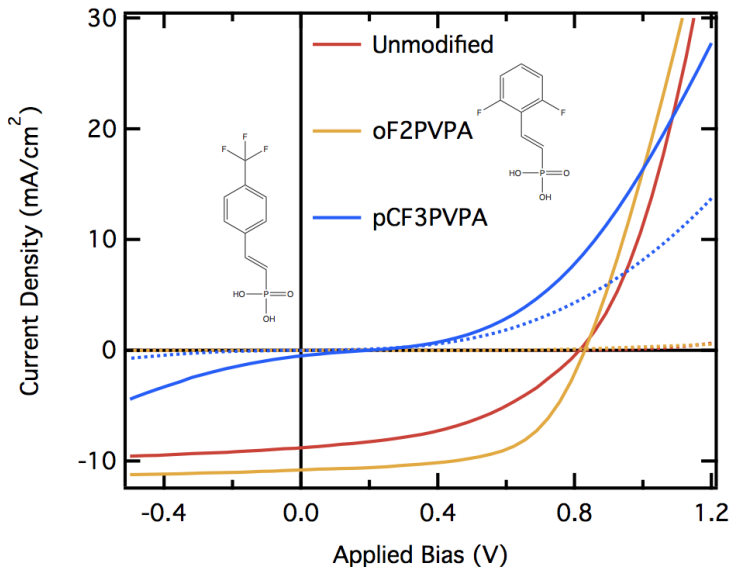


Figure 4.5: Applied voltage vs. current density for the devices listed in Table 4.3. Solid lines represent illuminated device characteristics, dotted lines represent dark. Inset are diagrams of the conjugated phosphonic acids.

The raw potential distribution for the unmodified and modified devices, given in Figure 4.6, show strikingly different line shapes in both forward and reverse applied bias. The unmodified device yields a sloping potential from the cathode into the active layer, with

the electric field extending through the majority of the active layer in reverse bias. The negative electric field in forward bias extends less than 70 nm through the active layer. The oF₂PVPA modified device shows slightly lower magnitude in field at the ZnO/active layer interface, but increased magnitude and greater symmetry of the electric field throughout the remainder of the active layer in forward and reverse bias. The pCF₃PVPA modified device, by contrast, has a much sharper transition from sloped to flat potential in the active layer, and the electric field drops off much more quickly approximately halfway through the active layer. Moreover, the electric field for this device is much more symmetric in field extension between forward and reverse applied bias, unlike the unmodified and oF₂PVPA-modified devices.

The differences in potential distribution correlate well with the performance of these devices. The unmodified device shows a reasonable short circuit current, indicating that carriers are successfully swept out of the device. This is corroborated by good extension of the electric field throughout the device with reverse applied bias (operating condition). oF₂PVPA modification improves both the short circuit current and fill factor of the device, which imply more charge extraction and less recombination. Again, the electric field distribution is consistent with this picture: the field is more uniform through the bulk of the active layer in forward bias, leading to more charge extraction and less chance for recombination. Furthermore, this device has slightly increased open circuit voltage, pointing to less voltage loss at the modified contact. This is also reflected in the electric field, where a slightly lower field magnitude is consistent with lower resistivity at the interface.

The charge density distributions within the modified devices, first derivatives of the electric field distributions given in Figure 4.7, are also telling of device operation. The charge density is a second derivative of the measured potential distribution, so there is significant noise in this data. However, some clues about device operation may still be seen. In the unmodified device, there is a clear barrier for charge extraction at the ZnO/P3HT:ICBA interface, where in operating condition we see positive charges in the ZnO and negative

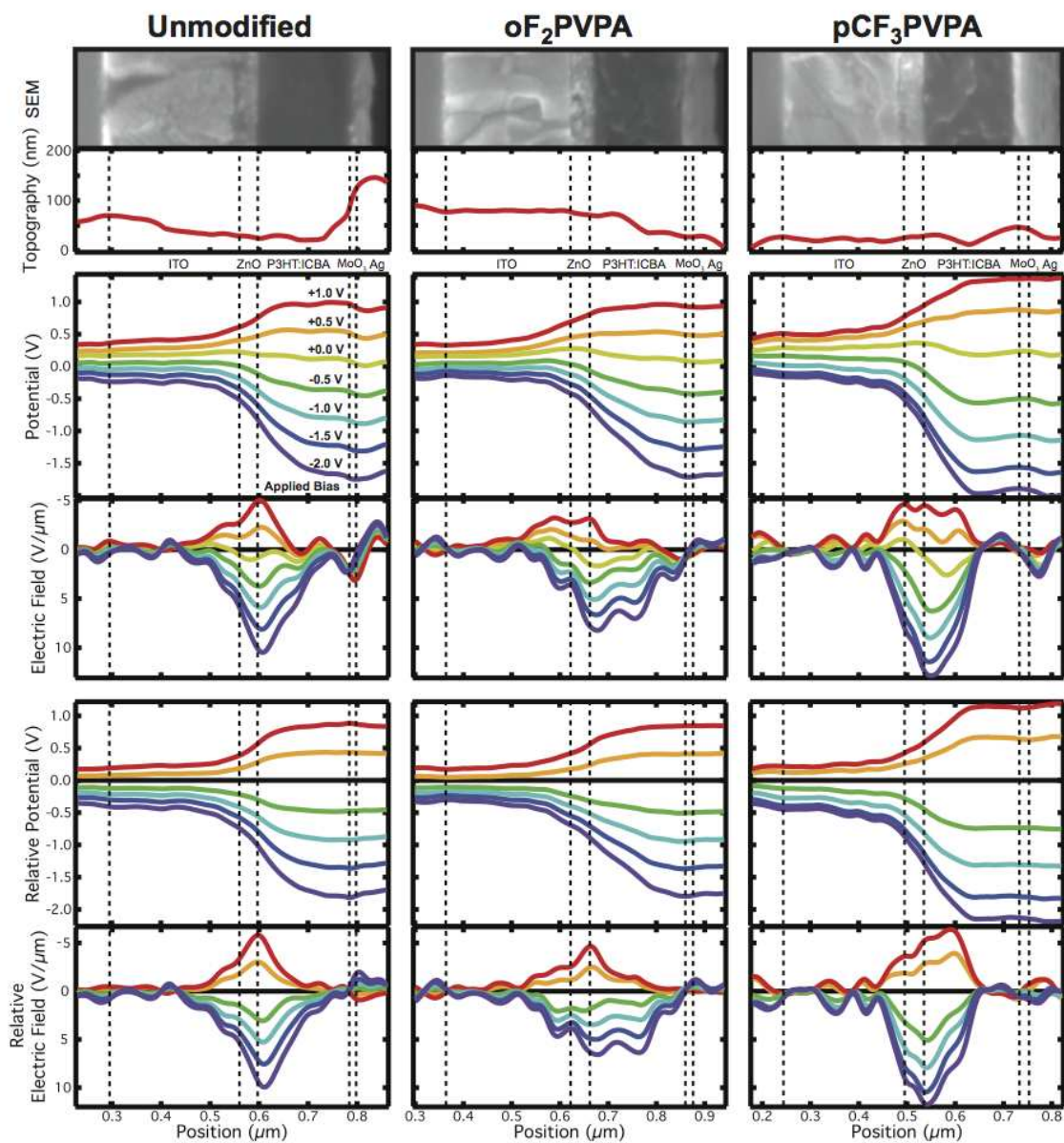


Figure 4.6: SEM images, topography, and raw and relative potential and electric field distributions for the unmodified and modified devices. Colors correspond to applied bias as listed for potential distributions on the unmodified device.

charges in the active layer. This barrier is reduced by oF_2PVPA modification of ZnO, for which we see a smaller buildup of charge on either side of the interface. For pCF_3PVPA modification, there is not simply more charge buildup at the interface. Rather, there appears to be two separate positive/negative charge regions: one at the ZnO/P3HT:ICBA interface, and a second a short distance into the BHJ. This may be caused by the very strong interfacial dipole of pCF_3PVPA opposing the natural work function difference of the interface, forming an energetic barrier for electron extraction to ZnO.

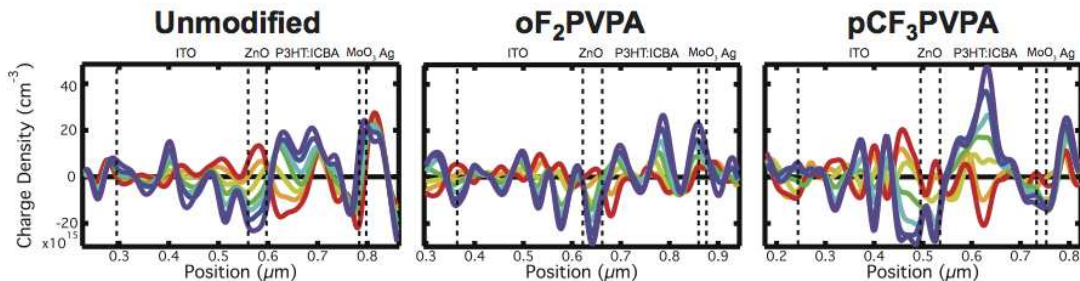


Figure 4.7: Charge density in modified inverted devices. Color scheme follows that of Figure 4.6.

4.4 Conclusions

We have shown that the potential distribution in a standard architecture organic BHJ device is greatly affected by biasing the device in air. In the As Fabricated and As Annealed (maximum efficiency for this device structure) X-SKPM measurements, there exists a near-uniform electric field extending throughout the active layer, aiding in the extraction of charge carriers from the device. Exposure to oxygen causes bulk p-doping of the active layer, causing a field-free region of the BHJ near the anode, and a large magnitude electric field at the cathode/BHJ interface. This has been shown for an oxygen p-doped device measured both in air and in a dry nitrogen system.

An inverted architecture device incorporating a ZnO electron transport layer and a MoO_x hole transport layer also exhibited a difference in the potential distribution upon air exposure,

though we believe the influence of surface effects dominate the behavior of this device. Specifically, ZnO is highly susceptible to adsorption of hydroxides on its surface, causing a much greater effective work function for ZnO on the cross-sectional surface than in the bulk of this device. This change in the ZnO work function manifested as a large electric field at the cathode and a field-free region near the anode only for the device measured in air, as the hydroxides desorb quickly in a dry nitrogen environment.[144]

We also have shown that an organic bulk heterojunction solar cell modified with oF₂PVPA, which has improved device characteristics over the unmodified version, shows an electric field more uniform in magnitude across the entire active layer of the device. Furthermore, our measurements indicate that there is a change in the space charge density within the BHJ as a result of ZnO modification. Field extension reduces recombination and improves charge extraction from the oF₂PVPA modified device, which correlates well with the increase in J_{SC} compared to the unmodified device. Modification with a detrimental molecule, pCF₃PVPA, produces the opposite result, limiting the electric field to a smaller region of the active layer near the pCF₃PVPA modified ZnO, and showing increased resistivity at the cathode interface.

The X-SKPM data we have presented here directly confirms both oxygen p-doping of P3HT-based BHJs, and the effect of surface hydroxides on the work function of ZnO. Furthermore, this study emphasizes the necessity of performing X-SKPM in an inert environment, as previous publications have failed to account for surface effects and active layer doping in the investigation of potential distributions within organic BHJ devices. The correlation of the potential distribution and modified device characteristics is helpful for understanding the role of dipolar molecular modifiers in a broader context, and may influence new methods of increasing device performance.

4.5 Acknowledgments

This work was funded by the U.S. DOE Contract No. DE-AC 3608-GO280308 with the National Renewable Energy Lab through the DOE Solar Energy Technology Program. The

authors thank the group of Alan Sellinger for providing conjugated phosphonic acids. Bobby To provided SEM images of device cross-sections.

CHAPTER 5

GENERAL CONCLUSIONS

Self-assembled monolayers of conjugated phosphonic acids on metal oxides cause large changes in the effective work function without changing the bulk properties of the underlying material. Consequently, these molecules are extremely useful for manipulating the charge transport level of a material, which has been exploited here in organic photovoltaic devices. Energy level tuning at a device interface improves charge collection from the bulk heterojunction, evidenced by increases in both short circuit current and electric field extension within the device. Direct measurement of the potential distribution in organic photovoltaic devices with X-SKPM was shown to be successful in an inert environment. In air, X-SKPM demonstrated the susceptibility of organic solar cells to surface effects on oxide interlayers and oxygen doping of the active layer.

5.1 Discussion and Impact

This work has been successful in advancing the path of dipolar modification of metal oxides for efficiency enhancement in organic solar cells. Consequences of the effect are much further reaching, as this technique may be applied to other device structures and materials, such as Perovskite, quantum dot, or silicon solar cells, organic and inorganic LEDs, and transistors. Because conjugated phosphonic acids bind to metal sites, these molecules may be used on a variety of materials to influence the built-in voltage, charge injection/extraction, and other properties of an electronic device that are influenced by contact work function.

Tuning the effective work function of the electron transport layer in a solar cell was expected to increase the open circuit voltage of the device. While conjugated phosphonic acids were effective in slightly raising the open circuit voltage of inverted bulk heterojunction photovoltaics, short circuit current was also improved with modification. This indicated that

the molecules may influence charge collection mechanics, which was investigated with cross-sectional scanning Kelvin probe microscopy (X-SKPM).

The direct measurement of potential distribution in an operating solar cell with X-SKPM sheds some light on the mechanism for efficiency improvement. Field extension in the active layer corresponding to an increase in the short circuit current signifies that potential distribution plays an important role in charge extraction in a solar cell. Specifically, expansion of the electric field in the active layer points to drift-dominated carrier extraction, rather than diffusion of charges to the contacts as often thought for organic photovoltaics. The field-efficiency correlation also prompts development of other strategies for enhancing the electric field in a device with the intention of improving charge separation and extraction.

Validation of the X-SKPM technique is a major step toward better understanding the operation of organic photovoltaics. Direct measurement of the potential distribution within a device provides the capability to test strategies for increasing the electric field in operational organic solar cells, as well as investigate the roles of various active layer, interlayer, and electrode materials. X-SKPM is also applicable to photovoltaic devices of other materials, depending on the prevalence of electronic defects that may influence the effective work function of the cross-sectional surface. The technique has already been used on quantum dot and Perovskite solar cells, as well as other electronic devices such as FETs and OLEDs. While power conversion efficiency improvement through interfacial modification in organic photovoltaics was realized, many questions about the mechanisms of device improvement remain. For one, electric field extension is shown to correlate with power conversion efficiency in modified devices. However, some studies claim that the field in a device has very little to do with performance. The extent to which the internal electric field influences device operation remains a very important topic that has not been fully explored. Examination of field extension/reduction in the other device structures mentioned could further inform general charge collection mechanics.

Another question raised by this work has to do with the limitations of dipole-induced shifting of the effective work function of a material inside a solar cell. A phosphonic acid was shown to decrease the effective work function of zinc oxide and increase the efficiency of the associated device. A conjugated phosphonic acid with the same aromatic group further decreased the work function, and further improved device characteristics. However the changes in zinc oxide work function did not correspond to expected value increases in the open circuit voltage of devices. The exact relationship between contact work function, built-in voltage, and open circuit voltage of an organic solar cell requires additional consideration. This relationship may also inform the limit of work function reduction/increase for an electron/hole transport layer at which device performance does not improve and contact-induced doping becomes a concern.

5.2 Recommendations for Future Research

The work presented in this thesis gives rise to a number of potential projects to pursue. One such direction is to modify hole transport materials in standard architecture devices to determine if the charge transport level alignment at the electron collector dominates device performance, or if the hole collector influences charge collection in the same way. Work on electron/hole transport material modification easily translates into other device structures and materials. For example, hole transport layer modification would be simplest in a standard architecture device in which the active layer is deposited onto the hole transport material such as nickel oxide. Additionally, several photovoltaic device structures including quantum dot, Perovskite, and bilayer organic solar cells use the same or similar materials for electron and hole collection, making these obvious choices to pursue for molecular dipole modification.

As mentioned earlier, it would also be interesting to push work function modification of a transport layer past the point of device improvement into the regime of contact-induced doping of the active layer. This was briefly addressed in this work with the use of MoO_x , which is a hole transport layer that has a very high work function when thermally evapo-

rated. However, systematically controlling the behavior of devices through the maximum performance of the materials with molecular modifiers may provide insight into the transport layer work function/built-in voltage/open circuit voltage relationship.

Cross-sectional scanning Kelvin probe microscopy also lends itself to these potential research topics, as the trend shown here between device performance and electric field could be tested in other types of solar cells. Specifically, modifying the electron transport layer titanium dioxide and measuring the potential distribution in quantum dot solar cells would be an interesting corollary to this work. Since X-SKPM is sensitive to doping of the active layer, it would also be of use for detecting contact-induced doping at extreme work functions of transport layer materials. Furthermore, because it is reliable in measuring the potential distribution in a device, it is capable of determining the effectiveness of methods for increasing the electric field in organic and hybrid solar cells such as morphology-controlled active layers, nanowire photoanodes, and ferroelectric polymers.

REFERENCES CITED

- [1] Slawomir Braun, William R Salaneck, and Mats Fahlman. Energy-Level Alignment at Organic/Metal and Organic/Organic Interfaces. *Adv. Mater.*, 21(14-15):1450–1472, 2009.
- [2] Yongye Liang and Luping Yu. A New Class of Semiconducting Polymers for Bulk Heterojunction Solar Cells with Exceptionally High Performance. *Acc. Chem. Res.*, 43(9):1227–1236, 2010.
- [3] E Bundgaard and F C Krebs. Low band gap polymers for organic photovoltaics. *Sol. Energy Mater. Sol. Cells*, 91(11):954–985, 2007.
- [4] Yen-Ju Cheng, Sheng-Hsiung Yang, and Chain-Shu Hsu. Synthesis of Conjugated Polymers for Organic Solar Cell Applications. *Chem. Rev.*, 109(11):5868–5923, 2009.
- [5] Youjun He, Hsiang-Yu Chen, Jianhui Hou, and Yongfang Li. Indene C60 Bisadduct: A New Acceptor for High-Performance Polymer Solar Cells. *J. Am. Chem. Soc.*, 132(4):1377–1382, 2010.
- [6] Jean Roncali. Molecular Bulk Heterojunctions: An Emerging Approach to Organic Solar Cells. *Acc. Chem. Res.*, 42(11):1719–1730, 2009.
- [7] Hin-Lap Yip and Alex K Y Jen. Recent advances in solution-processed interfacial materials for efficient and stable polymer solar cells. *Energy Environ. Sci.*, 5(3):5995–6011, 2012.
- [8] Roland Steim, F René Kogler, and Christoph J Brabec. Interface materials for organic solar cells. *J. Mater. Chem.*, 20(13):2499–2512, 2010.
- [9] V D Mihailetschi, P W M Blom, J C Hummelen, and M T Rispen. Cathode dependence of the open-circuit voltage of polymer:fullerene bulk heterojunction solar cells. *J. Appl. Phys.*, 94(10):6849–6854, 2003.
- [10] Riccardo Po, Chiara Carbonera, Andrea Bernardi, and Nadia Camaioni. The role of buffer layers in polymer solar cells. *Energy Environ. Sci.*, 4(2):285–310, 2011.
- [11] Li-Min Chen, Zheng Xu, Ziruo Hong, and Yang Yang. Interface investigation and engineering – achieving high performance polymer photovoltaic devices. *J. Mater. Chem.*, 20(13):2575–2598, 2010.

- [12] M S White, D C Olson, S E Shaheen, N Kopidakis, and D S Ginley. Inverted bulk-heterojunction organic photovoltaic device using a solution-derived ZnO underlayer. *Appl. Phys. Lett.*, 89(14):143517, 2006.
- [13] Yanming Sun, Jung Hwa Seo, Christopher J Takacs, Jason Seifter, and Alan J Heeger. Inverted Polymer Solar Cells Integrated with a Low-Temperature-Annealed Sol-Gel-Derived ZnO Film as an Electron Transport Layer. *Adv. Mater.*, 23(14):1679–1683, 2011.
- [14] A K K Kyaw, X W Sun, C Y Jiang, G Q Lo, D W Zhao, and D L Kwong. An inverted organic solar cell employing a sol-gel derived ZnO electron selective layer and thermal evaporated MoO₃ hole selective layer. *Appl. Phys. Lett.*, 93(22):221107, 2008.
- [15] Bradley A MacLeod, Bertrand J Tremolet de Villers, Philip Schulz, Paul F Ndione, Hyungchul Kim, Anthony J Giordano, Kai Zhu, Seth R Marder, Samuel Graham, Joseph J Berry, Antoine Kahn, and Dana C Olson. Stability of inverted organic solar cells with ZnO contact layers deposited from precursor solutions. *Energy Environ. Sci.*, 8:592–601, 2015.
- [16] Sarah R Cowan, Philip Schulz, Anthony J Giordano, Andres Garcia, Bradley A MacLeod, Seth R Marder, Antoine Kahn, David S Ginley, Erin L Ratcliff, and Dana C Olson. Chemically Controlled Reversible and Irreversible Extraction Barriers Via Stable Interface Modification of Zinc Oxide Electron Collection Layer in Polycarbazole-based Organic Solar Cells. *Adv. Funct. Mater.*, 24(29):4671–4680, 2014.
- [17] G Frank and H Kostlin. Electrical Properties and Defect Model of Tin-Doped Indium Oxide Layers. *Appl. Phys. A*, 27:197–206, 1982.
- [18] M J Alam and D C Cameron. Preparation and properties of transparent conductive aluminum-doped zinc oxide thin films by sol-gel process. *J. Vac. Sci. Technol. A*, 19(4):1642–1646, 2001.
- [19] Erin L Ratcliff, Ajaya K Sigdel, Mariola R Macech, Kenneth Nebesny, Paul A Lee, David S Ginley, Neal R Armstrong, and Joseph J Berry. Surface composition, work function, and electrochemical characteristics of gallium-doped zinc oxide. *Thin Solid Films*, 520(17):5652–5663, 2012.
- [20] D C Olson, S E Shaheen, M S White, W J Mitchell, M F A M van Hest, R T Collins, and D S Ginley. Band-Offset Engineering for Enhanced Open-Circuit Voltage in Polymer-Oxide Hybrid Solar Cells. *Adv. Funct. Mater.*, 17(2):264–269, 2007.
- [21] Enrique D Gomez and Yueh-Lin Loo. Engineering the organic semiconductor-electrode interface in polymer solar cells. *J. Mater. Chem.*, 20(32):6604–6611, 2010.

- [22] Hong Ma, Hin-Lap Yip, Fei Huang, and Alex K Y Jen. Interface Engineering for Organic Electronics. *Adv. Funct. Mater.*, 20(9):1371–1388, 2010.
- [23] Chao-Hsiang Hsieh, Yen-Ju Cheng, Pei-Jung Li, Chiu-Hsiang Chen, Martin Dubosc, Ru-Meng Liang, and Chain-Shu Hsu. Highly Efficient and Stable Inverted Polymer Solar Cells Integrated with a Cross-Linked Fullerene Material as an Interlayer. *J. Am. Chem. Soc.*, 132(13):4887–4893, 2010.
- [24] Tobias Stubhan, Michael Salinas, Alexander Ebel, Frederick C Krebs, Andreas Hirsch, Marcus Halik, and Christoph J Brabec. Increasing the Fill Factor of Inverted P3HT:PCBM Solar Cells Through Surface Modification of Al-Doped ZnO via Phosphonic Acid-Anchored C60 SAMs. *Adv. Funct. Mater.*, 2(5):532–535, 2012.
- [25] Steven K Hau, Hin-Lap Yip, Orb Acton, Nam Seob Baek, Hong Ma, and Alex K Y Jen. Interfacial modification to improve inverted polymer solar cells. *J. Mater. Chem.*, 18(42):5113–5119, 2008.
- [26] Matthew T Lloyd, Craig H Peters, Andres Garcia, Isaac V Kauvar, Joseph J Berry, Matthew O Reese, Michael D McGehee, David S Ginley, and Dana C Olson. Influence of the hole-transport layer on the initial behavior and lifetime of inverted organic photovoltaics. *Sol. Energy Mater. Sol. Cells*, 95(5):1382–1388, 2011.
- [27] Bonan Kang, L W Tan, and S R P Silva. Fluoropolymer indium-tin-oxide buffer layers for improved power conversion in organic photovoltaics. *Appl. Phys. Lett.*, 93(13):133302, 2008.
- [28] Thomas M Brenner. *Alternatives to Organic Acid Surface Modification of ZnO for Excitonic Photovoltaics*. PhD thesis, Colorado School of Mines, 2014.
- [29] Oliver T Hofmann, Jan-Christoph Deinert, Yong Xu, Patrick Rinke, Julia Stähler, Martin Wolf, and Matthias Scheffler. Large work function reduction by adsorption of a molecule with a negative electron affinity: Pyridine on ZnO(1010). *J. Chem. Phys.*, 139(17):174701, 2013.
- [30] Rose E Ruther, Ryan Franking, Alex M Huhn, Jaritza Gomez-Zayas, and Robert J Hamers. Formation of Smooth, Conformal Molecular Layers on ZnO Surfaces via Photochemical Grafting. *Langmuir*, 27(17):10604–10614, 2011.
- [31] Adi Salomon, Dvora Berkovich, and David Cahen. Molecular modification of an ionic semiconductor–metal interface: ZnO/molecule/Au diodes. *Appl. Phys. Lett.*, 82(7):1051–1053, 2003.

- [32] Hin-Lap Yip, Steven K Hau, Nam Seob Baek, and Alex K Y Jen. Self-assembled monolayer modified ZnO/metal bilayer cathodes for polymer/fullerene bulk-heterojunction solar cells. *Appl. Phys. Lett.*, 92(19):193313, 2008.
- [33] Hin-Lap Yip, Steven K Hau, Nam Seob Baek, Hong Ma, and Alex K Y Jen. Polymer Solar Cells That Use Self-Assembled-Monolayer- Modified ZnO/Metals as Cathodes. *Adv. Mater.*, 20(12):2376–2382, 2008.
- [34] C G Allen, D J Baker, T M Brenner, C C Weigand, J M Albin, K X Steirer, D C Olson, C Ladam, D S Ginley, R T Collins, and T E Furtak. Alkyl Surface Treatments of Planar Zinc Oxide in Hybrid Organic/Inorganic Solar Cells. *J. Phys. Chem. C*, 116(16):8872–8880, 2012.
- [35] Thomas M Brenner, Gang Chen, Erich P Meinig, Darick J Baker, Dana C Olson, Reuben T Collins, and Thomas E Furtak. Tuning zinc oxide/organic energy level alignment using mixed triethoxysilane monolayers. *J. Mater. Chem. C*, 1(37):5935, 2013.
- [36] Ye Eun Ha, Mi Young Jo, Juyun Park, Yong-Cheol Kang, Seong Il Yoo, and Joo Hyun Kim. Inverted Type Polymer Solar Cells with Self-Assembled Monolayer Treated ZnO. *J. Phys. Chem. C*, 117(6):2646–2652, 2013.
- [37] Zheng Xu, Li-Min Chen, Guanwen Yang, Chun-Hao Huang, Jianhui Hou, Yue Wu, Gang Li, Chain-Shu Hsu, and Yang Yang. Vertical Phase Separation in Poly(3-hexylthiophene): Fullerene Derivative Blends and its Advantage for Inverted Structure Solar Cells. *Adv. Funct. Mater.*, 19(8):1227–1234, 2009.
- [38] Mariano Campoy-Quiles, Toby Ferenczi, Tiziano Agostinelli, Pablo G Etchegoin, Youngkyoo Kim, Thomas D Anthopoulos, Paul N Stavrinou, Donal D C Bradley, and Jenny Nelson. Morphology evolution via self-organization and lateral and vertical diffusion in polymer:fullerene solar cell blends. *Nat. Mater.*, 7(2):158–164, 2008.
- [39] David S Germack, Calvin K Chan, R Joseph Kline, Daniel A Fischer, David J Gundlach, Michael F Toney, Lee J Richter, and Dean M DeLongchamp. Interfacial Segregation in Polymer/Fullerene Blend Films for Photovoltaic Devices. *Macromolecules*, 43(8):3828–3836, 2010.
- [40] Xavier Bulliard, Soo-Ghang Ihn, Sungyoung Yun, Yungi Kim, Dukhyun Choi, Jae-Young Choi, Min Kim, Myungsun Sim, Jong-Hwan Park, Woong Choi, and Kilwon Cho. Enhanced Performance in Polymer Solar Cells by Surface Energy Control. *Adv. Funct. Mater.*, 20(24):4381–4387, 2010.

- [41] Todd C Monson, Matthew T Lloyd, Dana C Olson, Yun-Ju Lee, and Julia W P Hsu. Photocurrent Enhancement in Polythiophene- and Alkanethiol-Modified ZnO Solar Cells. *Adv. Mater.*, 20(24):4755–4759, 2008.
- [42] Emanuele Smecca, Alessandro Motta, Maria Elena Fragalà, Yana Aleeva, and Guglielmo Guido Condorelli. Spectroscopic and Theoretical Study of the Grafting Modes of Phosphonic Acids on ZnO Nanorods. *J. Phys. Chem. C*, 117(10):5364–5372, 2013.
- [43] Christopher Wood, Hong Li, Paul Winget, and Jean-Luc Bredas. Binding Modes of Fluorinated Benzylphosphonic Acids on the Polar ZnO Surface and Impact on Work Function. *J. Phys. Chem. C*, 116(36):19125–19133, 2012.
- [44] Peter J Hotchkiss, Michał Malicki, Anthony J Giordano, Neal R Armstrong, and Seth R Marder. Characterization of phosphonic acid binding to zinc oxide. *J. Mater. Chem.*, 21(9):3107–3112, 2011.
- [45] Jixin Chen, Rose E Ruther, Yizheng Tan, Lee M Bishop, and Robert J Hamers. Molecular Adsorption on ZnO(1010) Single-Crystal Surfaces: Morphology and Charge Transfer. *Langmuir*, 28(28):10437–10445, 2012.
- [46] Craig L Perkins. Molecular Anchors for Self-Assembled Monolayers on ZnO: A Direct Comparison of the Thiol and Phosphonic Acid Moieties. *J. Phys. Chem. C*, 113(42):18276–18286, 2009.
- [47] Olena Taratula, Elena Galoppini, Dong Wang, Dorothy Chu, Zheng Zhang, Hanhong Chen, Gaurav Saraf, and Yicheng Lu. Binding Studies of Molecular Linkers to ZnO and MgZnO Nanotip Films. *J. Phys. Chem. B*, 110(13):6506–6515, 2006.
- [48] Beibei Zhang, Tao Kong, Wenzhi Xu, Ruigong Su, Yunhua Gao, and Guosheng Cheng. Surface Functionalization of Zinc Oxide by Carboxyalkylphosphonic Acid Self-Assembled Monolayers. *Langmuir*, 26(6):4514–4522, 2010.
- [49] Hong Li, Erin L Ratcliff, Ajaya K Sigdel, Anthony J Giordano, Seth R Marder, Joseph J Berry, and Jean-Luc Bredas. Modification of the Gallium-Doped Zinc Oxide Surface with Self-Assembled Monolayers of Phosphonic Acids: A Joint Theoretical and Experimental Study. *Adv. Funct. Mater.*, 24(23):3593–3603, 2014.
- [50] Anuradha Bulusu, Sergio A Paniagua, Bradley A MacLeod, Ajaya K Sigdel, Joseph J Berry, Dana C Olson, Seth R Marder, and Samuel Graham. Efficient Modification of Metal Oxide Surfaces with Phosphonic Acids by Spray Coating. *Langmuir*, 29(12):3935–3942, 2013.

- [51] Jaemin Kong, Jongjin Lee, Yonkil Jeong, Maengjun Kim, Sung-Oong Kang, and Kwanghee Lee. Biased internal potential distributions in a bulk-heterojunction organic solar cell incorporated with a TiOx interlayer. *Appl. Phys. Lett.*, 100(21):213305, 2012.
- [52] Jongjin Lee, Jaemin Kong, Heejoo Kim, Sung-Oong Kang, and Kwanghee Lee. Direct observation of internal potential distributions in a bulk heterojunction solar cell. *Appl. Phys. Lett.*, 99(24):243301, 2011.
- [53] L J A Koster, E C P Smits, V D Mihailetschi, and P W M Blom. Device model for the operation of polymer/fullerene bulk heterojunction solar cells. *Phys. Rev. B*, 72(8):085205, 2005.
- [54] Carsten Deibel and Vladimir Dyakonov. Polymer–fullerene bulk heterojunction solar cells. *Rep. Prog. Phys.*, 73(9):096401, 2010.
- [55] Juan Bisquert and Germà Garcia-Belmonte. On Voltage, Photovoltage, and Photocurrent in Bulk Heterojunction Organic Solar Cells. *J. Phys. Chem. Lett.*, 2(15):1950–1964, 2011.
- [56] J D Morris, Timothy L Atallah, Christopher J Lombardo, Heungman Park, Ananth Dodabalapur, and X Y Zhu. Mapping electric field distributions in biased organic bulk heterojunctions under illumination by nonlinear optical microscopy. *Appl. Phys. Lett.*, 102(3):033301, 2013.
- [57] Anthony J Morfa, Alexandre M Nardes, Sean E Shaheen, Nikos Kopidakis, and Jao van de Lagemaat. Time-of-Flight Studies of Electron-Collection Kinetics in Polymer:Fullerene Bulk-Heterojunction Solar Cells. *Adv. Funct. Mater.*, 21(13):2580–2586, 2011.
- [58] V D Mihailetschi, J Wildeman, and P W M Blom. Space-Charge Limited Photocurrent. *Phys. Rev. Lett.*, 94(12):126602, 2005.
- [59] Wolfgang Tress and Olle Inganäs. Simple experimental test to distinguish extraction and injection barriers at the electrodes of (organic) solar cells with S-shaped current–voltage characteristics. *Sol. Energy Mater. Sol. Cells*, 117(C):599–603, 2013.
- [60] Andrea Seemann, Tobias Sauermann, Christoph Lungenschmied, Oskar Armbruster, Siegfried Bauer, H J Egelhaaf, and Jens Hauch. Reversible and irreversible degradation of organic solar cell performance by oxygen. *Sol. Energy*, 85(6):1238–1249, 2011.
- [61] Germà Garcia-Belmonte, Antoni Munar, Eva M Barea, Juan Bisquert, Irati Ugarte, and Roberto Pacios. Charge carrier mobility and lifetime of organic bulk heterojunctions analyzed by impedance spectroscopy. *Org. Electron.*, 9(5):847–851, 2008.

- [62] Evan J Spadafora, Renaud Demadrille, Bernard Ratier, and Benjamin Grévin. Imaging the Carrier Photogeneration in Nanoscale Phase Segregated Organic Heterojunctions by Kelvin Probe Force Microscopy. *Nano Lett.*, 10(9):3337–3342, 2010.
- [63] Thilo Glatzel, Harald Hoppe, Niyazi S Sariciftci, Martha Ch Lux-Steiner, and Masaharu Komiyama. Kelvin Probe Force Microscopy Study of Conjugated Polymer/Fullerene Organic Solar Cells. *Jpn. J. Appl. Phys.*, 44(7B):5370–5373, 2005.
- [64] H Hoppe, T Glatzel, M Niggemann, A Hinsch, M Ch Lux-Steiner, and N S Sariciftci. Kelvin Probe Force Microscopy Study on Conjugated Polymer/Fullerene Bulk Heterojunction Organic Solar Cells. *Nano Lett.*, 5(2):269–274, 2005.
- [65] Rudiger Berger, Anna L Domanski, and Stefan A L Weber. Electrical characterization of organic solar cell materials based on scanning force microscopy. *Eur. Polym. J.*, 49(8):1907–1915, 2013.
- [66] Rebecca Saive, Michael Scherer, Christian Mueller, Dominik Daume, Janusz Schinke, Michael Kroeger, and Wolfgang Kowalsky. Imaging the Electric Potential within Organic Solar Cells. *Adv. Funct. Mater.*, 23(47):5854–5860, 2013.
- [67] Qi Chen, Lin Mao, Yaowen Li, Tao Kong, Na Wu, Changqi Ma, Sai Bai, Yizheng Jin, Dan Wu, Wei Lu, Bing Wang, and Liwei Chen. Quantitative operando visualization of the energy band depth profile in solar cells. *Nat. Commun.*, 6:1–9, 2015.
- [68] Michael Scherer, Rebecca Saive, Dominik Daume, Michael Kröger, and Wolfgang Kowalsky. Sample preparation for scanning Kelvin probe microscopy studies on cross sections of organic solar cells. *AIP Adv.*, 3(9):092134, 2013.
- [69] Sanjini U. Nanayakkara, Jao van de Lagemaat, and Joseph M. Luther. Scanning probe characterization of heterostructured colloidal nanomaterials. *Chem. Rev.*, 115(16):8157–8181, 2015. doi: 10.1021/cr500280t.
- [70] Zhicai He, Chengmei Zhong, Shijian Su, Miao Xu, Hongbin Wu, and Yong Cao. Enhanced power-conversion efficiency in polymersolar cells using an inverted device structure. *Nat. Photonics*, 6(9):591–595, 2012.
- [71] Jingbi You, Letian Dou, Ken Yoshimura, Takehito Kato, Kenichiro Ohya, Tom Moriarty, Keith Emery, Chun-Chao Chen, Jing Gao, Gang Li, and Yang Yang. A polymer tandem solar cell with 10.6% power conversion efficiency. *Nat. Commun.*, 4:1446–10, 2013.

- [72] Bradley A MacLeod, Philip Schulz, Sarah R Cowan, Andres Garcia, David S Ginley, Antoine Kahn, and Dana C Olson. Improved Performance in Bulk Heterojunction Organic Solar Cells with a Sol-Gel MgZnO Electron-Collecting Layer. *Adv. Funct. Mater.*, 4(13):1400073, 2014.
- [73] Jong Soo Kim, Jong-Hwan Park, Ji Hwang Lee, Jang Jo, Dong-Yu Kim, and Kilwon Cho. Control of the electrode work function and active layer morphology via surface modification of indium tin oxide for high efficiency organic photovoltaics. *Appl. Phys. Lett.*, 91(11):112111, 2007.
- [74] Erin L Ratcliff, Andres Garcia, Sergio A Paniagua, Sarah R Cowan, Anthony J Giordano, David S Ginley, Seth R Marder, Joseph J Berry, and Dana C Olson. Investigating the Influence of Interfacial Contact Properties on Open Circuit Voltages in Organic Photovoltaic Performance: Work Function Versus Selectivity. *Adv. Funct. Mater.*, 3(5):647–656, 2013.
- [75] Kristina M Knesting, Huanxin Ju, Cody W Schlenker, Anthony J Giordano, Andres Garcia, O’Neil L Smith, Dana C Olson, Seth R Marder, and David S Ginger. ITO Interface Modifiers Can Improve Voc in Polymer Solar Cells and Suppress Surface Recombination. *J. Phys. Chem. Lett.*, 4(23):4038–4044, 2013.
- [76] Eric L Hanson, Jing Guo, Norbert Koch, Jeffrey Schwartz, and Steven L Bernasek. Advanced Surface Modification of Indium Tin Oxide for Improved Charge Injection in Organic Devices. *J. Am. Chem. Soc.*, 127(28):10058–10062, 2005.
- [77] Asha Sharma, Peter J Hotchkiss, Seth R Marder, and Bernard Kippelen. Tailoring the work function of indium tin oxide electrodes in electrophosphorescent organic light-emitting diodes. *J. Appl. Phys.*, 105(8):084507, 2009.
- [78] Baohua Zhang, Chuanjiang Qin, Xiaodi Niu, Zhiyuan Xie, Yanxiang Cheng, Lixiang Wang, and Xinglin Li. On the origin of efficient electron injection at phosphonate-functionalized polyfluorene/aluminum interface in efficient polymer light-emitting diodes. *Appl. Phys. Lett.*, 97(4):043506, 2010.
- [79] Bradley A MacLeod, Noah E Horwitz, Erin L Ratcliff, Judith L Jenkins, Neal R Armstrong, Anthony J Giordano, Peter J Hotchkiss, Seth R Marder, Charles T Campbell, and David S Ginger. Built-In Potential in Conjugated Polymer Diodes with Changing Anode Work Function: Interfacial States and Deviation from the Schottky–Mott Limit. *J. Phys. Chem. Lett.*, 3(9):1202–1207, 2012.
- [80] Hong Li, Pavel Paramonov, and Jean-Luc Bredas. Theoretical study of the surface modification of indium tin oxide with trifluorophenyl phosphonic acid molecules: impact of coverage density and binding geometry. *J. Mater. Chem.*, 20(13):2630–2637, 2010.

- [81] Peter J Hotchkiss, Hong Li, Pavel B Paramonov, Sergio A Paniagua, Simon C Jones, Neal R Armstrong, Jean-Luc Bredas, and Seth R Marder. Modification of the Surface Properties of Indium Tin Oxide with Benzylphosphonic Acids: A Joint Experimental and Theoretical Study. *Adv. Mater.*, 21(44):4496–4501, 2009.
- [82] Georg Heimel, Lorenz Romaner, Egbert Zojer, and Jean-Luc Bredas. Toward Control of the Metal-Organic Interfacial Electronic Structure in Molecular Electronics: A First-Principles Study on Self-Assembled Monolayers of π -Conjugated Molecules on Noble Metals. *Nano Lett.*, 7(4):932–940, 2007.
- [83] Peter J Hotchkiss, Simon C Jones, Sergio A Paniagua, Asha Sharma, Bernard Kippelen, Neal R Armstrong, and Seth R Marder. The Modification of Indium Tin Oxide with Phosphonic Acids: Mechanism of Binding, Tuning of Surface Properties, and Potential for Use in Organic Electronic Applications. *Acc. Chem. Res.*, 45(3):337–346, 2012.
- [84] Asha Sharma, Andreas Haldi, Peter J Hotchkiss, Seth R Marder, and Bernard Kippelen. Effect of phosphonic acid surface modifiers on the work function of indium tin oxide and on the charge injection barrier into organic single-layer diodes. *J. Appl. Phys.*, 105(7):074511, 2009.
- [85] Kristina M Knesting, Peter J Hotchkiss, Bradley A MacLeod, Seth R Marder, and David S Ginger. Spatially Modulating Interfacial Properties of Transparent Conductive Oxides: Patterning Work Function with Phosphonic Acid Self-Assembled Monolayers. *Adv. Mater.*, 24(5):642–646, 2011.
- [86] Matthew Gliboff, Lingzi Sang, Kristina M Knesting, Matthew C Schalnath, Anoma Mudalige, Erin L Ratcliff, Hong Li, Ajaya K Sigdel, Anthony J Giordano, Joseph J Berry, Dennis Nordlund, Gerald T Seidler, Jean-Luc Bredas, Seth R Marder, Jeanne E Pemberton, and David S Ginger. Orientation of Phenylphosphonic Acid Self-Assembled Monolayers on a Transparent Conductive Oxide: A Combined NEXAFS, PM-IRRAS, and DFT Study. *Langmuir*, 29(7):2166–2174, 2013.
- [87] Leslie Charles Thomas. Interpretation of the Infrared Spectra of Organophosphorus Compounds. Heyden: London, 1st edition, 1974.
- [88] Sergio A Paniagua, Peter J Hotchkiss, Simon C Jones, Seth R Marder, Anoma Mudalige, F Saneeha Marrikar, Jeanne E Pemberton, and Neal R Armstrong. Phosphonic Acid Modification of Indium Tin Oxide Electrodes: Combined XPS/UPS/Contact Angle Studies. *J. Phys. Chem. C*, 112(21):7809–7817, 2008.
- [89] Mark T Greiner. Universal energy-level alignment of molecules on metal oxides. *Nat. Mater.*, 11(1):76–81, 2011.

- [90] Walid Al-Maksoud, Julien Mesnager, Farouk Jaber, Catherine Pinel, and Laurent Djakovitch. Synthesis of diethyl 2-(aryl)vinylphosphonates by the Heck reaction catalysed by well-defined palladium complexes. *J. Organomet. Chem.*, 694(20):3222–3231, 2009.
- [91] Pijus K Mandal and John S McMurray. Pd-C-Induced Catalytic Transfer Hydrogenation with Triethylsilane. *J. Org. Chem.*, 72(17):6599–6601, 2007.
- [92] Tae-Jun Ha and Ananth Dodabalapur. Photo stability of solution-processed low-voltage high mobility zinc-tin-oxide/ZrO₂ thin-film transistors for transparent display applications. *Appl. Phys. Lett.*, 102(12):123506, 2013.
- [93] Bo Sung Kim, Yeon Taek Jeong, Doohyoung Lee, TaeYoung Choi, Seung-Ho Jung, June Whan Choi, Chanwoo Yang, Kangmoon Jo, Byung-ju Lee, Eunhye Park, Doo Na Kim, Youngmin Kim, and Sungtae Shin. Solution-processed zinc-indium-tin oxide thin-film transistors for flat-panel displays. *Appl. Phys. Lett.*, 103(7):072110, 2013.
- [94] Duo Li, Juncong She, Shaozeng Xu, and Shaozhi Deng. Zinc Oxide Nanowire Lateral Field Emission Devices and its Application as Display Pixel Structures. *IEEE Trans. Electron Devices*, 60(9):2924–2930, 2013.
- [95] Tae Sang Kim, Joon Seok Park, Kyoung Seok Son, Ji Sim Jung, Kwang-Hee Lee, Wan Joo Maeng, Hyun-Suk Kim, Jang-Yeon Kwon, Bonwon Koo, and Sangyun Lee. Transparent AMOLED display driven by hafnium-indium-zinc oxide thin film transistor array. *Curr. Appl. Phys.*, 11(5):1253–1256, 2011.
- [96] Sang-Hee K Park, Chi-Sun Hwang, Minki Ryu, Shinhyuk Yang, Chunwon Byun, Jaeheon Shin, Jeong-Ik Lee, Kimoon Lee, Min Suk Oh, and Seongil Im. Transparent and Photo-stable ZnO Thin-film Transistors to Drive an Active Matrix Organic-Light-Emitting-Diode Display Panel. *Adv. Mater.*, 21(6):678–682, 2009.
- [97] Thomas R Andersen, Henrik F Dam, Birgitta Andreasen, Markus Hösel, Morten V Madsen, Suren A Gevorgyan, Roar R Søndergaard, Mikkel Jørgensen, and Fredrik C Krebs. A rational method for developing and testing stable flexible indium- and vacuum-free multilayer tandem polymer solar cells comprising up to twelve roll processed layers. *Sol. Energy Mater. Sol. Cells*, 120:735–743, 2014.
- [98] Ingrid Repins, Miguel A Contreras, Brian Egaas, Clay DeHart, John Scharf, Craig L Perkins, Bobby To, and Rommel Noufi. 19.9%-efficient ZnO/CdS/CuInGaSe₂ solar cell with 81.2% fill factor. *Prog. Photovolt: Res. Appl.*, 16(3):235–239, 2008.
- [99] Ning Zhang, Ke Yu, Qiong Li, Changqing Song, Lei Zhu, and Ziqiang Zhu. Room-temperature blue/violet laser emission from individual ultra-long ZnO microbelts. *Mater. Lett.*, 121(C):231–233, 2014.

- [100] T Pauporté, D Lincot, B Viana, and F Pellé. Toward laser emission of epitaxial nanorod arrays of ZnO grown by electrodeposition. *Appl. Phys. Lett.*, 89(23):233112, 2006.
- [101] Z K Tang, G K L Wong, P Yu, M Kawasaki, A Ohtomo, H Koinuma, and Y Segawa. Room-temperature ultraviolet laser emission from self-assembled ZnO microcrystallite thin films. *Appl. Phys. Lett.*, 72(25):3270–3272, 1998.
- [102] F H Nicoll. Ultraviolet ZnO Laser Pumped by an Electron Beam. *Appl. Phys. Lett.*, 9(1):13–15, 1966.
- [103] R Baraki, N Novak, T Frömling, T Granzow, and J Rödel. Bulk ZnO as piezotronic pressure sensor. *Appl. Phys. Lett.*, 105(11):111604, 2014.
- [104] Changjing Shao, Yongqin Chang, and Yi Long. High performance of nanostructured ZnO film gas sensor at room temperature. *Sens. Actuators, B*, 204:666–672, 2014.
- [105] Q Wan, Q H Li, Y J Chen, T H Wang, X L He, J P Li, and C L Lin. Fabrication and ethanol sensing characteristics of ZnO nanowire gas sensors. *Appl. Phys. Lett.*, 84(18):3654–3656, 2004.
- [106] P Mitra, A P Chatterjee, and H S Maiti. ZnO thin film sensor. *Mater. Lett.*, 35:33–38, 1998.
- [107] Xuan Sang Nguyen, Chuan Beng Tay, Eugene A Fitzgerald, and Soo Jin Chua. ZnO Coaxial Nanorod Homojunction UV Light-Emitting Diodes Prepared by Aqueous Solution Method. *Small*, 8(8):1204–1208, 2012.
- [108] Oleg Lupan, Thierry Pauporté, and Bruno Viana. Low-Voltage UV-Electroluminescence from ZnO-Nanowire Array/p-GaN Light-Emitting Diodes. *Adv. Mater.*, 22(30):3298–3302, 2010.
- [109] J H Lim, C K Kang, K K Kim, I K Park, D K Hwang, and S J Park. UV Electroluminescence Emission from ZnO Light-Emitting Diodes Grown by High-Temperature Radiofrequency Sputtering. *Adv. Mater.*, 18(20):2720–2724, 2006.
- [110] W Z Xu, Z Z Ye, Y J Zeng, L P Zhu, B H Zhao, L Jiang, J G Lu, H P He, and S B Zhang. ZnO light-emitting diode grown by plasma-assisted metal organic chemical vapor deposition. *Appl. Phys. Lett.*, 88(17):173506, 2006.
- [111] Yafit Itzhaik, Gary Hodes, and Hagai Cohen. Band Alignment and Internal Field Mapping in Solar Cells. *J. Phys. Chem. Lett.*, 2(22):2872–2876, 2011.

- [112] R Ranjusha, R Sreeja, P A Mini, K R V Subramanian, Shantikumar V Nair, and Avinash Balakrishnan. Electrical and optical characteristics of surface treated ZnO nanotubes. *Mater. Res. Bull.*, 47(8):1887–1891, 2012.
- [113] J S Kim, R H Friend, and F Cacialli. Surface energy and polarity of treated indium–tin–oxide anodes for polymer light-emitting diodes studied by contact-angle measurements. *J. Appl. Phys.*, 86(5):2774–2778, 1999.
- [114] J S Kim, P K H Ho, D S Thomas, R H Friend, F Cacialli, G-W Bao, and S F Y Li. X-ray photoelectron spectroscopy of surface-treated indium-tin oxide thin films. *Chemical Physics Letters*, 315:307–312, 1999.
- [115] J S Kim, M Granström, R H Friend, N Johansson, W R Salaneck, R Daik, W J Feast, and F Cacialli. Indium–tin oxide treatments for single- and double-layer polymeric light-emitting diodes: The relation between the anode physical, chemical, and morphological properties and the device performance. *J. Appl. Phys.*, 84(12):6859–6870, 1998.
- [116] Renjia Zhou, Romain Stalder, Dongping Xie, Weiran Cao, Ying Zheng, Yixing Yang, Marc Plaisant, Paul H Holloway, Kirk S Schanze, John R Reynolds, and Jiangeng Xue. Enhancing the Efficiency of Solution-Processed Polymer:Colloidal Nanocrystal Hybrid Photovoltaic Cells Using Ethanethiol Treatment. *ACS Nano*, 7(6):4846–4854, 2013.
- [117] C G Allen, D J Baker, J M Albin, H E Oertli, D T Gillaspie, D C Olson, T E Furtak, and R T Collins. Surface Modification of ZnO Using Triethoxysilane-Based Molecules. *Langmuir*, 24(23):13393–13398, 2008.
- [118] C Noguees and P Lang. Self-Assembled Alkanethiol Monolayers on a Zn Substrate: Structure and Organization. *Langmuir*, 23(16):8385–8391, 2007.
- [119] Hongping Zhang and Steven Baldelli. Alkanethiol Monolayers at Reduced and Oxidized Zinc Surfaces with Corrosion Protection: A Sum Frequency Generation and Electrochemistry Investigation. *J. Phys. Chem. B*, 110(47):24062–24069, 2006.
- [120] J Christopher Love, Lara A Estroff, Jennah K Kriebel, Ralph G Nuzzo, and George M Whitesides. Self-Assembled Monolayers of Thiolates on Metals as a Form of Nanotechnology. *Chem. Rev.*, 105(4):1103–1170, 2005.
- [121] Scott H Brewer, Derek A Brown, and Stefan Franzen. Formation of Thiolate and Phosphonate Adlayers on Indium Tin Oxide: Optical and Electronic Characterization. *Langmuir*, 18(18):6857–6865, 2002.

- [122] T J Gardner, C Daniel Frisbie, and M S Wrighton. Systems for Orthogonal Self-Assembly of Electroactive Monolayers on Au and ITO: An Approach to Molecular Electronics. *J. Am. Chem. Soc.*, 117:6927–6933, 1995.
- [123] Thilo Bauer, Thomas Schmaltz, Thomas Lenz, Marcus Halik, Bernd Meyer, and Timothy Clark. Phosphonate- and Carboxylate-Based Self-Assembled Monolayers for Organic Devices: A Theoretical Study of Surface Binding on Aluminum Oxide with Experimental Support. *ACS Appl. Mater. Interfaces*, 5(13):6073–6080, 2013.
- [124] Nir Kedem, Sylke Blumstengel, Fritz Henneberger, Hagai Cohen, Gary Hodes, and David Cahen. Morphology-, synthesis- and doping-independent tuning of ZnO work function using phenylphosphonates. *Phys. Chem. Chem. Phys.*, 16(18):8310–8319, 2014.
- [125] Jennifer L Braid, Unsal Koldemir, Alan Sellinger, Reuben T Collins, Thomas E Furtak, and Dana C Olson. Conjugated Phosphonic Acid Modified Zinc Oxide Electron Transport Layers for Improved Performance in Organic Solar Cells. *ACS Appl. Mater. Interfaces*, 6(21):19229–19234, 2014.
- [126] Eric L Bruner, Norbert Koch, Amelia R Span, Steven L Bernasek, Antoine Kahn, and Jeffrey Schwartz. Controlling the Work Function of Indium Tin Oxide: Differentiating Dipolar from Local Surface Effects. *J. Am. Chem. Soc.*, 124(13):3192–3193, 2002.
- [127] G te Velde, F M Bickelhaupt, E J Baerends, C Fonesca Guerra, S J A Van Gisbergen, J G Snijders, and T Ziegler. Chemistry with ADF. *J. Comput. Chem.*, 22(9):931–967, 2001.
- [128] C Fonesca Guerra, J G Snijders, G te Velde, and E J Baerends. Towards an order-N DFT method. *Theor. Chem. Acc.*, 99:391–403, 1998.
- [129] S H Vosko, L Wilk, and M Nusair. Accurate spin-dependent electron liquid correlation energies for local spin density calculations: a critical analysis. *National Research Council of Canada*, pages 1–12, 1980.
- [130] C Lee, W Yang, and R G Parr. Development of the Colle-Salvetti correlation-energy formula into a functional of the electron density. *Phys. Rev. B*, 37(2):785–789, 1988.
- [131] Charles S Demmer, Niels Krogsgaard-Larsen, and Lennart Bunch. Review on Modern Advances of Chemical Methods for the Introduction of a Phosphonic Acid Group. *Chem. Rev.*, 111(12):7981–8006, 2011.
- [132] Franca Bigi, Maria Lina Conforti, Raimondo Maggi, Annalisa Piccinno, and Giovanni Sartori. Clean synthesis in water: uncatalysed preparation of ylidenemalononitriles. *Green Chem.*, 2(3):101–103, 2000.

- [133] S Khodabakhsh, D Poplavskyy, S Heutz, J Nelson, D D C Bradley, H Murata, and T S Jones. Using Self-Assembling Dipole Molecules to Improve Hole Injection in Conjugated Polymers. *Adv. Funct. Mater.*, 14(12):1205–1210, 2004.
- [134] Lingyi Meng, Dong Wang, Qikai Li, Yuanping Yi, Jean-Luc Bredas, and Zhigang Shuai. An improved dynamic Monte Carlo model coupled with Poisson equation to simulate the performance of organic photovoltaic devices. *J. Chem. Phys.*, 134(12):124102, 2011.
- [135] P W M Blom, V D Mihailetschi, L J A Koster, and D E Markov. Device Physics of Polymer:Fullerene Bulk Heterojunction Solar Cells. *Adv. Mater.*, 19(12):1551–1566, 2007.
- [136] Rebecca Saive, Christian Mueller, Janusz Schinke, Robert Lovrincic, and Wolfgang Kowalsky. Understanding S-shaped current-voltage characteristics of organic solar cells: Direct measurement of potential distributions by scanning Kelvin probe. *Appl. Phys. Lett.*, 103(24):243303, 2013.
- [137] Antonio Guerrero, Pablo P Boix, Luís F Marchesi, Teresa Ripolles-Sanchis, Ernesto C Pereira, and Germà Garcia-Belmonte. Oxygen p-doping induced photogeneration loss in P3HT:PCBM solar cells. *Sol. Energy Mater. Sol. Cells*, 100:185–191, 2012.
- [138] Unsal Koldemir, Jennifer L Braid, Amanda Morgenstern, Mark Eberhart, Reuben T Collins, Dana C Olson, and Alan Sellinger. Molecular Design for Tuning Work Functions of Transparent Conducting Electrodes. *J. Phys. Chem. Lett.*, 6(12):2269–2276, 2015.
- [139] Irfan Irfan, Alexander James Turinske, Zhenan Bao, and Yongli Gao. Work function recovery of air exposed molybdenum oxide thin films. *Appl. Phys. Lett.*, 101(9):093305, 2012.
- [140] J Wang, L Xu, Yun-Ju Lee, M De Anda Villa, A V Malko, and Julia W P Hsu. Effects of Contact-Induced Doping on the Behaviors of Organic Photovoltaic Devices. *Nano Lett.*, 15(11):7627–7632, 2015.
- [141] B J Jin, S H Bae, S Y Lee, and S Im. Effects of native defects on optical and electrical properties of ZnO prepared by pulsed laser deposition. *Mater. Sci. Eng., B*, 71:301–305, 2000.
- [142] Leonard J Brillson and Yicheng Lu. ZnO Schottky barriers and Ohmic contacts. *J. Appl. Phys.*, 109(12):121301, 2011.

- [143] Fang-Ling Kuo, Yun Li, Marvin Solomon, Jincheng Du, and Nigel D Shepherd. Work-function tuning of zinc oxide films by argon sputtering and oxygen plasma: an experimental and computational study. *J. Phys. Chem.*, 45(6):065301, 2012.
- [144] Andreas Klein and Frank Säuberlich. Surfaces and Interfaces of Sputter-Deposited ZnO Films. In *Transparent Conductive Zinc Oxide*, pages 125–185. Springer, 2008.

APPENDIX A - SUPPLEMENTAL INFORMATION FOR CHAPTER 4

The devices investigated with X-SKPM in Chapter 4 were two of six devices on a single sample. The operational characteristics for those two whole devices before cleaving or X-SKPM measurement are given in Table A.1. We intended to show the effects of annealing and air exposure on the potential distribution, and obviously device performance is also affected by these factors. Therefore, starting with devices of equivalent performance is essential for isolating changes in device operation from variation between devices. The whole standard devices showed remarkably similar performance, with only small differences in each parameter.

Table A.1: Whole standard architecture device characteristics

	V _{OC} (V)	J _{SC} (mA/cm ²)	FF (%)	PCE (%)
As Fabricated - Whole	0.37	8.92	50.7	1.65
Annealed - Whole	0.36	8.87	52.5	1.66

The two inverted devices used to test annealing and air exposure also came from one sample, and their whole device characteristics are given in Table A.2. Again, device parameters vary by only small amounts, with PCEs being only 2.5% different.

Table A.2: Whole inverted architecture device characteristics

	V _{OC} (V)	J _{SC} (mA/cm ²)	FF (%)	PCE (%)
As-Fabricated - Whole	0.78	9.33	70.6	5.14
Annealed - Whole	0.78	9.10	70.7	5.01

Phosphonic acid modified devices were taken from three different samples, as the modifiers cannot be applied to different devices on the same sample. The modified devices were compared with the unmodified inverted device, and whole device characteristics for all three are shown in Table A.3. Here, device characteristics do not match between devices, as we

expect the modifiers to significantly increase performance in the case of oF₂PVPA, and decrease performance for pCF₃PVPA. While device characteristics do change during X-SKPM investigation, the device performance is not significantly impacted by cleaving.

Table A.3: Whole modified inverted device characteristics

	V _{OC} (V)	J _{SC} (mA/cm ²)	FF (%)	PCE (%)
Unmodified - Whole	0.78	9.33	70.6	5.14
oF ₂ PVPA - Whole	0.81	9.51	70.7	5.45
pCF ₃ PVPA - Whole	0.18	2.35	25.1	0.11

APPENDIX B - PERMISSIONS

Permissions from the publisher and non-committee co-authors to include the publications reproduced in Chapters 2 and 3 are included here. Permissions to use Figure 1.5, Figure 1.6, Figure 1.7, Figure 1.8, and Figure 1.10 follow.

American Chemical Society's Policy on Theses and Dissertations

If your university requires you to obtain permission, you must use the RightsLink permission system. See RightsLink instructions at <http://pubs.acs.org/page/copyright/permissions.html>.

This is regarding request for permission to include **your** paper(s) or portions of text from **your** paper(s) in your thesis. Permission is now automatically granted; please pay special attention to the **implications** paragraph below. The Copyright Subcommittee of the Joint Board/Council Committees on Publications approved the following:

Copyright permission for published and submitted material from theses and dissertations

ACS extends blanket permission to students to include in their theses and dissertations their own articles, or portions thereof, that have been published in ACS journals or submitted to ACS journals for publication, provided that the ACS copyright credit line is noted on the appropriate page(s).

Publishing **implications** of electronic publication of theses and dissertation material

Students and their mentors should be aware that posting of theses and dissertation material on the Web prior to submission of material from that thesis or dissertation to an ACS journal may affect publication in that journal. Whether Web posting is considered prior publication may be evaluated on a case-by-case basis by the journal's editor. If an ACS journal editor considers Web posting to be "prior publication", the paper will not be accepted for publication in that journal. If you intend to submit your unpublished paper to ACS for publication, check with the appropriate editor prior to posting your manuscript electronically.

Reuse/Republishing of the Entire Work in Theses or Collections: Authors may reuse all or part of the Submitted, Accepted or Published Work in a thesis or dissertation that the author writes and is required to submit to satisfy the criteria of degree-granting institutions. Such reuse is permitted subject to the ACS' "Ethical Guidelines to Publication of Chemical Research" (<http://pubs.acs.org/page/policy/ethics/index.html>); the author should secure written confirmation (via letter or email) from the respective ACS journal editor(s) to avoid potential conflicts with journal prior publication*/embargo policies. Appropriate citation of the Published Work must be made. If the thesis or dissertation to be published is in electronic format, a direct link to the Published Work must also be included using the ACS Articles on Request author-directed link – see <http://pubs.acs.org/page/policy/articlesonrequest/index.html>

* Prior publication policies of ACS journals are posted on the ACS website at <http://pubs.acs.org/page/policy/prior/index.html>

If your paper has **not** yet been published by ACS, please print the following credit line on the first page of your article: "Reproduced (or 'Reproduced in part') with permission from [JOURNAL NAME], in press (or 'submitted for publication'). Unpublished work copyright [CURRENT YEAR] American Chemical Society." Include appropriate information.

If your paper has already been published by ACS and you want to include the text or portions of the text in your thesis/dissertation, please print the ACS copyright credit line on the first page of your article: "Reproduced (or 'Reproduced in part') with permission from [FULL REFERENCE CITATION.] Copyright [YEAR] American Chemical Society." Include appropriate information.

Submission to a Dissertation Distributor: If you plan to submit your thesis to UMI or to another dissertation distributor, you should not include the unpublished ACS paper in your thesis if the thesis will be disseminated electronically, until ACS has published your paper. After publication of the paper by ACS, you may release the entire thesis (**not the individual ACS article by itself**) for electronic dissemination through the distributor; ACS's copyright credit line should be printed on the first page of the ACS paper.



Jennifer Braid <jdrerup@mymail.mines.edu>

Permission to use ACS Conjugated Phosphonic Acid paper in my thesis

Unsal Koldemir <ukoldemir@gmail.com>

Fri, Mar 25, 2016 at 3:18 PM

To: Jennifer Braid <jdrerup@mymail.mines.edu>

Jen,
You can use this paper in your thesis.

Best,

Unsal Koldemir

25 Mar 2016 21:46 tarihinde "Jennifer Braid" <jdrerup@mymail.mines.edu> yazdı:

Hi Unsal,

Mines requires that I obtain your permission to use our publication in my thesis. Could you please reply granting your permission for the following paper? This email transcript will appear in my thesis.

Conjugated Phosphonic Acid Modified Zinc Oxide Electron Transport Layers for Improved Performance in Organic Solar Cells

DOI: 10.1021/am505182c ACS Appl. Mater. Interfaces 2014, 6, 19229-19234

Thank you,
Jen



Jennifer Braid <jdrerup@mymail.mines.edu>

Permission to use Molecular Design JPCL perspective in my thesis

Amanda Morgenstern <amorgens@mymail.mines.edu>

Fri, Mar 25, 2016 at 2:02 PM

To: Jennifer Braid <jdrerup@mymail.mines.edu>

I, Amanda Morgenstern, give you permission to use our publication, Molecular Design for Tuning Work Functions of Transparent Conducting Electrodes, in your thesis.

Amanda Morgenstern
amorgens@mines.edu
Chemistry PhD Candidate
Molecular Theory Group
Colorado School of Mines

On Fri, Mar 25, 2016 at 1:45 PM, Jennifer Braid <jdrerup@mymail.mines.edu> wrote:

Hello co-authors,

Mines requires that I obtain your permission to use our publication in my thesis. Could you please reply granting your permission for the following paper? This email transcript will appear in my thesis.

Molecular Design for Tuning Work Functions of Transparent Conducting Electrodes

DOI: 10.1021/acs.jpcllett.5b00420 J. Phys. Chem. Lett. 2015, 6, 2269-2276

Thank you,

Jen



Jennifer Braid <jdrerup@mymail.mines.edu>

Permission to use Molecular Design JPCL perspective in my thesis

Unsal Koldemir <ukoldemir@gmail.com>

Fri, Mar 25, 2016 at 2:08 PM

To: Jennifer Braid <jdrerup@mymail.mines.edu>

Hi jen,

You can use the paper in your thesis.

Congratulations for your defense in advance.

Best

Unsal Koldemir

25 Mar 2016 21:45 tarihinde "Jennifer Braid" <jdrerup@mymail.mines.edu> yazdı:

Hello co-authors,

Mines requires that I obtain your permission to use our publication in my thesis. Could you please reply granting your permission for the following paper? This email transcript will appear in my thesis.

Molecular Design for Tuning Work Functions of Transparent Conducting Electrodes

DOI: 10.1021/acs.jpcllett.5b00420 J. Phys. Chem. Lett. 2015, 6, 2269-2276

Thank you,

Jen



Jennifer Braid <jdrerup@mymail.mines.edu>

Permission to use Molecular Design JPCL perspective in my thesis

Mark Eberhart <meberhar@mines.edu>
To: Jennifer Braid <jdrerup@mymail.mines.edu>

Fri, Mar 25, 2016 at 2:21 PM

Yes this is fine.

Mark Eberhart
meberhar@mines.edu

On Mar 25, 2016, at 1:45 PM, Jennifer Braid <jdrerup@mymail.mines.edu> wrote:

Hello co-authors,

Mines requires that I obtain your permission to use our publication in my thesis. Could you please reply granting your permission for the following paper? This email transcript will appear in my thesis.

Molecular Design for Tuning Work Functions of Transparent Conducting Electrodes

DOI: 10.1021/acs.jpcllett.5b00420 J. Phys. Chem. Lett. 2015, 6, 2269-2276

Thank you,

Jen

AIP PUBLISHING LLC LICENSE TERMS AND CONDITIONS

Mar 27, 2016

This Agreement between Jennifer L Braid ("You") and AIP Publishing LLC ("AIP Publishing LLC") consists of your license details and the terms and conditions provided by AIP Publishing LLC and Copyright Clearance Center.

License Number	3837280948633
License date	Mar 27, 2016
Licensed Content Publisher	AIP Publishing LLC
Licensed Content Publication	Journal of Applied Physics
Licensed Content Title	Cathode dependence of the open-circuit voltage of polymer:fullerene bulk heterojunction solar cells
Licensed Content Author	V. D. Mihailetschi, P. W. M. Blom, J. C. Hummelen, et al.
Licensed Content Date	Oct 31, 2003
Licensed Content Volume Number	94
Licensed Content Issue Number	10
Type of Use	Thesis/Dissertation
Requestor type	Student
Format	Print and electronic
Portion	Figure/Table
Number of figures/tables	1
Title of your thesis / dissertation	Understanding efficiency improvement in organic photovoltaics with molecular modifiers
Expected completion date	May 2016
Estimated size (number of pages)	100
Requestor Location	Jennifer L Braid 605 21st St Apt E None GOLDEN, CO 80401 United States Attn: Jennifer L Braid
Billing Type	Invoice
Billing Address	Jennifer L Braid 605 21st St Apt E None GOLDEN, CO 80401 United States Attn: Jennifer L Braid
Total	0.00 USD
Terms and Conditions	

AIP Publishing LLC -- Terms and Conditions: Permissions Uses

AIP Publishing hereby grants to you the non-exclusive right and license to use and/or distribute the Material according to the use specified in your order, on a one-time basis, for the specified term, with a maximum distribution equal to the number that you have ordered. Any links or other content accompanying the Material are not the subject of this license.

1. You agree to include the following copyright and permission notice with the reproduction of the Material: "Reprinted from [FULL CITATION]. with the permission of AIP Publishing." For an article, the credit line and permission notice must be printed on the first page of the article or book chapter. For photographs, covers, or tables, the notice may appear with the Material, in a footnote, or in the reference list.
2. If you have licensed reuse of a figure, photograph, cover, or table, it is your responsibility to ensure that the material is original to AIP Publishing and does not contain the copyright of another entity, and that the copyright notice of the figure, photograph, cover, or table does not indicate that it was reprinted by AIP Publishing, with permission, from another source. Under no circumstances does AIP Publishing purport or intend to grant permission to reuse material to which it does not hold appropriate rights.
You may not alter or modify the Material in any manner. You may translate the Material into another language only if you have licensed translation rights. You may not use the Material for promotional purposes.
3. The foregoing license shall not take effect unless and until AIP Publishing or its agent, Copyright Clearance Center, receives the Payment in accordance with Copyright Clearance Center Billing and Payment Terms and Conditions, which are incorporated herein by reference.
4. AIP Publishing or Copyright Clearance Center may, within two business days of granting this license, revoke the license for any reason whatsoever, with a full refund payable to you. Should you violate the terms of this license at any time, AIP Publishing, or Copyright Clearance Center may revoke the license with no refund to you. Notice of such revocation will be made using the contact information provided by you. Failure to receive such notice will not nullify the revocation.
5. AIP Publishing makes no representations or warranties with respect to the Material. You agree to indemnify and hold harmless AIP Publishing, and their officers, directors, employees or agents from and against any and all claims arising out of your use of the Material other than as specifically authorized herein.
6. The permission granted herein is personal to you and is not transferable or assignable without the prior written permission of AIP Publishing. This license may not be amended except in a writing signed by the party to be charged.
7. If purchase orders, acknowledgments or check endorsements are issued on any forms containing terms and conditions which are inconsistent with these provisions, such inconsistent terms and conditions shall be of no force and effect. This document, including the CCC Billing and Payment Terms and Conditions, shall be the entire agreement between the parties relating to the subject matter hereof.

This Agreement shall be governed by and construed in accordance with the laws of the State of New York. Both parties hereby submit to the jurisdiction of the courts of New York County for purposes of resolving any disputes that may arise hereunder.

V1.1

Questions? customercare@copyright.com or +1-855-239-3415 (toll free in the US) or +1-978-646-2777.

JOHN WILEY AND SONS LICENSE TERMS AND CONDITIONS

Mar 27, 2016

This Agreement between Jennifer L Braid ("You") and John Wiley and Sons ("John Wiley and Sons") consists of your license details and the terms and conditions provided by John Wiley and Sons and Copyright Clearance Center.

License Number	3837280139352
License date	Mar 27, 2016
Licensed Content Publisher	John Wiley and Sons
Licensed Content Publication	Advanced Materials
Licensed Content Title	Energy-Level Alignment at Organic/Metal and Organic/Organic Interfaces
Licensed Content Author	Slawomir Braun,William R. Salaneck,Mats Fahlman
Licensed Content Date	Mar 2, 2009
Pages	23
Type of Use	Dissertation/Thesis
Requestor type	University/Academic
Format	Print and electronic
Portion	Figure/table
Number of figures/tables	1
Original Wiley figure/table number(s)	Figure 7
Will you be translating?	No
Title of your thesis / dissertation	Understanding efficiency improvement in organic photovoltaics with molecular modifiers
Expected completion date	May 2016
Expected size (number of pages)	100
Requestor Location	Jennifer L Braid 605 21st St Apt E None GOLDEN, CO 80401 United States Attn: Jennifer L Braid
Billing Type	Invoice
Billing Address	Jennifer L Braid 605 21st St Apt E None GOLDEN, CO 80401 United States Attn: Jennifer L Braid
Total	0.00 USD
Terms and Conditions	

TERMS AND CONDITIONS

This copyrighted material is owned by or exclusively licensed to John Wiley & Sons, Inc. or one of its group companies (each a "Wiley Company") or handled on behalf of a society with which a Wiley Company has exclusive publishing rights in relation to a particular work (collectively "WILEY"). By clicking "accept" in connection with completing this licensing transaction, you agree that the following terms and conditions apply to this transaction (along with the billing and payment terms and conditions established by the Copyright Clearance Center Inc., ("CCC's Billing and Payment terms and conditions"), at the time that you opened your RightsLink account (these are available at any time at <http://myaccount.copyright.com>).

Terms and Conditions

- The materials you have requested permission to reproduce or reuse (the "Wiley Materials") are protected by copyright.
- You are hereby granted a personal, non-exclusive, non-sub licensable (on a stand-alone basis), non-transferable, worldwide, limited license to reproduce the Wiley Materials for the purpose specified in the licensing process. This license, **and any CONTENT (PDF or image file) purchased as part of your order**, is for a one-time use only and limited to any maximum distribution number specified in the license. The first instance of republication or reuse granted by this license must be completed within two years of the date of the grant of this license (although copies prepared before the end date may be distributed thereafter). The Wiley Materials shall not be used in any other manner or for any other purpose, beyond what is granted in the license. Permission is granted subject to an appropriate acknowledgement given to the author, title of the material/book/journal and the publisher. You shall also duplicate the copyright notice that appears in the Wiley publication in your use of the Wiley Material. Permission is also granted on the understanding that nowhere in the text is a previously published source acknowledged for all or part of this Wiley Material. Any third party content is expressly excluded from this permission.
- With respect to the Wiley Materials, all rights are reserved. Except as expressly granted by the terms of the license, no part of the Wiley Materials may be copied, modified, adapted (except for minor reformatting required by the new Publication), translated, reproduced, transferred or distributed, in any form or by any means, and no derivative works may be made based on the Wiley Materials without the prior permission of the respective copyright owner. **For STM Signatory Publishers clearing permission under the terms of the [STM Permissions Guidelines](#) only, the terms of the license are extended to include subsequent editions and for editions in other languages, provided such editions are for the work as a whole in situ and does not involve the separate exploitation of the permitted figures or extracts**, You may not alter, remove or suppress in any manner any copyright, trademark or other notices displayed by the Wiley Materials. You may not license, rent, sell, loan, lease, pledge, offer as security, transfer or assign the Wiley Materials on a stand-alone basis, or any of the rights granted to you hereunder to any other person.
- The Wiley Materials and all of the intellectual property rights therein shall at all times remain the exclusive property of John Wiley & Sons Inc, the Wiley Companies, or their respective licensors, and your interest therein is only that of having possession of and the right to reproduce the Wiley Materials pursuant to Section 2 herein during the continuance of this Agreement. You agree that you own no right, title or interest in or to the Wiley Materials or any of the intellectual property rights therein. You shall have no rights hereunder other than the license as provided for above in Section 2. No right, license or interest to any trademark, trade name, service mark or other branding ("Marks") of WILEY or its licensors is granted hereunder, and you agree that you shall not assert any such right, license or interest with respect thereto
- NEITHER WILEY NOR ITS LICENSORS MAKES ANY WARRANTY OR REPRESENTATION OF ANY KIND TO YOU OR ANY THIRD PARTY, EXPRESS, IMPLIED OR STATUTORY, WITH RESPECT TO THE MATERIALS OR THE ACCURACY OF ANY INFORMATION CONTAINED IN THE MATERIALS, INCLUDING, WITHOUT LIMITATION, ANY IMPLIED WARRANTY OF MERCHANTABILITY, ACCURACY, SATISFACTORY QUALITY, FITNESS FOR A PARTICULAR PURPOSE, USABILITY, INTEGRATION OR NON-INFRINGEMENT AND ALL SUCH WARRANTIES ARE HEREBY EXCLUDED BY WILEY AND ITS LICENSORS AND WAIVED BY YOU.
- WILEY shall have the right to terminate this Agreement immediately upon breach of this Agreement by you.
- You shall indemnify, defend and hold harmless WILEY, its Licensors and their respective directors, officers, agents

and employees, from and against any actual or threatened claims, demands, causes of action or proceedings arising from any breach of this Agreement by you.

- IN NO EVENT SHALL WILEY OR ITS LICENSORS BE LIABLE TO YOU OR ANY OTHER PARTY OR ANY OTHER PERSON OR ENTITY FOR ANY SPECIAL, CONSEQUENTIAL, INCIDENTAL, INDIRECT, EXEMPLARY OR PUNITIVE DAMAGES, HOWEVER CAUSED, ARISING OUT OF OR IN CONNECTION WITH THE DOWNLOADING, PROVISIONING, VIEWING OR USE OF THE MATERIALS REGARDLESS OF THE FORM OF ACTION, WHETHER FOR BREACH OF CONTRACT, BREACH OF WARRANTY, TORT, NEGLIGENCE, INFRINGEMENT OR OTHERWISE (INCLUDING, WITHOUT LIMITATION, DAMAGES BASED ON LOSS OF PROFITS, DATA, FILES, USE, BUSINESS OPPORTUNITY OR CLAIMS OF THIRD PARTIES), AND WHETHER OR NOT THE PARTY HAS BEEN ADVISED OF THE POSSIBILITY OF SUCH DAMAGES. THIS LIMITATION SHALL APPLY NOTWITHSTANDING ANY FAILURE OF ESSENTIAL PURPOSE OF ANY LIMITED REMEDY PROVIDED HEREIN.
- Should any provision of this Agreement be held by a court of competent jurisdiction to be illegal, invalid, or unenforceable, that provision shall be deemed amended to achieve as nearly as possible the same economic effect as the original provision, and the legality, validity and enforceability of the remaining provisions of this Agreement shall not be affected or impaired thereby.
- The failure of either party to enforce any term or condition of this Agreement shall not constitute a waiver of either party's right to enforce each and every term and condition of this Agreement. No breach under this agreement shall be deemed waived or excused by either party unless such waiver or consent is in writing signed by the party granting such waiver or consent. The waiver by or consent of a party to a breach of any provision of this Agreement shall not operate or be construed as a waiver of or consent to any other or subsequent breach by such other party.
- This Agreement may not be assigned (including by operation of law or otherwise) by you without WILEY's prior written consent.
- Any fee required for this permission shall be non-refundable after thirty (30) days from receipt by the CCC.
- These terms and conditions together with CCC's Billing and Payment terms and conditions (which are incorporated herein) form the entire agreement between you and WILEY concerning this licensing transaction and (in the absence of fraud) supersedes all prior agreements and representations of the parties, oral or written. This Agreement may not be amended except in writing signed by both parties. This Agreement shall be binding upon and inure to the benefit of the parties' successors, legal representatives, and authorized assigns.
- In the event of any conflict between your obligations established by these terms and conditions and those established by CCC's Billing and Payment terms and conditions, these terms and conditions shall prevail.
- WILEY expressly reserves all rights not specifically granted in the combination of (i) the license details provided by you and accepted in the course of this licensing transaction, (ii) these terms and conditions and (iii) CCC's Billing and Payment terms and conditions.
- This Agreement will be void if the Type of Use, Format, Circulation, or Requestor Type was misrepresented during the licensing process.
- This Agreement shall be governed by and construed in accordance with the laws of the State of New York, USA, without regards to such state's conflict of law rules. Any legal action, suit or proceeding arising out of or relating to these Terms and Conditions or the breach thereof shall be instituted in a court of competent jurisdiction in New York County in the State of New York in the United States of America and each party hereby consents and submits to the personal jurisdiction of such court, waives any objection to venue in such court and consents to service of process by registered or certified mail, return receipt requested, at the last known address of such party.

WILEY OPEN ACCESS TERMS AND CONDITIONS

Wiley Publishes Open Access Articles in fully Open Access Journals and in Subscription journals offering Online Open. Although most of the fully Open Access journals publish open access articles under the terms of the Creative Commons

Attribution (CC BY) License only, the subscription journals and a few of the Open Access Journals offer a choice of Creative Commons Licenses. The license type is clearly identified on the article.

The Creative Commons Attribution License

The [Creative Commons Attribution License \(CC-BY\)](#) allows users to copy, distribute and transmit an article, adapt the article and make commercial use of the article. The CC-BY license permits commercial and non-

Creative Commons Attribution Non-Commercial License

The [Creative Commons Attribution Non-Commercial \(CC-BY-NC\) License](#) permits use, distribution and reproduction in any medium, provided the original work is properly cited and is not used for commercial purposes.(see below)

Creative Commons Attribution-Non-Commercial-NoDerivs License

The [Creative Commons Attribution Non-Commercial-NoDerivs License](#) (CC-BY-NC-ND) permits use, distribution and reproduction in any medium, provided the original work is properly cited, is not used for commercial purposes and no modifications or adaptations are made. (see below)

Use by commercial "for-profit" organizations

Use of Wiley Open Access articles for commercial, promotional, or marketing purposes requires further explicit permission from Wiley and will be subject to a fee.

Further details can be found on Wiley Online Library <http://olabout.wiley.com/WileyCDA/Section/id-410895.html>

Other Terms and Conditions:

v1.10 Last updated September 2015

Questions? customercare@copyright.com or +1-855-239-3415 (toll free in the US) or +1-978-646-2777.



**ROYAL SOCIETY OF CHEMISTRY LICENSE
TERMS AND CONDITIONS**

Mar 27, 2016

This Agreement between Jennifer L Braid ("You") and Royal Society of Chemistry ("Royal Society of Chemistry") consists of your license details and the terms and conditions provided by Royal Society of Chemistry and Copyright Clearance Center.

License Number	3837311084644
License date	Mar 27, 2016
Licensed Content Publisher	Royal Society of Chemistry
Licensed Content Publication	Journal of Materials Chemistry C
Licensed Content Title	Tuning zinc oxide/organic energy level alignment using mixed triethoxysilane monolayers
Licensed Content Author	Thomas M. Brenner,Gang Chen,Erich P. Meinig,Darick J. Baker,Dana C. Olson,Reuben T. Collins,Thomas E. Furtak
Licensed Content Date	Jul 31, 2013
Licensed Content Volume Number	1
Licensed Content Issue Number	37
Type of Use	Thesis/Dissertation
Requestor type	academic/educational
Portion	figures/tables/images
Number of figures/tables /images	1
Format	print and electronic
Distribution quantity	100000
Will you be translating?	no
Order reference number	None
Title of the thesis/dissertation	Understanding efficiency improvement in organic photovoltaics with molecular modifiers
Expected completion date	May 2016
Estimated size	100
Requestor Location	Jennifer L Braid 605 21st St Apt E GOLDEN, CO 80401 United States Attn: Jennifer L Braid

Billing Type	Invoice
Billing Address	Jennifer L Braid 605 21st St Apt E GOLDEN, CO 80401 United States Attn: Jennifer L Braid
Total	0.00 USD

Terms and Conditions

This License Agreement is between {Requestor Name} ("You") and The Royal Society of Chemistry ("RSC") provided by the Copyright Clearance Center ("CCC"). The license consists of your order details, the terms and conditions provided by the Royal Society of Chemistry, and the payment terms and conditions.

RSC / TERMS AND CONDITIONS

INTRODUCTION

The publisher for this copyrighted material is The Royal Society of Chemistry. By clicking "accept" in connection with completing this licensing transaction, you agree that the following terms and conditions apply to this transaction (along with the Billing and Payment terms and conditions established by CCC, at the time that you opened your RightsLink account and that are available at any time at .

LICENSE GRANTED

The RSC hereby grants you a non-exclusive license to use the aforementioned material anywhere in the world subject to the terms and conditions indicated herein. Reproduction of the material is confined to the purpose and/or media for which permission is hereby given.

RESERVATION OF RIGHTS

The RSC reserves all rights not specifically granted in the combination of (i) the license details provided by your and accepted in the course of this licensing transaction; (ii) these terms and conditions; and (iii) CCC's Billing and Payment terms and conditions.

REVOCATION

The RSC reserves the right to revoke this license for any reason, including, but not limited to, advertising and promotional uses of RSC content, third party usage, and incorrect source figure attribution.

THIRD-PARTY MATERIAL DISCLAIMER

If part of the material to be used (for example, a figure) has appeared in the RSC publication with credit to another source, permission must also be sought from that source. If the other source is another RSC publication these details should be included in your RightsLink request. If the other source is a third party, permission must be obtained from the third party. The RSC disclaims any responsibility for the reproduction you make of items owned by a third party.

PAYMENT OF FEE

If the permission fee for the requested material is waived in this instance, please be advised that any future requests for the reproduction of RSC materials may attract a fee.

ACKNOWLEDGEMENT

The reproduction of the licensed material must be accompanied by the following acknowledgement:

Reproduced ("Adapted" or "in part") from {Reference Citation} (or Ref XX) with permission of The Royal Society of Chemistry.

If the licensed material is being reproduced from New Journal of Chemistry (NJC), Photochemical & Photobiological Sciences (PPS) or Physical Chemistry Chemical Physics (PCCP) you must include one of the following acknowledgements:

For figures originally published in NJC:

Reproduced (“Adapted” or “in part”) from {Reference Citation} (or Ref XX) with permission of The Royal Society of Chemistry (RSC) on behalf of the European Society for Photobiology, the European Photochemistry Association and the RSC.

For figures originally published in PPS:

Reproduced (“Adapted” or “in part”) from {Reference Citation} (or Ref XX) with permission of The Royal Society of Chemistry (RSC) on behalf of the Centre National de la Recherche Scientifique (CNRS) and the RSC.

For figures originally published in PCCP:

Reproduced (“Adapted” or “in part”) from {Reference Citation} (or Ref XX) with permission of the PCCP Owner Societies.

HYPertext LINKS

With any material which is being reproduced in electronic form, you must include a hypertext link to the original RSC article on the RSC’s website. The recommended form for the hyperlink is <http://dx.doi.org/10.1039/DOI suffix>, for example in the link <http://dx.doi.org/10.1039/b110420a> the DOI suffix is ‘b110420a’. To find the relevant DOI suffix for the RSC article in question, go to the Journals section of the website and locate the article in the list of papers for the volume and issue of your specific journal. You will find the DOI suffix quoted there.

LICENSE CONTINGENT ON PAYMENT

While you may exercise the rights licensed immediately upon issuance of the license at the end of the licensing process for the transaction, provided that you have disclosed complete and accurate details of your proposed use, no license is finally effective unless and until full payment is received from you (by CCC) as provided in CCC's Billing and Payment terms and conditions. If full payment is not received on a timely basis, then any license preliminarily granted shall be deemed automatically revoked and shall be void as if never granted. Further, in the event that you breach any of these terms and conditions or any of CCC's Billing and Payment terms and conditions, the license is automatically revoked and shall be void as if never granted. Use of materials as described in a revoked license, as well as any use of the materials beyond the scope of an unrevoked license, may constitute copyright infringement and the RSC reserves the right to take any and all action to protect its copyright in the materials.

WARRANTIES

The RSC makes no representations or warranties with respect to the licensed material.

INDEMNITY

You hereby indemnify and agree to hold harmless the RSC and the CCC, and their respective officers, directors, trustees, employees and agents, from and against any and all claims arising out of your use of the licensed material other than as specifically authorized pursuant to this licence.

NO TRANSFER OF LICENSE

This license is personal to you or your publisher and may not be sublicensed, assigned, or transferred by you to any other person without the RSC's written permission.

NO AMENDMENT EXCEPT IN WRITING

This license may not be amended except in a writing signed by both parties (or, in the case

of "Other Conditions, v1.2", by CCC on the RSC's behalf).

OBJECTION TO CONTRARY TERMS

You hereby acknowledge and agree that these terms and conditions, together with CCC's Billing and Payment terms and conditions (which are incorporated herein), comprise the entire agreement between you and the RSC (and CCC) concerning this licensing transaction, to the exclusion of all other terms and conditions, written or verbal, express or implied (including any terms contained in any purchase order, acknowledgment, check endorsement or other writing prepared by you). In the event of any conflict between your obligations established by these terms and conditions and those established by CCC's Billing and Payment terms and conditions, these terms and conditions shall control.

JURISDICTION

This license transaction shall be governed by and construed in accordance with the laws of the District of Columbia. You hereby agree to submit to the jurisdiction of the courts located in the District of Columbia for purposes of resolving any disputes that may arise in connection with this licensing transaction.

LIMITED LICENSE

The following terms and conditions apply to specific license types:

Translation

This permission is granted for non-exclusive world English rights only unless your license was granted for translation rights. If you licensed translation rights you may only translate this content into the languages you requested. A professional translator must perform all translations and reproduce the content word for word preserving the integrity of the article.

Intranet

If the licensed material is being posted on an Intranet, the Intranet is to be password-protected and made available only to bona fide students or employees only. All content posted to the Intranet must maintain the copyright information line on the bottom of each image. You must also fully reference the material and include a hypertext link as specified above.

Copies of Whole Articles

All copies of whole articles must maintain, if available, the copyright information line on the bottom of each page.

Other Conditions

v1.2

Gratis licenses (referencing \$0 in the Total field) are free. Please retain this printable license for your reference. No payment is required.

If you would like to pay for this license now, please remit this license along with your payment made payable to "COPYRIGHT CLEARANCE CENTER" otherwise you will be invoiced within 48 hours of the license date. Payment should be in the form of a check or money order referencing your account number and this invoice number {Invoice Number}.

Once you receive your invoice for this order, you may pay your invoice by credit card.

Please follow instructions provided at that time.

Make Payment To:

Copyright Clearance Center

Dept 001

P.O. Box 843006

Boston, MA 02284-3006

For suggestions or comments regarding this order, contact Rightslink Customer Support:

customercare@copyright.com or +1-855-239-3415 (toll free in the US) or +1-978-646-2777.

Questions? customercare@copyright.com or +1-855-239-3415 (toll free in the US) or +1-978-646-2777.



JOHN WILEY AND SONS LICENSE TERMS AND CONDITIONS

Mar 27, 2016

This Agreement between Jennifer L Braid ("You") and John Wiley and Sons ("John Wiley and Sons") consists of your license details and the terms and conditions provided by John Wiley and Sons and Copyright Clearance Center.

License Number	3837280588755
License date	Mar 27, 2016
Licensed Content Publisher	John Wiley and Sons
Licensed Content Publication	Advanced Functional Materials
Licensed Content Title	Chemically Controlled Reversible and Irreversible Extraction Barriers Via Stable Interface Modification of Zinc Oxide Electron Collection Layer in Polycarbazole-based Organic Solar Cells
Licensed Content Author	Sarah R. Cowan, Philip Schulz, Anthony J. Giordano, Andres Garcia, Bradley A. MacLeod, Seth R. Marder, Antoine Kahn, David S. Ginley, Erin L. Ratcliff, Dana C. Olson
Licensed Content Date	Apr 22, 2014
Pages	10
Type of Use	Dissertation/Thesis
Requestor type	University/Academic
Format	Print and electronic
Portion	Figure/table
Number of figures/tables	1
Original Wiley figure/table number(s)	Figure 3
Will you be translating?	No
Title of your thesis / dissertation	Understanding efficiency improvement in organic photovoltaics with molecular modifiers
Expected completion date	May 2016
Expected size (number of pages)	100
Requestor Location	Jennifer L Braid 605 21st St Apt E None GOLDEN, CO 80401 United States Attn: Jennifer L Braid
Billing Type	Invoice
Billing Address	Jennifer L Braid 605 21st St Apt E None GOLDEN, CO 80401 United States Attn: Jennifer L Braid

Total **0.00 USD**

[Terms and Conditions](#)

TERMS AND CONDITIONS

This copyrighted material is owned by or exclusively licensed to John Wiley & Sons, Inc. or one of its group companies (each a "Wiley Company") or handled on behalf of a society with which a Wiley Company has exclusive publishing rights in relation to a particular work (collectively "WILEY"). By clicking "accept" in connection with completing this licensing transaction, you agree that the following terms and conditions apply to this transaction (along with the billing and payment terms and conditions established by the Copyright Clearance Center Inc., ("CCC's Billing and Payment terms and conditions"), at the time that you opened your RightsLink account (these are available at any time at <http://myaccount.copyright.com>).

Terms and Conditions

- The materials you have requested permission to reproduce or reuse (the "Wiley Materials") are protected by copyright.
- You are hereby granted a personal, non-exclusive, non-sub licensable (on a stand-alone basis), non-transferable, worldwide, limited license to reproduce the Wiley Materials for the purpose specified in the licensing process. This license, **and any CONTENT (PDF or image file) purchased as part of your order**, is for a one-time use only and limited to any maximum distribution number specified in the license. The first instance of republication or reuse granted by this license must be completed within two years of the date of the grant of this license (although copies prepared before the end date may be distributed thereafter). The Wiley Materials shall not be used in any other manner or for any other purpose, beyond what is granted in the license. Permission is granted subject to an appropriate acknowledgement given to the author, title of the material/book/journal and the publisher. You shall also duplicate the copyright notice that appears in the Wiley publication in your use of the Wiley Material. Permission is also granted on the understanding that nowhere in the text is a previously published source acknowledged for all or part of this Wiley Material. Any third party content is expressly excluded from this permission.
- With respect to the Wiley Materials, all rights are reserved. Except as expressly granted by the terms of the license, no part of the Wiley Materials may be copied, modified, adapted (except for minor reformatting required by the new Publication), translated, reproduced, transferred or distributed, in any form or by any means, and no derivative works may be made based on the Wiley Materials without the prior permission of the respective copyright owner. **For STM Signatory Publishers clearing permission under the terms of the [STM Permissions Guidelines](#) only, the terms of the license are extended to include subsequent editions and for editions in other languages, provided such editions are for the work as a whole in situ and does not involve the separate exploitation of the permitted figures or extracts**, You may not alter, remove or suppress in any manner any copyright, trademark or other notices displayed by the Wiley Materials. You may not license, rent, sell, loan, lease, pledge, offer as security, transfer or assign the Wiley Materials on a stand-alone basis, or any of the rights granted to you hereunder to any other person.
- The Wiley Materials and all of the intellectual property rights therein shall at all times remain the exclusive property of John Wiley & Sons Inc, the Wiley Companies, or their respective licensors, and your interest therein is only that of having possession of and the right to reproduce the Wiley Materials pursuant to Section 2 herein during the continuance of this Agreement. You agree that you own no right, title or interest in or to the Wiley Materials or any of the intellectual property rights therein. You shall have no rights hereunder other than the license as provided for above in Section 2. No right, license or interest to any trademark, trade name, service mark or other branding ("Marks") of WILEY or its licensors is granted hereunder, and you agree that you shall not assert any such right, license or interest with respect thereto
- NEITHER WILEY NOR ITS LICENSORS MAKES ANY WARRANTY OR REPRESENTATION OF ANY KIND TO YOU OR ANY THIRD PARTY, EXPRESS, IMPLIED OR STATUTORY, WITH RESPECT TO THE MATERIALS OR THE ACCURACY OF ANY INFORMATION CONTAINED IN THE MATERIALS, INCLUDING, WITHOUT LIMITATION, ANY IMPLIED WARRANTY OF MERCHANTABILITY, ACCURACY, SATISFACTORY QUALITY, FITNESS FOR A PARTICULAR PURPOSE, USABILITY, INTEGRATION OR NON-INFRINGEMENT AND ALL SUCH WARRANTIES ARE HEREBY EXCLUDED BY WILEY AND ITS LICENSORS AND WAIVED BY YOU.
- WILEY shall have the right to terminate this Agreement immediately upon breach of this Agreement by you.

- You shall indemnify, defend and hold harmless WILEY, its Licensors and their respective directors, officers, agents and employees, from and against any actual or threatened claims, demands, causes of action or proceedings arising from any breach of this Agreement by you.
- IN NO EVENT SHALL WILEY OR ITS LICENSORS BE LIABLE TO YOU OR ANY OTHER PARTY OR ANY OTHER PERSON OR ENTITY FOR ANY SPECIAL, CONSEQUENTIAL, INCIDENTAL, INDIRECT, EXEMPLARY OR PUNITIVE DAMAGES, HOWEVER CAUSED, ARISING OUT OF OR IN CONNECTION WITH THE DOWNLOADING, PROVISIONING, VIEWING OR USE OF THE MATERIALS REGARDLESS OF THE FORM OF ACTION, WHETHER FOR BREACH OF CONTRACT, BREACH OF WARRANTY, TORT, NEGLIGENCE, INFRINGEMENT OR OTHERWISE (INCLUDING, WITHOUT LIMITATION, DAMAGES BASED ON LOSS OF PROFITS, DATA, FILES, USE, BUSINESS OPPORTUNITY OR CLAIMS OF THIRD PARTIES), AND WHETHER OR NOT THE PARTY HAS BEEN ADVISED OF THE POSSIBILITY OF SUCH DAMAGES. THIS LIMITATION SHALL APPLY NOTWITHSTANDING ANY FAILURE OF ESSENTIAL PURPOSE OF ANY LIMITED REMEDY PROVIDED HEREIN.
- Should any provision of this Agreement be held by a court of competent jurisdiction to be illegal, invalid, or unenforceable, that provision shall be deemed amended to achieve as nearly as possible the same economic effect as the original provision, and the legality, validity and enforceability of the remaining provisions of this Agreement shall not be affected or impaired thereby.
- The failure of either party to enforce any term or condition of this Agreement shall not constitute a waiver of either party's right to enforce each and every term and condition of this Agreement. No breach under this agreement shall be deemed waived or excused by either party unless such waiver or consent is in writing signed by the party granting such waiver or consent. The waiver by or consent of a party to a breach of any provision of this Agreement shall not operate or be construed as a waiver of or consent to any other or subsequent breach by such other party.
- This Agreement may not be assigned (including by operation of law or otherwise) by you without WILEY's prior written consent.
- Any fee required for this permission shall be non-refundable after thirty (30) days from receipt by the CCC.
- These terms and conditions together with CCC's Billing and Payment terms and conditions (which are incorporated herein) form the entire agreement between you and WILEY concerning this licensing transaction and (in the absence of fraud) supersedes all prior agreements and representations of the parties, oral or written. This Agreement may not be amended except in writing signed by both parties. This Agreement shall be binding upon and inure to the benefit of the parties' successors, legal representatives, and authorized assigns.
- In the event of any conflict between your obligations established by these terms and conditions and those established by CCC's Billing and Payment terms and conditions, these terms and conditions shall prevail.
- WILEY expressly reserves all rights not specifically granted in the combination of (i) the license details provided by you and accepted in the course of this licensing transaction, (ii) these terms and conditions and (iii) CCC's Billing and Payment terms and conditions.
- This Agreement will be void if the Type of Use, Format, Circulation, or Requestor Type was misrepresented during the licensing process.
- This Agreement shall be governed by and construed in accordance with the laws of the State of New York, USA, without regards to such state's conflict of law rules. Any legal action, suit or proceeding arising out of or relating to these Terms and Conditions or the breach thereof shall be instituted in a court of competent jurisdiction in New York County in the State of New York in the United States of America and each party hereby consents and submits to the personal jurisdiction of such court, waives any objection to venue in such court and consents to service of process by registered or certified mail, return receipt requested, at the last known address of such party.

WILEY OPEN ACCESS TERMS AND CONDITIONS

Wiley Publishes Open Access Articles in fully Open Access Journals and in Subscription journals offering Online Open. Although most of the fully Open Access journals publish open access articles under the terms of the Creative Commons Attribution (CC BY) License only, the subscription journals and a few of the Open Access Journals offer a choice of Creative Commons Licenses. The license type is clearly identified on the article.

The Creative Commons Attribution License

The [Creative Commons Attribution License \(CC-BY\)](#) allows users to copy, distribute and transmit an article, adapt the article and make commercial use of the article. The CC-BY license permits commercial and non-

Creative Commons Attribution Non-Commercial License

The [Creative Commons Attribution Non-Commercial \(CC-BY-NC\) License](#) permits use, distribution and reproduction in any medium, provided the original work is properly cited and is not used for commercial purposes.(see below)

Creative Commons Attribution-Non-Commercial-NoDerivs License

The [Creative Commons Attribution Non-Commercial-NoDerivs License](#) (CC-BY-NC-ND) permits use, distribution and reproduction in any medium, provided the original work is properly cited, is not used for commercial purposes and no modifications or adaptations are made. (see below)

Use by commercial "for-profit" organizations

Use of Wiley Open Access articles for commercial, promotional, or marketing purposes requires further explicit permission from Wiley and will be subject to a fee.

Further details can be found on Wiley Online Library <http://olabout.wiley.com/WileyCDA/Section/id-410895.html>

Other Terms and Conditions:

v1.10 Last updated September 2015

Questions? customercare@copyright.com or +1-855-239-3415 (toll free in the US) or +1-978-646-2777.



RightsLink®

[Home](#)[Create Account](#)[Help](#)

Title: Scanning Probe Characterization of Heterostructured Colloidal Nanomaterials

Author: Sanjini U. Nanayakkara, Jao van de Lagemaat, Joseph M. Luther

Publication: Chemical Reviews

Publisher: American Chemical Society

Date: Aug 1, 2015

Copyright © 2015, American Chemical Society

[LOGIN](#)

If you're a **copyright.com user**, you can login to RightsLink using your copyright.com credentials. Already a **RightsLink user** or want to [learn more?](#)

PERMISSION/LICENSE IS GRANTED FOR YOUR ORDER AT NO CHARGE

This type of permission/license, instead of the standard Terms & Conditions, is sent to you because no fee is being charged for your order. Please note the following:

- Permission is granted for your request in both print and electronic formats, and translations.
- If figures and/or tables were requested, they may be adapted or used in part.
- Please print this page for your records and send a copy of it to your publisher/graduate school.
- Appropriate credit for the requested material should be given as follows: "Reprinted (adapted) with permission from (COMPLETE REFERENCE CITATION). Copyright (YEAR) American Chemical Society." Insert appropriate information in place of the capitalized words.
- One-time permission is granted only for the use specified in your request. No additional uses are granted (such as derivative works or other editions). For any other uses, please submit a new request.

If credit is given to another source for the material you requested, permission must be obtained from that source.

[BACK](#)[CLOSE WINDOW](#)

Copyright © 2016 [Copyright Clearance Center, Inc.](#) All Rights Reserved. [Privacy statement.](#) [Terms and Conditions.](#)
Comments? We would like to hear from you. E-mail us at customercare@copyright.com